ANALYSIS OF SYNAPTOTAGMIN-SNARE COMPLEX INTERACTIONS BY ONE-DIMENSIONAL NMR SPECTROSCOPY

APPROVED BY SUPERVISORY COMMITTEE

_____

Jose Rizo-Rey, Ph.D.

_____

Luke Rice, Ph.D.

_____

Chad Brautigam, Ph.D.

_____

Hongtao Yu, Ph.D.

Dedication

To my loved ones

ANALYSIS OF SYNAPTOTAGMIN-SNARE COMPLEX INTERACTIONS BY ONE-DIMENSIONAL NMR SPECTROSCOPY

by

AMY ZHOU

DISSERTATION

Presented to the Faculty of the Graduate School of Biomedical Sciences

The University of Texas Southwestern Medical Center at Dallas

In Partial Fulfillment of the Requirements

For the Degree of

DOCTOR OF PHILOSOPHY

The University of Texas Southwestern Medical Center

Dallas, TX

May, 2015

Acknowledgements

I would like to thank Dr. Jose Rizo-Rey for the opportunity to pursue my doctoral studies in his lab. His patient teaching helped me grasp the concepts and techniques of NMR and other biophysical tools. His attention to detail taught me a great deal about the process of scientific research. His enthusiasm and encouragement allowed me to stay positive and push forward with my projects even during the difficult times. I have learned from him the importance of being humble and critical of oneself, and these qualities allowed me to mature not only as a scientist, but as a person. I am very fortunate to have been under Jose's guidance for the past four years.

My dissertation committee members, Dr. Luke Rice, Dr. Chad Brautigam, and Dr. Hongtao Yu, have been invaluable throughout my studies in critiquing my data and inspiring me to brainstorm for the next experiments. I greatly appreciate their advice and insights. I would also like to thank the members of the Rizo-Rey lab for a very positive environment in which to do science. In particular, Kyle Brewer guided me through my initial lab rotation. Dr. Lijing Su and Alpay Seven helped me in my experiments with liposomes. I also appreciate the fruitful discussions and supportive friendships I shared with these other lab members: Dr. Cong Ma, Dr. Luning He, Dr. Junjie Xu, Yilun Sun, Dr. Yibin Xu, Dr. Wei Li, Dr. Mengru Ho, Dr. Marcelo Roggero, and Dr. Victoria Esser.

The Medical Scientist Training Program has been very supportive. I am grateful for the kindness and helpfulness of Dr. Andrew Zinn, Ms. Robin Downing and Ms. Stephanie Robertson. Finally, I would like to thank my dear friends as well as my parents, Xiaoxia Li and Jianqin Zhou, for their unwavering love, patience, and understanding during my challenging but exciting graduate school journey.

ANALYSIS OF SYNAPTOTAGMIN-SNARE COMPLEX INTERACTIONS BY ONE-DIMENSIONAL NMR SPECTROSCOPY

AMY ZHOU

The University of Texas Southwestern Medical Center at Dallas, 2015

JOSE RIZO-REY, Ph.D.

The mechanism of calcium-triggered neurotransmitter release is mediated by numerous proteins at the neuronal synapse. The SNARE proteins form a complex that mediates fusion between the synaptic vesicle and plasma membrane. The protein synaptotagmin-1 is the major sensor for the calcium concentration. Synaptotagmin-1 and the SNARE complex are therefore believed to interact in order to couple the calcium concentration to membrane fusion. The detailed mechanism of the interaction is still unclear, because the technical difficulties in probing the system have rendered it intractable with respect to traditional biochemical and biophysical methods.

I will present an analytical method based on one-dimensional NMR spectroscopy that overcomes these limitations. The experiments are based on the current working model that synaptotagmin-1 facilitates the SNAREs' role in membrane fusion in a calcium-dependent manner. My data suggest that the synaptotagmin-1/SNARE complex interaction is calcium-dependent and mediated primarily by the synaptotagmin C2B domain. Further, the polybasic region of C2B constitutes the primary binding site, while the two arginine residues at the bottom of the domain mediate additional interactions that lead to aggregation and precipitation. These results help clarify the complex mechanism of synaptotagmin-1/SNARE coupling, as well as to illustrate the usefulness of 1D NMR to study such protein-protein interactions.

Alternative methods to probe such interactions are explored. The advantage of a related competition assay lies in its sampling of the primary binding site with little interference of the other binding mode(s). However, experimental artifacts hindered the application of the assay to my system. A diffusion-based method is another route for studying protein-protein interactions, provided there is sufficient dynamic range to allow for meaningful interpretations.

The SNARE-, calcium-, and lipid-binding profiles of an extended synaptotagmin-like protein (E-Syt) were also characterized. E-Syts are of interest because they can shed light on the evolution of proteins in the synaptotagmin family. In addition, they can reveal general governing principles of tandem C2-domain proteins which often function in signal transduction and membrane trafficking.

TABLE OF CONTENTS

PRIOR PUBLICATIONS

Amy Zhou, Kyle D. Brewer, and Josep Rizo. Analysis of SNARE Complex/Synaptotagmin-1 interactions by One-Dimensional NMR Spectroscopy. *Biochemistry.* 2013, 52(20): 3446–3456.

Urs O. Häfeli, Kelly Gilmour, **Amy Zhou,** Stanley Lee, and Michael E. Hayden. Modeling of magnetic bandages for drug targeting: Button vs. Halbach arrays. *Journal of Magnetism and Magnetic Materials.* 2007, 311(1): 323-329.

LIST OF FIGURES

LIST OF ABBREVIATIONS

1D, 2D, 3D	One, two and three-dimensional
BSA	Bovine serum albumin
CD	Circular dichroism
Co-IP	co-immunoprecipitation assay
CNS	Central nervous system
DLS	Dynamic light scattering
DOPS	1,2-dioleoyl-sn-glycero-3-phospho-L-serine
DTT	Dithiothreitol
E. coli	*Eschericheria coli*
EDTA	Ethylenediamine tetraacetic acid
EGTA	Ethylene glycol-bis(2-aminoethylether)-tetraacetic acid
EPR	Electron paramagnetic resonance
EPSC	Excitatory post-synaptic current
ESyt	Extended Synaptotagmin-like protein
FPLC	Fast performance liquid chromatography
FRET	Förster (fluorescence) resonance energy transfer
GST	Glutathione S-Transferase
HEPES	N-(2-hydroxyethyl) piperizine-N'2-ethanesulphonic acid
HSQC	Heteronuclear single quantum coherence spectroscopy
IPTG	Isopropyl β-D-thiogalactopyranoside
K_d	Dissociation constant
kDa	Kilodalton
LB	Luria broth
ml	Milliliter

nm	Nanometer
NMJ	Neuromuscular junction
NMR	nuclear magnetic resonance
NSF	N-ethylmaleimide-sensitive factor
OD	Optical density
PBS	Phosphate buffered saline
PCR	Polymerase chain reaction
PIP_2	Phosphatidylinositol-4,5-bisphosphate
PKC	Protein kinase C
pN	Piconewton
POPC	1-palmitoyl, 2-oleoyl-sn-glycero-3-phosphocholine
POPE	1-palmitoyl-2-oleoyl-sn-glycero-3-phosphoethanolamine
ppm	Part(s) per million
RIMs	Rab3-interacting molecules
RT	Room temperature
SDS-PAGE	Sodium dodecyl sulfate-polyacrylamide gel
SM proteins	Sec1/Munc18 proteins
SMR	Strongest methyl resonance
SN1	The N-terminal SNARE motif of rat SNAP25
SN3	The C-terminal SNARE motif of rat SNAP25
SNAP	Soluble NSF attachment protein (different from SNAP-25)
SNAP-25	Synaptosomal associated protein of 25 kDa (different from SNAPs)
SNARE	SNAP receptor
SV	Synaptic vesicle
Syb	Synaptobrevin (same as VAMP)

Syt1, Syt2	Synaptotagmin-1, synaptotagmin-2
TMR	Trans-membrane region
Tris	Tris (hydroxymethyl) aminomethane
TROSY	Transverse relaxation optimized spectroscopy
t-SNARE	Target membrane-associated SNARE
UV	Ultraviolet
VAMP	Vesicle associated membrane protein (same as Syb)
v-SNARE	Vesicle-associated SNARE
WT	Wildtype

Chapter 1. General Introduction

1.1 The neuron – structure and function

The human brain is arguably the most complex organ in both its normal physiological and altered pathological states. This complexity arises in part from the network of connections among its neurons: each neuron can receive inputs from, and transmit outputs to, multiple other neurons. Given the hundreds of billions of neurons in the brain (Purves et al. 2001; Shatz 2001), the combinatorial possibilities lead to the intricate patterns of connections.

The neuron was first visualized microscopically in the early 1800's by G.G. Valentin. In the late 1800's, Santiago Ramón y Cajal proposed the idea of neurons as the primary functional units of the nervous system (Cajal 1906). His neuron doctrine stated that, as opposed to a syncytium of cells, the brain is composed of neuronal cells that are discrete structural and functional units connected through specialized junctions (Lopez-Munoz et al. 2006). The doctrine holds true to this day in most, if not all, nervous systems that have been studied.

A neuron consists of a cell body or soma, an axon, and one or more dendrites (Figure 1). Neurons communicate with each other as follows: an action potential travels from the cell body along the axon as a wave of local membrane depolarizations, until it reaches the axon terminal. The terminal is the transmitting end of the cell. It is separated from the receiving neuronal cell body or dendrite by the synaptic cleft (Figure 2). The synapse contains the molecular machinery that facilitates the transmission of electrical and chemical signals (Kandel et al. 2000; Purves et al. 2001). This dissertation concerns the pre-synaptic proteins that control such transmission.

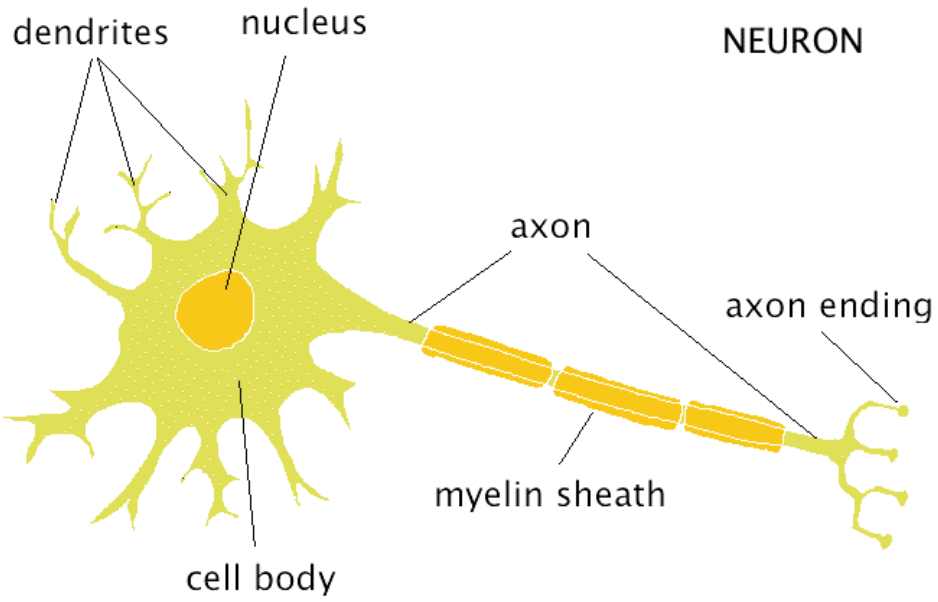

Figure 1. Illustration of a neuron. The cell body, dendrites, and axon are shown. The axon is a long projection that is sometimes encased in a myelin sheath which facilitates signal transmission (Boeree 2009).

1.2 The synapse and synaptic vesicle exocytosis

The modern understanding of neurotransmission is based on seminal work elucidating both the electrical (Hodgkin and Huxley 1952) and chemical components (Fatt and Katz 1952; Del Castillo and Katz 1954). This dissertation focuses on the chemical component. Bernad Katz proposed the quantal theory of transmitter release in 1954, after observing that the post-synaptic potential at frog neuromuscular junctions consisted of multiple, small quanta of acetylcholine. The presynaptic terminal contained a corresponding pool of such quanta, with presynaptic stimulation causing the synchronous release of some part of this pool. Furthermore, they noted that calcium controlled the probability of a given quantum being released (Del Castillo and Katz 1954). These observations, along with the first EM images of the synapse (De Robertis and Bennett 1955; Palay 1960), led to the hypothesis that neurotransmitters are stored in synaptic vesicles. Quantal transmission is a result of neurotransmitter release from these vesicles (Del Castillo and Katz 1956; Palay 1956).

Storage vesicles are categorized by their size and content. The synaptic vesicles (SVs) alluded to above are also known as small clear-core vesicles. They are one of three types of storage vesicles. At 40-60 nm in diameter, SVs contain small molecular neurotransmitters such as acetylcholine, amino acids, and other non-peptides. After releasing their contents into the synaptic cleft, the vesicles are endocytosed, recycled, and re-filled with neurotransmitters for the next round of fusion (Ceccarelli et al. 1973; Heuser and Reese 1973). A second type, the large dense-core vesicles, are 90-250 nm and contains neuropeptides. They are localized to endocrine cells. The third type - the small/large dense-core vesicles - contain biogenic amines. Their size depends on the type of neurons (Purves et al. 2001). The focus here is on the mechanism of

exocytosis of synaptic vesicles. But many aspects of this mechanism can be generalized to other forms of vesicle exocytosis.

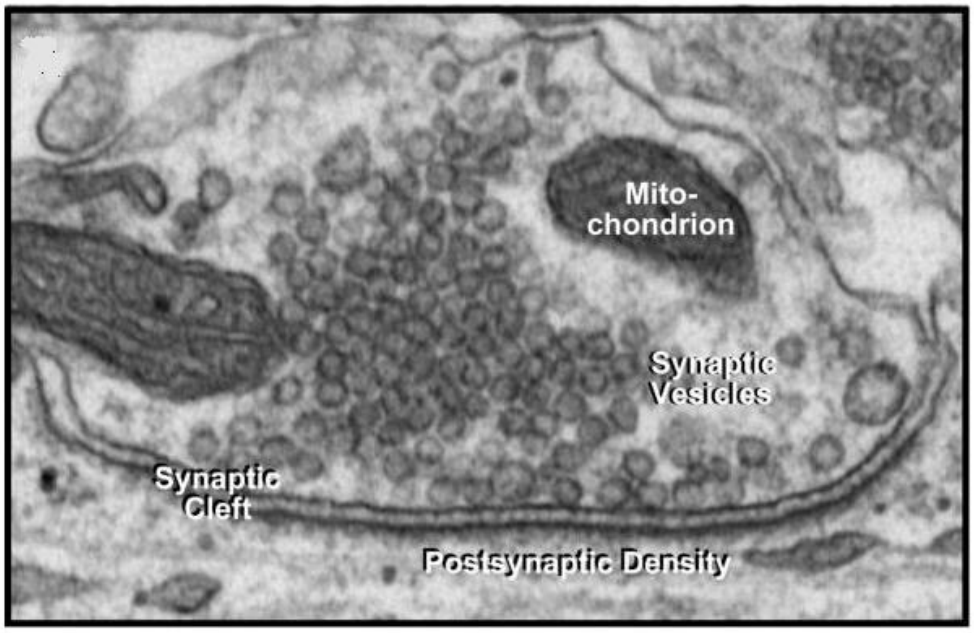

Figure 2. Electron micrograph of a synapse (Sudhof 2008). The synaptic vesicles located in the pre-synaptic cell are filled with neurotransmitters. Upon the action-potential driven increase in intracellular [Ca^{2+}], these vesicles fuse with the pre-synaptic plasma membrane, releasing their content into the synaptic cleft. From there, the neurotransmitters can diffuse and interact with post-synaptic receptors.

Neurotransmitter release is initiated when an action potential propagates along the axon to the pre-synaptic terminal. There, it depolarizes the plasma membrane which causes the opening of voltage-gated Ca^{2+}-channels and a transient increase in the intracellular Ca^{2+} concentration. This brings about the fusion of the synaptic vesicles with the plasma membrane, and neurotransmitters are released into the synaptic cleft. This fundamental mechanism was first described at the neuromuscular junction in 1967 (Katz and Miledi 1967). Its temporal profile has since been characterized in many model synapses (Augustine et al. 1985; Sabatini and Regehr 1996), especially in the calyx of Held in the rat brainstem (Meinrenken et al. 2003). These studies demonstrated the tight coordination of presynaptic action potential, Ca^{2+} influx, and vesicle fusion, such that the sequence of events occurs on the order of a few hundred microseconds. Such speed and precision is mediated by cytosolic, vesicle- and plasma membrane-anchored proteins. They mediate the targeting of vesicles to the plasma membrane (docking), the preparation of vesicles for fusion (priming), and membrane fusion in response to Ca^{2+} influx (Figure 3). The research presented here focuses on a subset of the proteins that function in the final Ca^{2+}-triggered membrane fusion step: synaptotagmin-1 and the SNARE proteins, as introduced in the next section.

While the focus of this work is on the proteins involved in action potential-driven neurotransmitter release, there are two other forms of Ca^{2+}-dependent synaptic exocytosis: spontaneous “mini” release and asynchronous release (Pang and Sudhof 2010). Spontaneous mini release represents the background nerve terminal activity triggered by spontaneous Ca^{2+} fluctuations. It can be observed in all neurons at varying frequencies: from once per 2-3 hours to once per 3 minutes per synapse, depending on the type of neuron. Asynchronous release

typically becomes more apparent when the main synaptotagmin Ca^{2+} sensor is ablated (Geppert et al. 1994).

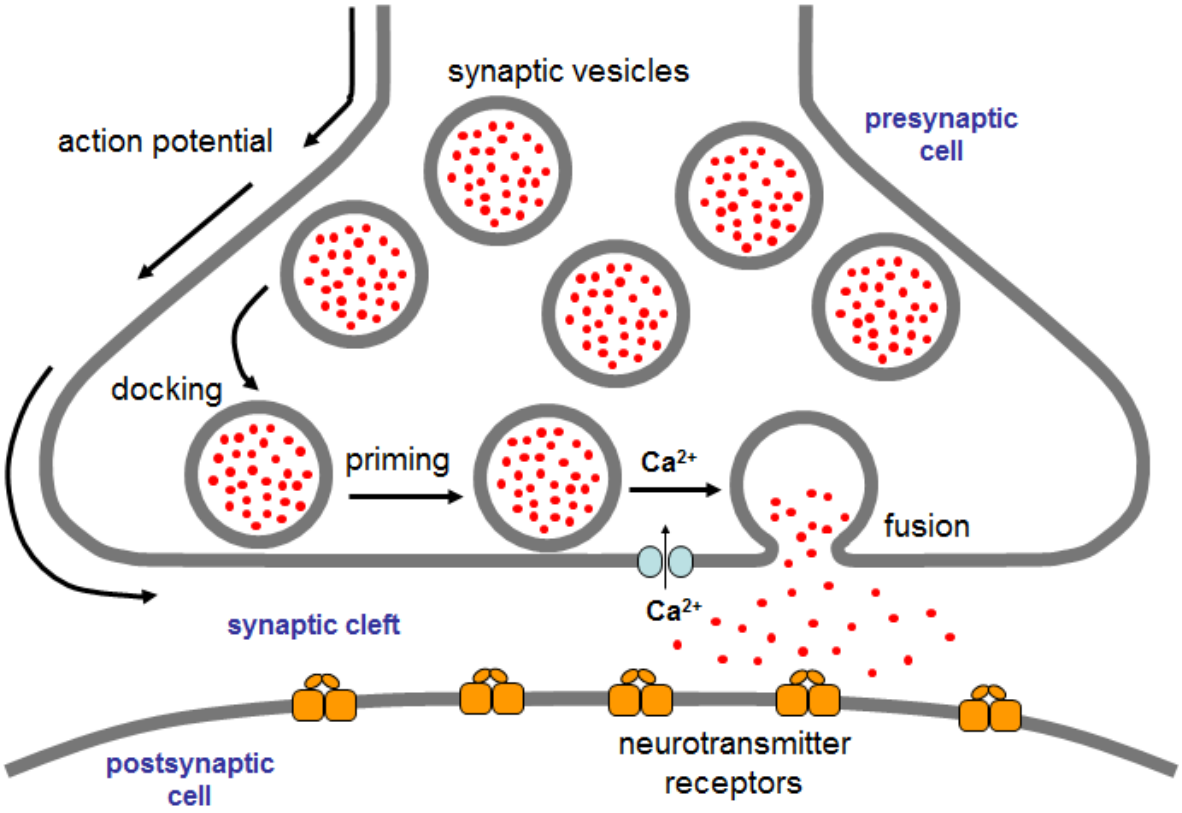

Figure 3. The sequence of events in neurotransmitter release. Neurotransmitter release is initiated when an action potential propagates along the axon to the end of the pre-synaptic terminal. There, it depolarizes the plasma membrane which causes the opening of voltage-gated Ca^{2+}-channels and a transient increase in the intracellular Ca^{2+} concentration. This brings about the fusion of the synaptic vesicles with the plasma membrane, and neurotransmitters are released into the synaptic cleft (figure courtesy of mentor Jose Rizo-Rey).

The strength of a synapse is measured by the change in the postsynaptic membrane potential as a result of the presynaptic action potential. The strength depends on the size and number of individual connections between the pre- and post-synaptic neurons. Changes to the strength of existing synapses is believed to contribute to the plasticity of the adult brain, even though this capacity to change is most prominent in the neural circuits of young, developing brains. Such plasticity in adults enables the acquisition of memory, learning of new skills, and response to injury, among many other functions. It appears to arise from post-translational modification of proteins, alterations in gene expression, and some formation of new axon-dendrite connections (Purves et al. 2001). The characterization of neuronal synapses it thus of great interest and importance.

1.3 Proteins involved in the regulation of synaptic vesicle exocytosis

1.3.1 Overview

The rise in intracellular calcium concentration leads to neurotransmitter release within a few hundred microseconds. The sequential steps in such a fast process require exquisite temporal and spatial control. Such control is achieved through many proteins localized at the synapse. The core protein machinery includes N-ethylmaleimide-sensitive factor (NSF), soluble NSF adaptor proteins (SNAPs), the neuronal SNAP receptors (SNAREs) syntaxin-1, SNAP-25 and synaptobrevin, and the Sec1/Munc18 (SM) protein Munc18-1 (Brunger 2005; Jahn and Scheller 2006; Rizo and Rosenmund 2008; Sudhof and Rothman 2009; Ma et al. 2013). These proteins have homologs in most types of intracellular membrane trafficking, implicating their conservation across all forms of membrane fusion. In addition, there are neuron-specific proteins in the regulation of Ca^{2+} triggered neurotransmitter release, including the Ca^{2+} sensor synaptotagmin-1 (Fernandez-Chacon et al. 2001), the priming factors RIMs, the active zone protein Munc13, and the SNARE complex associating protein complexin. Calcium induces the synaptotagmin-mediated displacement of complexin from the SNARE complex, thereby triggering fast exocytosis (Tang et al. 2006). All these proteins are present in several isoforms with differential distributions, suggesting a general organizational principle of the mammalian brain (Geppert et al. 1991).

1.3.2 Synaptotagmin and its role as a Ca^{2+} sensor

Synaptotagmins are a large family of membrane trafficking proteins characterized by an N-terminal trans-membrane region, a variable length linker, and two cytoplasmic C2 domains – C2A and C2B. They are evolutionary conserved through vertebrates and invertebrates, but are

absent from plants and unicellular eukaryotes (Sudhof 2012). Synaptotagmin was first identified through an antibody screen for synaptic proteins, and found to be an SV-specific membrane protein with wide distribution in neurons and neurosecretory tissue (Matthew et al. 1981). The synaptotagmin cytoplasmic domains display homology to the regulatory C2 region of PKC. C2-domains are widespread modules of 130–140 residues initially defined as the second constant sequence - hence C2 - in protein kinase C-isoforms (Coussens et al. 1986). Proteins containing these domains are typically involved in signal transduction and membrane trafficking. The classical isoforms of PKC depend on Ca^{2+} for activation, and phospholipid binding to many C2 domains are Ca^{2+}-dependent (Rizo and Sudhof 1998). However, not all C2 domains bind Ca^{2+}: there are Ca^{2+}-dependent and independent forms that interact with a diverse set of targets. For example, while the C2A domain of the extended synaptotagmin-like protein isoform 2 - ESyt-2 - binds Ca^{2+}, its C2B domain does not (see chapter 4).

The C2 domains of synaptotagmin-1 (Syt1) bind Ca^{2+} and mediate Ca^{2+}-dependent phospholipid binding (Brose et al. 1992; Davletov and Sudhof 1993; Chapman et al. 1995; Li et al. 1995). These functions are essential for Ca^{2+}-triggered neurotransmitter release, and is particularly true for the C2B domain (Mackler et al. 2002; Nishiki and Augustine 2004; Shin et al. 2009). The Ca^{2+}-binding ability of the C2A domain contributes to the overall cooperativity of Ca^{2+}-triggered release as well, but C2B is believed to be functionally more important (Fernandez-Chacon et al. 2002; Robinson et al. 2002; Shin et al. 2009). Calcium binding does not induce substantial conformational changes in synaptotagmin, but causes an electrostatic potential change that mediates phospholipid binding and insertion of hydrophobic residues into the membrane bilayer (Shao et al. 1997; Chapman and Davis 1998; Zhang et al. 1998).

The importance of synaptotagmin in mediating Ca^{2+}-dependent neurotransmitter release was first demonstrated *in vivo* in *D. melanogaster* and *C. elegans* (Littleton et al. 1993; Nonet et al. 1993). Later, it was shown that mice homozygous for a mutation in the Syt1 gene died within 48 hours after birth. The hippocampal neurons cultured from these mice show severe impairment of the synchronous component of Ca^{2+}-dependent release, but not the asynchronous or the Ca^{2+}-independent (also known as the spontaneous) component (Geppert et al. 1994). The functional importance of Ca^{2+}-dependent phospholipid-Syt1 interactions was shown through point mutations in Syt1: the mutations that impaired or enhanced Ca^{2+}-dependent phospholipid binding led to parallel effects on the efficiency of neurotransmitter release (Fernandez-Chacon et al. 2001; Rhee et al. 2005). These studies further established Syt1 as the major Ca^{2+} sensor for fast neurotransmitter release (Sudhof 2012).

The C2 domains of synaptotagmin contain two β-sheets, each consisting of four β-strands (Ubach et al. 1998). The overall structure is often referred to as a β-sandwich (Figure 5), with a long axis of 50 Å. The Ca^{2+}-binding loops are positioned on one side of the β-sandwich structure, and the Ca^{2+}-coordinating properties are determined mostly by the positions of the aspartate and serine residues. These residues are often not in close proximity in the primary sequence space, but form a cluster within 6 Å in the three-dimensional structure (Sutton et al. 1995; Fernandez et al. 2001).

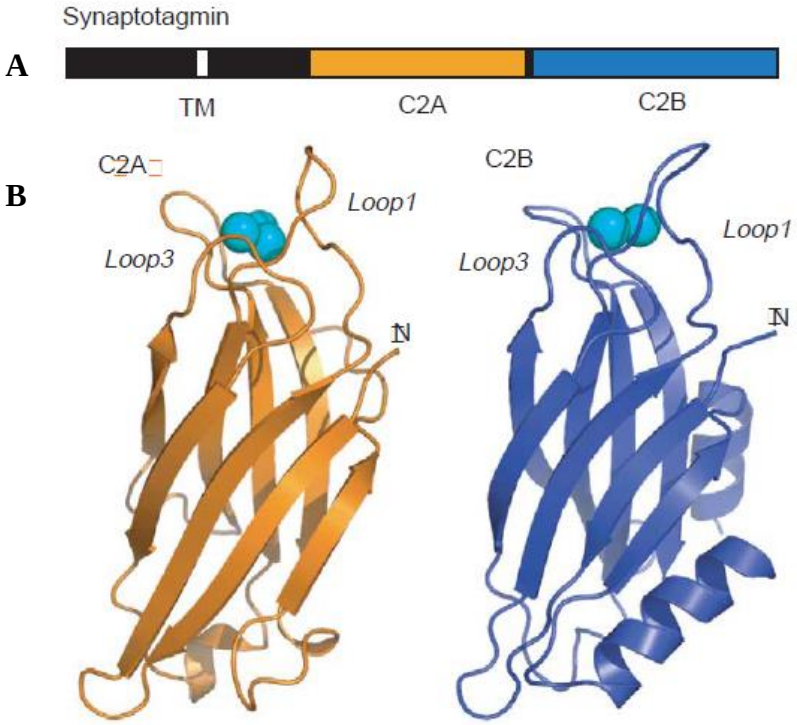

Figure 5. The structure of synaptotagmin-1. A. The domain diagram of synaptotagmin-1 showing its transmembrane region (TM), C2A domain (yellow), and C2B domain (blue). **B.** Ribbon diagrams of the C2A and C2B domains with Ca^{2+} ions (cyan spheres) bound to the top loops formed by the eight-strand β-sandwich. The two domains are flexibly linked (Rizo et al. 2006).

Ca^{2+} binding does not induce major conformational changes, but is believed to act as an electrostatic switch (Shao et al. 1996; Shao et al. 1997; Fernandez et al. 2001; Ubach et al. 2001). This is because these top loops also mediate the Ca^{2+}-dependent binding of synaptotagmin to phospholipids (Chapman and Davis 1998; Zhang et al. 1998; Fernandez et al. 2001). The intrinsic affinities of the different Ca^{2+} binding pockets of Syt1 C2 domains range from a K_d of 60 µM to above 1 mM (Ubach et al. 1998). The affinities are enhanced 2-3 orders of magnitude in the presence of negatively charged phospholipids (Davletov and Sudhof 1993), leading to the highest affinity being ~5 µM. This suggests the phospholipids contribute negative charges that, along with the residues on Syt1, complete the Ca^{2+}-coordinating spheres. (Fernandez-Chacon et al. 2001; Fernandez et al. 2001). *In vivo*, neurotransmitter release is associated with intracellular Ca^{2+} concentrations ranging from ~10 µM to ~200 µM, depending on the type of neuronal cells used (Heidelberger et al. 1994).

Synaptotagmin has been shown to bind the opposing membranes in the presence of calcium, bringing the membranes close together. The C2B domain is sufficient for this role, which is a consequence of the abundance of basic residues on the C2B domain (Arac et al. 2006) (Figure 6).

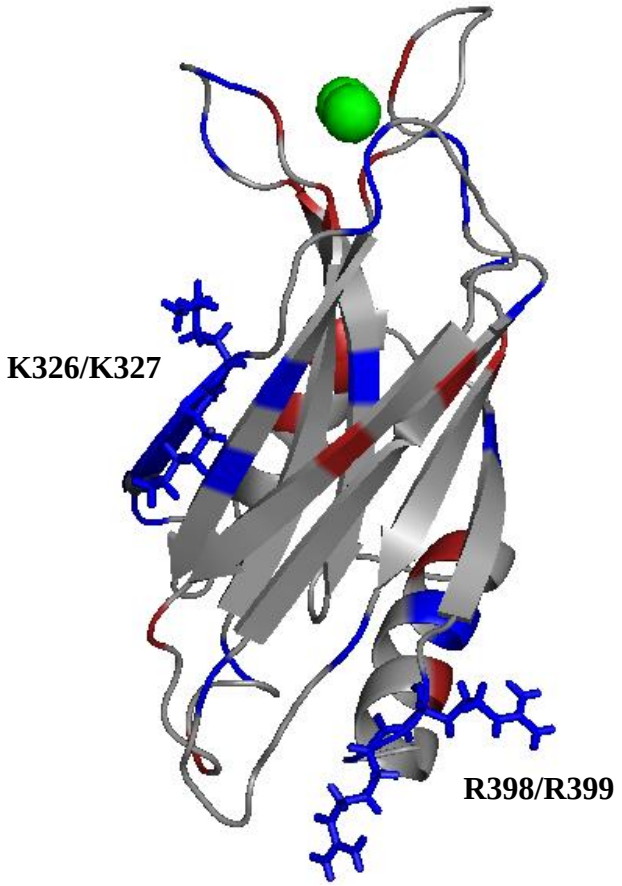

Figure 6. Ribbon diagram of the C2B domain of synaptotagmin-1. Amino acid residues with positively-charged side chains are shown in blue, negatively-charged in red. Ca^{2+} ions are shown in green. The polybasic lateral side with the lysine side chains shown as sticks will be mutated: K326A/K327A. The two arginine residues opposite of the Ca^{2+} ions will be mutated as well: R398Q/R399Q.

The functional relevance of the above *in vitro* results was confirmed when mutation of the two arginines to glutamines, R398Q/R399Q, almost completely abolished neurotransmitter release as measured by the EPSC in hippocampal neurons. In addition, the mutation strongly impaired liposome clustering and SNARE-dependent lipid mixing (Xue et al. 2008). Another region of interest is on the polybasic side of the C2B β-sandwich. It has been implicated in binding negatively charged phospholipids such as PIP_2 (Bai et al. 2004). Mutation in the polybasic region through neutralization of the two lysine residues, K326A/K327A, led to a 36% drop in evoked neurotransmitter release in the drosophila NMJ (Mackler and Reist 2001) and around 50% drop in the EPSC of hippocampal neurons (Li et al. 2006). Synaptotagmin functions mediated by the C2B polybasic motif are therefore necessary for full-length synaptotagmin function *in vivo* (Mackler and Reist 2001).

To date, 16 different isoforms of mammalian synaptotagmin have been identified, eight of which are known to bind calcium (Sudhof 2012). The calcium sensitivities and tissue distributions of the isoforms may overlap but are not identical (Pang and Sudhof 2010). For example, Syt1 and Syt2 have been established as the active Ca^{2+} sensors in synaptic exocytosis (Ullrich et al. 1994). They are both abundantly expressed on synaptic vesicles but are differentially distributed in the brain (Geppert et al. 1991; Fykse et al. 1993). In addition to synaptic vesicles, synaptotagmin is also a component of the neuropeptide-containing large dense-core vesicles (Walch-Solimena et al. 1993). The conserved function of synaptotagmin operates in most forms of Ca^{2+}-regulated exocytosis: the degranulation of mast cells, acrosome exocytosis in sperm cells, hormone secretion from endocrine cells, and neuropeptide release (Sudhof and Rizo 2012). The abundance of synaptotagmin isoforms and their non-identical functions are believed to contribute to the functional and tissue heterogeneity and specificity in membrane trafficking.

Synaptotagmins do not have clear homologs in yeast, therefore their evolutionary history and properties are not well known. A family of yeast membrane proteins known as the tricalbins is thought to be related to synaptotagmins. They consist of tandem C2-domains, and their mammalian counterparts are a family of extended synaptotagmin-like proteins (E-Syts) (Min et al. 2007). Detailed studies of E-Syts can therefore shed light on the evolution of synaptotagmin.

1.3.3 The SNARE complex and its role in membrane fusion

The SNAREs are a family of cytoplasmically oriented integral membrane proteins. They are characterized by the α-helical SNARE motifs which are 60-70 residues long and composed of eight heptad repeats (Figure 7). Their importance in membrane fusion was first shown at the synapse where synaptobrevin, SNAP-25, and syntaxin-1 were specifically cleaved by the Clostridial *tetani* and Clostridial *botulinum* neurotoxins. This led to a block of presynaptic membrane fusion and neurotransmitter release without changes in synaptic morphology (Link et al. 1992; Schiavo et al. 1992; Blasi et al. 1993; Blasi et al. 1993). *In vivo*, neurotoxin cleavage of the proteins manifested as muscle spasms (tetanus) and paralysis (botulism) (Schiavo et al. 2000; Simpson 2004). Soon after their identification, synaptobrevin, SNAP-25, and syntaxin-1 were isolated from the bovine brain (Sollner et al. 1993) through affinity purification with the cytosolic fusion proteins NSF (Block et al. 1988) and SNAP (Block et al. 1988). They formed a stoichiometric complex, and were named the SNARE complex short for the SNAP receptor complex.

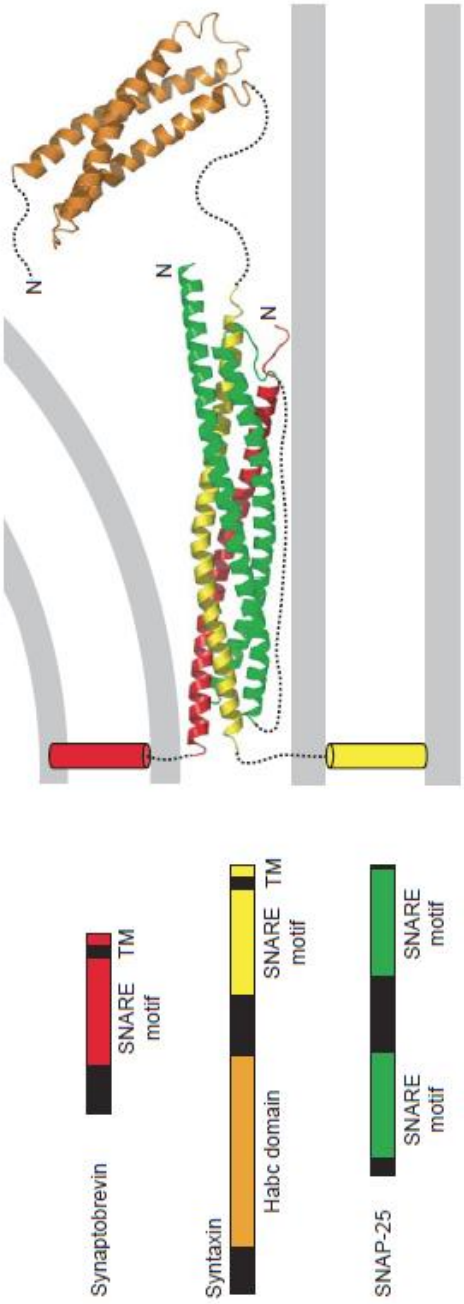

Figure 7. Structure and function of the neuronal SNAREs. Domain diagrams of the SNARE proteins. The three proteins show the characteristic α-helical SNARE motifs and form a tight four-helix bundle. The transmembrane domains are shown as cylinders and the flexible linkers as lines. The diagram is based on the NMR structure of the syntaxin Habc domain (Fernandez et al. 1998) and the crystal structure of the SNARE four-helix bundle (Sutton et al. 1998). This dissertation focuses on the soluble four-helix bundle. The SNAREs in the context of the lipid bilayers can bridge the vesicle and plasma membranes (Rizo et al. 2006).

Subsequent *in vitro* work showed that the complex can form in the absence of NSF and SNAP, and that it can bind synaptotagmin (Sollner et al. 1993). It is highly stable and SDS-resistant (Hayashi et al. 1994).

Many SNAREs and their homologs have since been characterized in yeast, plants, and animals (Rothman 1994; Bennett 1995; Linial 1997), each specific for a type of vesicle or target membrane. The vesicle is the secretory storage vehicle characteristic of the tissue type in which the protein is localized. The target membranes include the ER and nuclear envelopes, Golgi, endosomes, lysosomes, and apical and basolateral plasma membranes (Sudhof et al. 1993). The fusion of a vesicle with its target membrane involves the pairing of the corresponding v-SNARE and t-SNARE that reside in these opposite membranes (Sollner 2003). The process is believed to be initiated with the N- to C-terminal zippering of the *trans*-SNARE complex that bridges the junction between the opposing membranes. Complete zippering likely leads to the opening of the fusion-pore, but it is also possible that it only leads to membrane stress and/or curvature (Figure 8), and that fusion-pore opening requires subsequent mediation by other proteins such as synaptotagmin (Sudhof and Rizo 2012). All other SNARE complexes are now believed to be structurally similar to the synaptic complex and mediate membrane fusion via analogous mechanisms (Jahn et al. 2003). The SNAREs are thus thought to be essential in all forms of intracellular membrane fusion. Further, it has been demonstrated *in vitro* that they constitute sufficient minimal machinery for membrane fusion (Weber et al. 1998; Van Den Bogaart et al. 2010). However, recent work has elucidated the necessity of the SM proteins in mediating the initiation and propagation of such processes (Ma et al. 2013).

While most SNARE proteins contain one α-helical SNARE motif, SNAP-25 and its homologs contain two. It is anchored to the membrane via palmitoylation, while synaptobrevin

and syntaxin-1 are anchored through their C-terminal transmembrane domains (Figure 7). The three synaptic SNAREs thus form a parallel four-helix bundle, as observed via EPR (Poirier et al. 1998) and crystallography (Sutton et al. 1998). Syntaxin-1 and its homologs contain an additional N-terminal Habc domain (Fernandez et al. 1998) that lends to its further functional complexity in fusion (Sudhof and Rizo 2012). This dissertation work focuses on the soluble four-helix bundle portion of the synaptic SNARE proteins.

1.4 General goals of the dissertation

Synaptotagmin and the SNARE complex are believed to interact in order to couple the increase in intracellular Ca^{2+} concentration to membrane fusion, thereby bringing about synaptic vesicle exocytosis and neurotransmitter release. This dissertation is based on the current working model that synaptotagmin facilitates SNAREs' role in membrane fusion in a Ca^{2+}-dependent manner (Figure 8). The precise mechanism by which this occurs is still unknown and will be the focus of chapter 2, where I applied 1D NMR spectroscopy to understand the synaptotagmin-SNARE complex interactions. Chapter 3 explores alternative methods to probe such protein-protein interactions. The technical difficulties encountered highlight the complexity of the system and can inform the characterization of other protein-protein systems. Finally, NMR spectroscopy is applied again in chapter 4 to characterize the Ca^{2+}-binding properties of an extended synaptotagmin-like protein, ESyt2. My results highlight the general properties as well as the varying features of tandem C2-domain proteins.

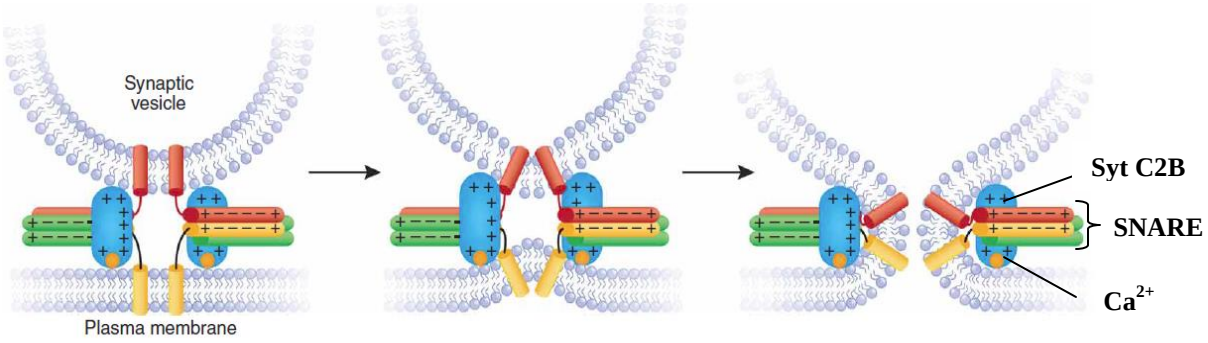

Figure 8. Current working model of how synaptotagmin-1 assists the SNARE complex in fusing the vesicle and plasma membranes in a Ca^{2+}-dependent manner (Rizo and Rosenmund 2008). The SNARE complex is shown as a multi-colored bundle as in Figure 7. Only the C2B domain of Syt1 is shown (blue), highlighting its overall positive charge (see also Figure 6). The Ca^{2+} ions are schematically represented as single orange spheres.

Chapter 2. Quantitative Analysis of Synaptotagmin-1/SNARE Complex Interactions

2.1 Introduction

Neurotransmitter release depends critically on the calcium sensor synaptotagmin-1, and the SNARE complex which mediates fusion between the synaptic vesicle and plasma membrane. Previous characterizations of the synaptotagmin-1/SNARE complex interactions are outlined below. These will lead to current questions, some of which are addressed through the experiments in this chapter.

2.1.1 The interactions of synaptotagmin-1 with the SNAREs

The function of synaptotagmin-1 depends on its interactions with the SNAREs – this is believed to be key in coupling Ca^{2+} sensing to membrane fusion. However, the nature of these interactions is unclear. This is because many modes of interactions have been described, sometimes leading to equivocal conclusions.

Synaptotagmin-1 has been shown to bind the neuronal SNARE protein syntaxin-1 in both Ca^{2+}-dependent and Ca^{2+}-independent fashions. This binding was reported to be mediated by the syntaxin-1 SNARE motif or Habc domain, and involves the synaptotagmin-1 C2A, C2B, or both domains (Bennett et al. 1992; Chapman et al. 1995; Li et al. 1995; Kee and Scheller 1996; Shao et al. 1997; Fernandez et al. 1998; Matos et al. 2000). Various studies have also reported that synaptotagmin-1 binds to SNAP-25, the syntaxin-1/SNAP-25 heterodimer, and to the SNARE complex. These interactions were again characterized as either Ca^{2+}-dependent or independent, and to be mediated by the synaptotagmin C2A and/or C2B domains (Davis et al. 1999; Gerona et al. 2000; Zhang et al. 2002; Rickman and Davletov 2003; Rickman et al. 2004; Bowen et al. 2005; Tang et al. 2006; Dai et al. 2007; Lynch et al. 2007).

There are numerous characterizations of the binding sites between synaptotagmin-1 and the SNARE complex, but no clear consensus has been reached. Binding has been shown to involve a negatively charged region in the SNAP-25 N-terminal (Zhang et al. 2002; Rickman et al. 2006) or C-terminal SNARE motif (Zhang et al. 2002; Dai et al. 2007). It also included the polybasic region on the lateral side of the synaptotagmin C2B domain, but there is disagreement as to whether the two arginine residues at the bottom of the domain are also involved (Rickman et al. 2006; Dai et al. 2007; Gaffaney et al. 2008; Xue et al. 2008). A single-molecule FRET model suggests the SNARE complex is closest to the bottom of the C2B domain (Choi et al. 2010)

Attempts have also been made to obtain a structure of the complex of synaptotagmin-1 and the SNAREs. In the same single-molecule FRET study, the results are not conclusive because the two entities are not in physical contact (Choi et al. 2010). In an electron paramagnetic resonance study, the results agree with previous findings that the polybasic side of the C2B domain is involved. Further, it suggests that synaptotagmin is configured to bind opposing membranes when in association with the SNAREs (Lai et al. 2011), in agreement with the working model in this dissertation. But the study also asserts that the complex of synaptotagmin-1 and the SNAREs takes on multiple conformations, which does not account for the ability of Syt1 to bridge the opposing membranes. Therefore, the physiologically relevant mode or modes of interaction are still unknown.

Some of the aforementioned conclusions may be a consequence of the limitations of the assays, as well as the stickiness or promiscuity of the proteins – for example syntaxin-1 (Rizo et al. 2006). Therefore, not all the documented interactions may be physiologically relevant. Nevertheless, because synaptotagmin-1 functions in the later steps of exocytosis - when the

SNARE complex is believed to be at least partially assembled - the Syt1/SNARE complex interaction is very likely pertinent to the process of Ca^{2+}-evoked neurotransmitter release. This dissertation work is based on a current working model, wherein synaptotagmin cooperates with the SNAREs to bring the synaptic vesicle and plasma membranes together in a Ca^{2+}-dependent manner, mostly through the positive electrostatic potential of the synaptotagmin C2B domain (Arac et al. 2006) (Figure 8). I sought to clarify the Ca^{2+}-dependence of the interaction as well as the protein surfaces involved.

2.1.2 Technical difficulties in studying synaptotagmin-1/SNARE complex interactions

Methods based on affinity chromatography enabled the identification of synaptotagmins, SNAREs, and other proteins of the neurotransmitter release machinery (Perin et al. 1990; Bennett et al. 1992; Hata et al. 1993; Sollner et al. 1993; Mcmahon et al. 1995). Yeast-two-hybrid, pull-down, and co-IP assays are also useful in identifying protein binding partners. But when it comes to characterizing these phenomena in purified protein systems, many interactions observed through these methods cannot be reproduced (Fernandez et al. 2001; Ubach et al. 2001; Basu et al. 2005). Such inconsistencies may arise if the assay is not sufficiently sensitive as a result of steric hindrance by the protein tags or the reaction matrix. Conversely, the assay may not be sufficiently specific if weak, non-specific interactions are enhanced and detected as positive results, when in fact they are artifacts of the assay. In addition, non-protein contaminants can mediate or mask protein-protein interactions and require rigorous purification protocols – for example, the affinity of the positively-charged synaptotagmin C2B domain for nucleic acids (Fernandez et al. 2001; Ubach et al. 2001). These assay limitations may account for some of the ambiguities in the synaptotagmin-1/SNARE complex results to date.

The synaptotagmin-1/SNARE complex macromolecular assembly has been difficult to characterize. I attempted to use isothermal titration calorimetry and fluorescence anisotropy, but both methods carry limitations given the relatively weak affinity, the low enthalpies of binding, and the tendency of the proteins to precipitate as shown in (Dai et al. 2007) and in sections 2.3.2 and 2.3.7.

I sought to optimize an analytical method that could overcome these limitations. The method used involves 1D NMR spectroscopy (Arac et al. 2003), where the signal representing synaptotagmin-1 changes as a function of the amount of SNARE complex bound. This assay offers high sensitivity even at low micromolar protein concentrations because the proton signals are not dispersed into a second dimension as in 2D NMR spectroscopy (Arac et al. 2003). I was able to define the relative contributions of the different binding modes, as well as the effects of point mutations on binding. It allowed for a quantitative correlation between the effects of these mutations on binding *in vitro* and their functional effects *in vivo*. My data suggest that 1) the synaptotagmin-1/SNARE complex interaction is Ca^{2+}-dependent, 2) the interaction is mediated primarily by the synaptotagmin C2B domain, 3) the polybasic region of C2B constitutes the primary binding site for the SNARE complex, and 4) the two arginines at the bottom of the domain mediate additional, weaker interactions that lead to aggregation and precipitation of the macromolecular assembly. These results help clarify the complex mechanism of synaptotagmin-1/SNARE coupling, as well as to illustrate the usefulness of 1D NMR to study such protein-protein interactions.

2.2 Materials & Methods

2.2.1 Protein expression and purification

Constructs for expression of rat synaptotagmin-1 C2A domain (residues 140-267), C2B domain (residues 271-421), C2AB fragment (residues 140-421), as well as the SNARE motifs of rat synaptobrevin (residues 29–93), rat syntaxin-1A (residues 191–253), and human SNAP-25B (residues 11–82 and 141–203) were available in the lab (Xue et al. 2008; Ma et al. 2013). Mutations were performed using the QuickChange site-directed mutagenesis kit (Stratagene). All proteins were expressed as GST-fusions in *Escherichia coli* BL21 DE3 cells. One colony of bacteria on the transformation plate was used to inoculate 50 ml of LB broth with 100 µg/mL ampicillin added. This small culture was grown at 37 °C and 250 rpm overnight. The next day, it was transferred to 1 L of LB medium with 100 µg/ml ampicillin added. It was incubated at 37 °C and 250 rpm for 2.5-3 hours till the OD_{600} reached 0.8-0.9. The temperature was then lowered to 25 °C and the media allowed to equilibrate at the new temperature for 30 minutes. Subsequently, 0.4 mM IPTG was added to induce protein expression. Induction was carried out at 25 °C and 250 rpm for 16-20 hours to allow protein expression to proceed to completion.

For isotopically labeled synaptotagmin domains, the same growth and expression protocol was followed except the LB medium was replaced with M9 minimal medium with $^{13}C_6$-glucose as the sole carbon source and $^{15}NH_4Cl$ as the sole nitrogen source. Each liter of M9 minimal medium consists of 6.8 g Na_2HPO_4, 3.0 g KH_2PO_4, 0.5 g NaCl, 1.0 g $^{15}NH_4Cl$, 2.0 mM $MgSO_4$, 100 µM $CaCl_2$, 2 ml trace elements, and 3.0 g $^{13}C_6$ –glucose. If ^{13}C labeling was not required, 4.0 g of D-glucose was used instead. 100 µg/ml Ampicillin and 100 µl of 0.5% (w/v) thiamine were added immediately prior to incubation at 37 °C.

The cells were centrifuged at 4000 rpm or around 10,000 g for 30 minutes in a swing bucket rotor (Sorvall RC-3C Plus). The SNARE protein cell pellets were suspended in PBS containing 1 mM each of EDTA, EGTA, AEBSF, and Sigma inhibitor cocktail. The suspension was frozen in liquid nitrogen then stored at -80 °C until further purification took place. The SNARE proteins were purified by affinity chromatography similarly to synaptotagmin below, but with PBS instead of Lysis Buffer. The elution from the affinity column was further purified by gel filtration into the same final buffer as synaptotagmin: 25 mM HEPES-NaOH pH 7.4, 125 mM NaCl. The SNARE motifs of synaptobrevin, syntaxin-1 and SNAP-25 were mixed in an equimolar ratio and incubated overnight at 4°C to assemble the SNARE complex. Isolated SNARE motifs that did not incorporate into SNARE complexes were removed by extensive concentration-dilution in a 10 kDa Amicon centrifugal filter. The purity of the final SDS-resistant complex was verified with SDS-PAGE and Coomassie blue staining.

For synatptoagmin C2AB, C2A, and C2B fragments, the cell pellets were resuspended in cold Lysis Buffer (40 mM Tris-HCl pH 8.2, 200 mM NaCl) with 1% (v/v) Triton X-100, 2 mM DTT, and protease inhibitors added (1 mM each of Sigma Inhibitor cocktail, ABESF, EGTA, and EDTA). The suspension was frozen in liquid nitrogen and thawed in RT water bath. The freeze-thaw cycle facilitates breakage of the cell wall. The cells were passed four times through an EmulsiFlex-C5 cell homogenizer (Avestin) at 13,000 psi and centrifuged at 19000 rpm (Sorvall RC 6 Plus Centrifuge) or around 40,000 g for 30 minutes. The supernatant was incubated for one hour at RT with 100 mg pre-dissolved protamine sulfate (Sigma-Aldrich). Since protamine sulfate also precipitates proteins, this step was skipped if the protein expression level is low. But subsequent Benzonase nuclease and cation exchange chromatography steps were performed in order to rid the sample of nucleic-acid contaminants. The mixture was

centrifuged again at 19000 rpm for 30 minutes, and the supernatant was passed through 0.45 µm syringe filter before mixing with prewashed Glutathione Sepharose 4B beads (GE Healthcare) at a ratio of 1 ml of beads slurry per 1 L of initial culture. Incubation was either three hours at RT or overnight at 4°C. The resin was extensively washed with 200 ml each of the following buffers in sequence: Lysis Buffer, Lysis Buffer with 50 mM $CaCl_2$, and Lysis Buffer with 50 mM $CaCl_2$ and 1 M NaCl.

The resin was then equilibrated with Benzonase Buffer (50 mM Tris-HCl, pH 8.0, 2 mM $MgCl_2$, 2 mM DTT) before the addition of 20 ml Benzonase buffer and 5 µl Benzonase Nuclease (Novagen, 25 KUN) and rotation at RT for 2-3 hours. The Benzonase wash was discarded and the resin extensively washed with high ionic strength benzonase buffer at 1 M NaCl. This step was performed to rid the residual nucleic acids bound to the resin and/or protein. The resin was then equilibrated with Thrombin Cleavage buffer (TCB: 50 mM Tris-HCl, pH 8.0, 150 mM NaCl, 2.5 mM $CaCl_2$, 2 mM DTT). Thrombin cleavage was carried out at RT for 3 hrs or 4°C overnight in 10 ml TCB and 0.08 mg/ml thrombin (Sigma-Aldrich). The protein cleaved from the GST tag was eluted. Elution was repeated with TCB until UV $Abs_{280} < 0.1$ to recover the maximal amount of protein from the resin.

For the WT and mutant C2AB and C2A fragments, the elution fractions were combined and diluted with buffer A (50 mM NaAc pH 6.2, 5 mM $CaCl_2$) so that [NaCl] ≤ 100 mM. Cation-exchange on Source S column (GE Life Sciences) was performed in buffer A with a linear gradient from 0.1 to 0.7 M NaCl in 30 column volumes. This was followed by gel filtration on Superdex 75 (25 mM HEPES-NaOH pH 7.4, 125 mM NaCl) and concentration using a 10 kDa centrifugal filter unit (Amicon) for a final protein concentration of 50 - 300 µM.

For the WT and mutant C_2B domain, the elution fractions were concentrated with 2.5 mM EDTA added to chelate the calcium ions in the TCB. This step was performed to avoid calcium phosphate precipitation on the Superdex 75 column in the phosphate-containing gel filtration buffer (0.2 M phosphate, pH 6.3, 0.3 M NaCl). The gel filtration elution was buffer-exchanged using a 10 kDa centrifugal filter unit into 20 mM MES pH 6.3, in order to avoid such precipitation. The protein was then loaded onto SourceS column where cation-exchange was carried out in 20 mM MES, pH 6.3, 20 mM $CaCl_2$ using a linear gradient from 0.1 to 0.6 M NaCl in 40 column volumes. Two distinct peaks always emerged (see Figure 9), and both represent proteins of the correct molecular weight. However, only the latter peak was devoid of nucleic acid contaminants. It was collected and buffer exchanged into the same final buffer as the other proteins: 25 mM HEPES-NaOH pH 7.4, 125 mM NaCl. Finally, 0.5 mM TCEP and 1 mM ABESF were added to all the purified proteins, but EDTA and EDTA-containing inhibitor cocktails were avoided. Proper folding of the synaptotagmin-1 C2AB and C2B fragment mutants was confirmed through ^{1}H-^{15}N TROSY-HSQC spectra.

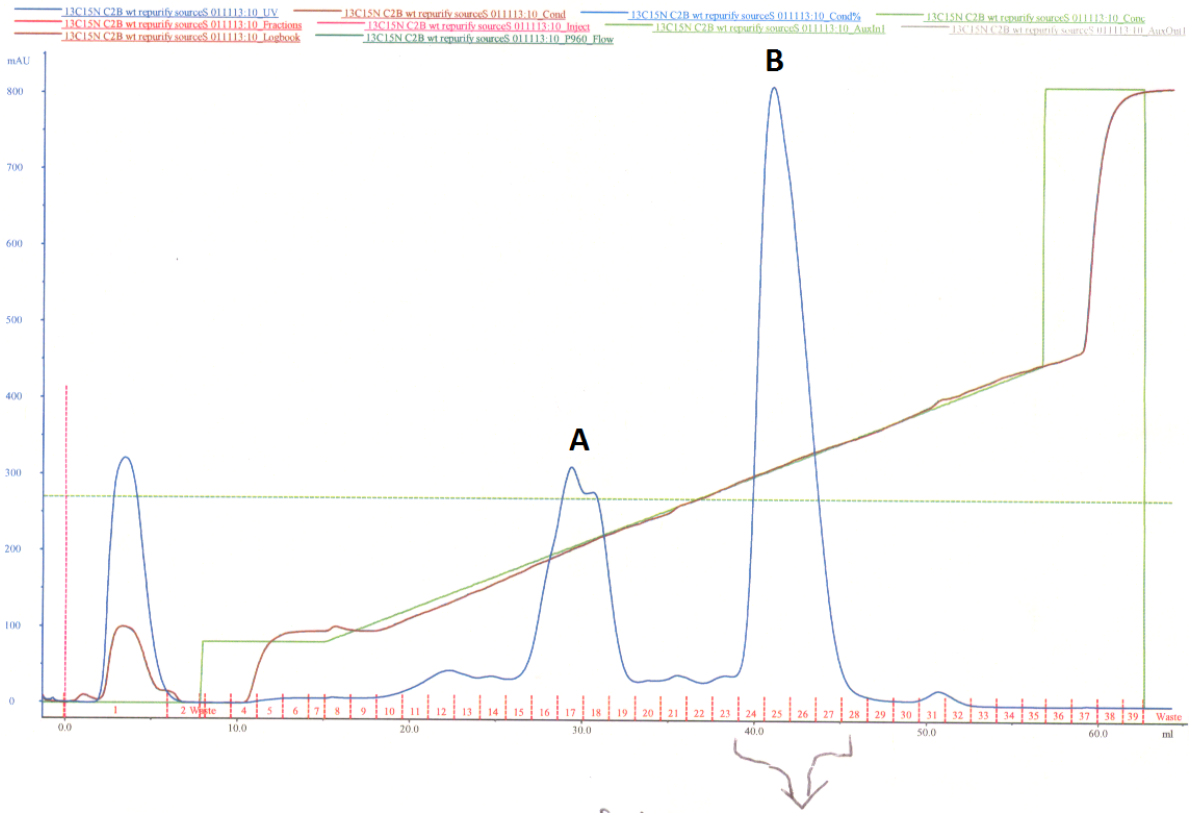

Figure 9. The final step in the purification of the synaptotagmin-1 C2B domain. Cation exchange source S column is used to separate the pure sample from acidic contaminants. The pure sample is represented by peak B and elutes later at higher ionic strength than peak A.

2.2.2 NMR spectroscopy

All NMR spectra were acquired at 25°C on Varian INOVA 500 MHz or 600 MHz spectrometers. Samples were prepared in 25 mM HEPES and 125 mM NaCl at pH 7.4 with 5% D_2O. Standard conditions included 1 mM Ca^{2+} unless otherwise indicated. For Ca^{2+}-free samples, 1 mM EDTA was added.

1D ^{13}C-edited ^{1}H spectra were obtained by acquiring the first trace of a ^{1}H-^{13}C heteronuclear single quantum coherence spectrum (HSQC) as described before (Arac et al. 2003). The 1D mode allows for high sensitivity even at low micromolar protein concentrations because the ^{1}H signals are not dispersed into a second dimension. Total acquisition times were 20-40 minutes for spectra acquired on cold probes and 1 hour for spectra acquired on room temperature probes. Spectra were analyzed with the VnmrJ software (Agilent Technologies Inc., Santa Clara, CA).

The overall broadening caused by binding of the unlabeled SNARE complex should in principle extend to most of the cross-peaks from the labeled synaptotagmin. However, cross-peaks from flexible regions may remain largely unaffected if they are not involved in binding, because internal motions lead to very sharp resonances for flexible regions regardless of the molecular size (Rizo et al. 2012). An example of this notion was shown in the ^{1}H-^{15}N HSQC spectrum of the synaptic SNARE protein synaptobrevin, where its 116 residues were reconstituted into 100 nm lipid vesicles (Brewer et al. 2011). Even though the effective molecular weight of the vesicles is in the 100-MDa range, the HSQC cross-peaks of residues 1–74 were still observable with high sensitivity even at 9 μM protein concentration because these residues remain flexible.

2.2.3 Titrations with the SNARE complex

Samples contained a constant concentration of 3 μM uniformly ^{13}C-labeled C2AB or C2B and the indicated concentrations of unlabeled SNARE complex. A new sample was prepared for each titration point, rather than adding SNARE complex to the same sample. The 1% natural abundance of ^{13}C isotope in the unlabeled SNARE complex was accounted for as follows: I acquired the ^{13}C-edited 1D spectrum of a 20 μM unlabeled SNARE complex sample. This spectrum was subtracted from each titration point spectrum, by a fraction equal to the particular [SNARE] in that sample divided by 20 μM. Assuming a 1:1 equilibrium-binding model, where the synaptotagmin C2AB or C2B is considered as the protein P_T and the SNARE complex as the ligand L_T, the strongest methyl resonance (SMR) intensity I after the natural abundance correction can be expressed as a function of the total SNARE complex concentration L_T, by equation (1):

$$I = I_f + \frac{(I_b - I_f)(P_T + L_T + K_d - \sqrt{(P_T + L_T + K_d)^2 - 4P_T L_T})}{2P_T} \quad (1)$$

where I_f represents the SMR intensity of the free, unbound ^{13}C-labeled protein, I_b is the SMR intensity of the labeled protein bound to the SNARE complex, and K_d is the dissociation constant. The experimental data were fit to this equation using Sigma Plot (Systat Software Inc.) to extract the optimal I_f, I_b and K_d values. After an initial fit, the optimal value of I_f was used to normalize all the intensities, which allows comparison between data sets obtained at different times and on different instruments. Hence, the value of I_f after normalization is equal to 1 and the I_b values are expressed as a fraction of I_f. The values of I_b and K_d described below and their errors

were obtained by fitting 3-4 separate data sets and then calculating the average and standard deviations of the values obtained.

2.2.4 Synaptotagmin-1 fragment/SNARE complex precipitation assays

Samples containing 10 μM WT or mutant synaptotagmin-1 C2AB fragment or C2B domain were mixed with 10 or 20 μM SNARE complex under the same conditions as the NMR experiments: 25 mM HEPES-NaOH, 125 mM NaCl, 1 mM Ca^{2+}, pH 7.4. The total reaction volume was 50 μl. After 5 minutes incubation at room temperature, the samples were centrifuged at 13,000 rpm for 1.5 minutes in a benchtop centrifuge (Eppendorf AG 5415 D), and the supernatant was separated from the pellet. The pellet was resuspended in 50 μl buffer, and 5 μl of each of the supernatant and pellet fractions were analyzed by SDS-PAGE using 15% (w/v) polyacrylamide gels in Tris-Glycine-SDS running buffer, followed by Coomassie blue staining.

2.3 Results

2.3.1 2D NMR spectroscopy confirms the purity and proper folding of the WT and mutant synaptotagmin-1 fragments

Although ^{15}N-labeling is not necessary for the 1D NMR binding assay, I used uniformly ^{15}N,^{13}C-labeled Syt1 fragments in order to record ^{1}H-^{15}N HSQC and TROSY-HSQC spectra. As shown in

Figure 10, the C2B domain mutants display well-dispersed peaks similar to the WT, with only a few chemical shift differences. This indicates that the mutations perturbed the local chemical environments for some residues, but did not induce overall structural changes in the protein. Any difference observed in the 1D NMR binding assays would therefore be specific to

the residue changes, and not a consequence of large structural perturbations that would drastically alter the synaptotagmin-1/SNARE complex interaction. Similar results were obtained with the C2AB fragment mutants (data not shown).

A.

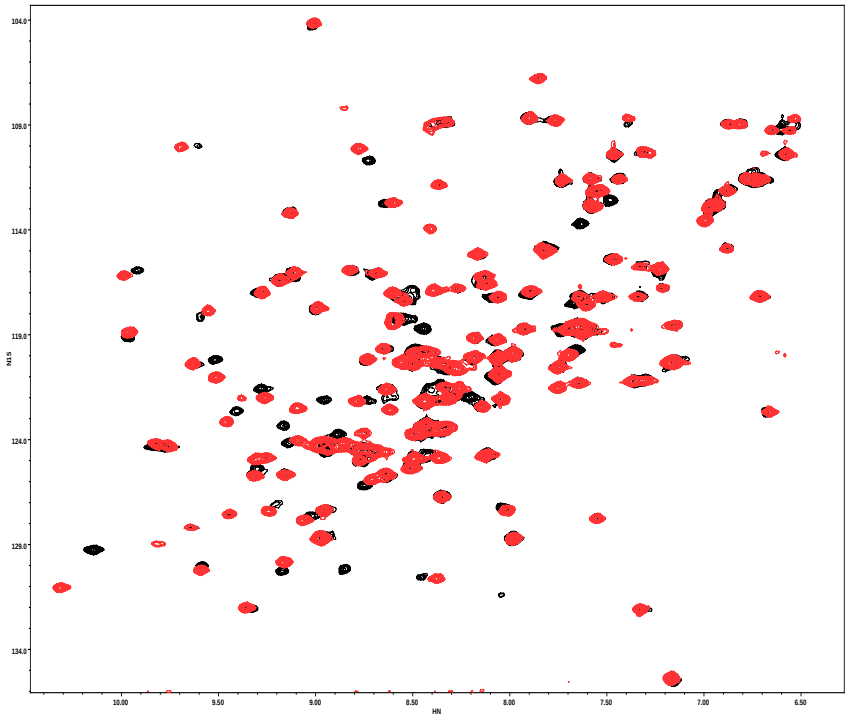
104.0
109.0
114.0
119.0
124.0
129.0
134.0
N15
10.00
9.50
9.00
8.50
8.00
7.50
7.00
6.50
HN

B.

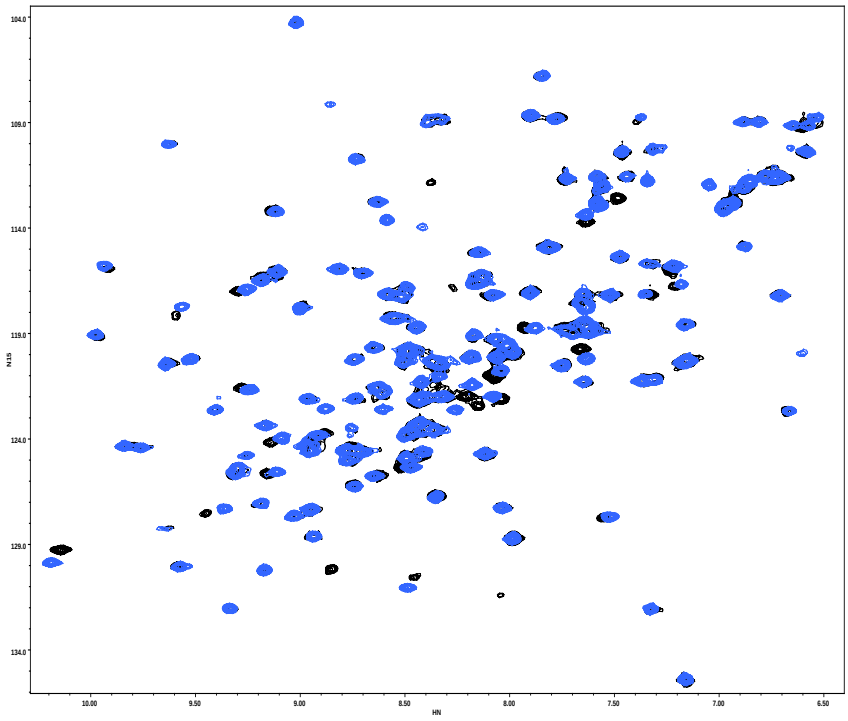
104.0
109.0
114.0
119.0
124.0
129.0
134.0
N15
10.00
9.50
9.00
8.50
8.00
7.50
7.00
6.50
HN

Figure 10. ^{1}H-^{15}N HSQC of uniformly ^{15}N,^{13}C-labeled synaptotagmin-1 C2B domain. **A.** The C2B KK mutant (red) is overlaid with C2B WT (black). **B.** The C2B RR mutant (blue) is overlaid with the C2B WT (black).

The presence of nucleic acid contaminants is a concern for synaptotagmin-1 fragments, which carry an overall positive charge at pH 7.4. As an illustration, Figure 11 contrasts the impure and pure C2B domain. The impure sample was not subject to the final cation exchange step (see section 2.2.1), and exhibited multiplicity for some of the residue cross-peaks. This is despite it not displaying significant UV absorbance at 260 nm, which would be characteristic of nucleic acid contamination. The cross-peak multiplicity shows that some contaminants remain bound to the polybasic region (Ubach et al. 2001). The pure sample gives a single set of cross-peaks in the HSQC spectra, which is the optimal detection method to date in the lab to ensure such sample purity.

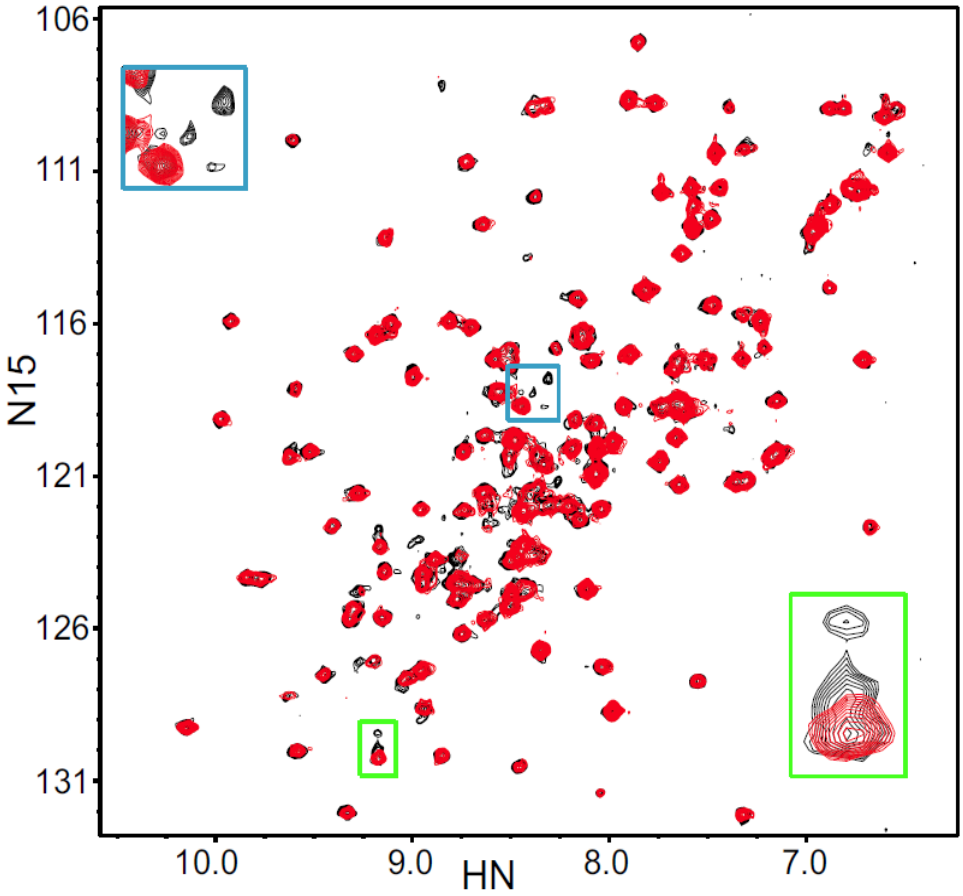

Figure 11. ^{1}H-^{15}N HSQC spectra of WT synaptotagmin-1 C2B domain that was fully purified (red) or that was purified without the final cation exchange chromatography (black). The insets are expansions of cross-peaks that are unique for the purified C2B domain but exhibit multiplicity in the impure C2B domain.

2.3.2 Determination of protein concentrations for binding assay

At physiological pH and 1 mM Ca^{2+}, neither the C2AB fragment nor the SNARE complex alone precipitated at up to 200 µM. In the absence of Ca^{2+}, the addition of C2AB to the SNARE complex did not cause visible precipitation at up to 100 µM. When all three factors - 1 mM Ca^{2+}, C2AB, and SNARE – were present, however, visible cloudiness of the solution was observed when both protein concentrations were above approximately 10 µM, indicating precipitation of the sample. This could be avoided if the concentration of either C2AB or the SNARE complex was kept at ~4 µM or below. The ^{13}C-labeled synaptotagmin-1 fragments were thus kept at 3 µM in all the 1D NMR assays, while the concentration of the SNARE complex incresed from 0 to 40 µM.

2.3.3 General observations from the 1D binding assay

As introduced in section 2.2.3, the assay measures the intensity of the SMR in 1D ^{13}C-edited proton NMR spectra. It follows the signal of the ^{13}C-labeled synaptotagmin fragment, and quantifies the decrease in intensity upon binding to the unlabeled SNARE complex. Binding results in the formation of a larger molecular weight complex, thereby slowing down its tumbling rate in solution. This in turn increases the transverse relaxation rate of the sample which leads to resonance broadening and manifests as a decrease in the signal intensity of the peak (Figure 12A). Because the SNARE complex is a long rigid helical bundle with a larger hydrodynamic radius than the C2AB fragment, it was chosen to be the unlabeled ligand that is added to the labeled C2AB at increasing concentrations. The reverse experiment of labeling the SNARE complex works as well (Arac et al. 2003), but the procedure as described gave sufficient dynamic range for quantification of the interaction.

This method provides high sensitivity even at 3 μM synaptotagmin concentration, because the methyl signals are not spread in additional dimensions as in multidimensional NMR experiments. Since synaptotagmin-1/SNARE complex interactions are highly sensitive to the ionic strength (Tang et al. 2006), all experiments described in this study were performed with a constant ionic strength that resembles physiological conditions.

Figure 12B shows the theoretical, simulated titration data based on equation 1. The simulation was carried out for two different affinities, holding the I_f and I_b constant at 1.0 and 0.4 respectively. With increasing concentrations of SNARE complex, the SMR signal of the labeled synaptotagmin fragment is expected to decrease. This decrease becomes more dramatic with tighter affinity, or lower K_d value.

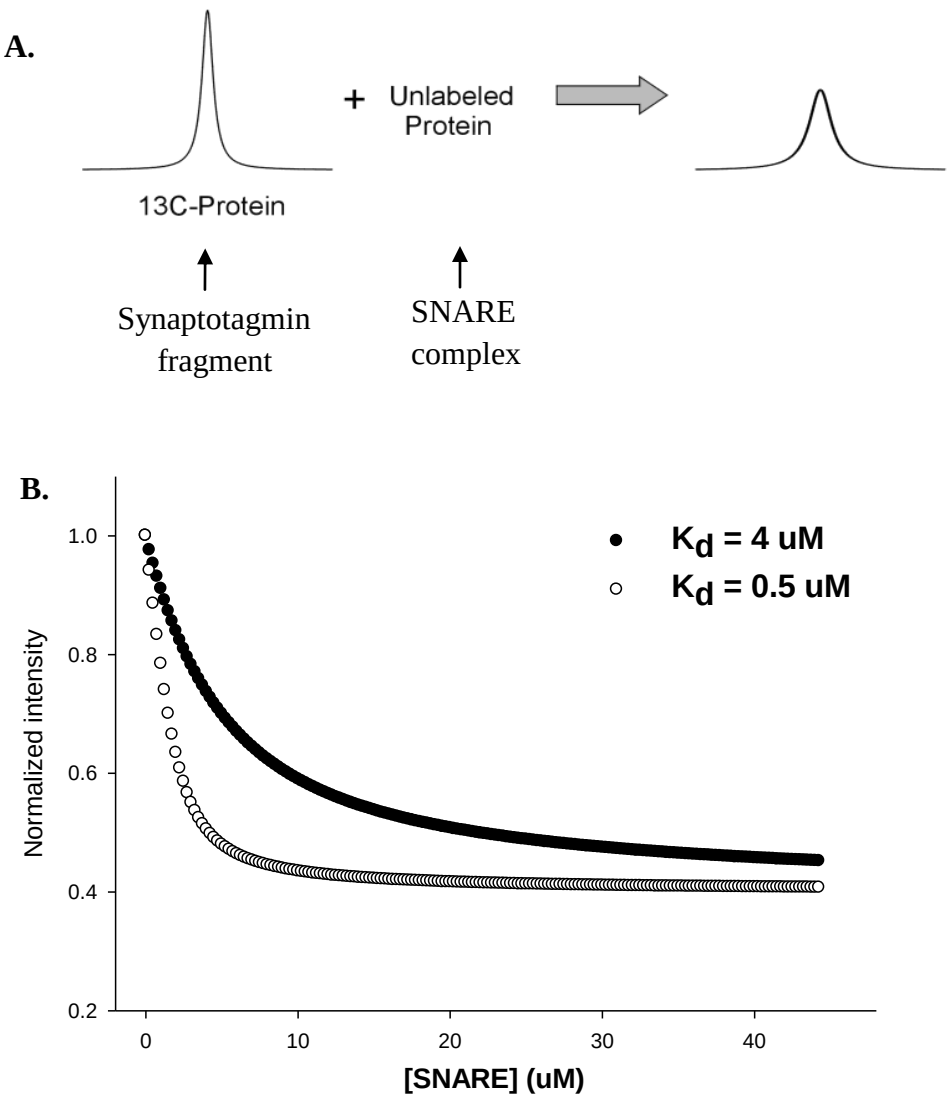

Figure 12. Principles of the binding assay. A. The SMR signal of the ^{13}C-labeled synaptotagmin-1 C2AB fragment decreases upon binding to the unlabeled SNARE complex. Binding results in the formation of a larger molecular weight complex, thereby slowing down its tumbling rate in solution. This in turn increases the transverse relaxation rate of the sample which leads to resonance broadening and manifests as a decrease in the signal intensity. **B.** Simulation of equation 1 for two different K_d values. I_b is fixed at 0.4. Tighter affinity leads to greater decrease in signal as a function of SNARE complex concentration.

2.3.4 Calcium enhances synaptotagmin-1/SNARE complex binding

When 3.5 μM SNARE complex was added to 3 μM labeled C2AB, there was a small decrease in the SMR intensity under the Ca^{2+}-free condition of 1 mM EDTA, indicating weak binding. A much larger decrease was observed when the same experiment was performed in the presence of 1 mM Ca^{2+} (Figure 13A). Since Ca^{2+} itself did not affect the SMR intensity, these results showed that, as expected, Ca^{2+} strongly enhances binding of C2AB to the SNARE complex.

Subsequently, Ca^{2+} titration was performed at the constant protein concentrations of 3.5 μM SNARE complex and 3 μM labeled C2AB. It revealed a progressive decrease in SMR intensity as a function of increasing [Ca^{2+}], saturating at about 300 μM Ca^{2+}. Figure 13C shows a sample calcium titration. Fitting three such independent titrations to a Hill equation yielded an average of 58 ± 8 μM for the microscopic dissociation constant, and a Hill coefficient of 1.2 ± 0.3. These results suggest there is almost no cooperativity among the C2 domain Ca^{2+} binding sites in enhancing SNARE complex binding. If the SNARE complex itself does not directly coordinate the Ca^{2+} ions, this is an expected result because there is no cooperativity among the five intrinsic Ca^{2+} binding sites of synaptotagmin-1 (Ubach et al. 1998; Fernandez et al. 2001).

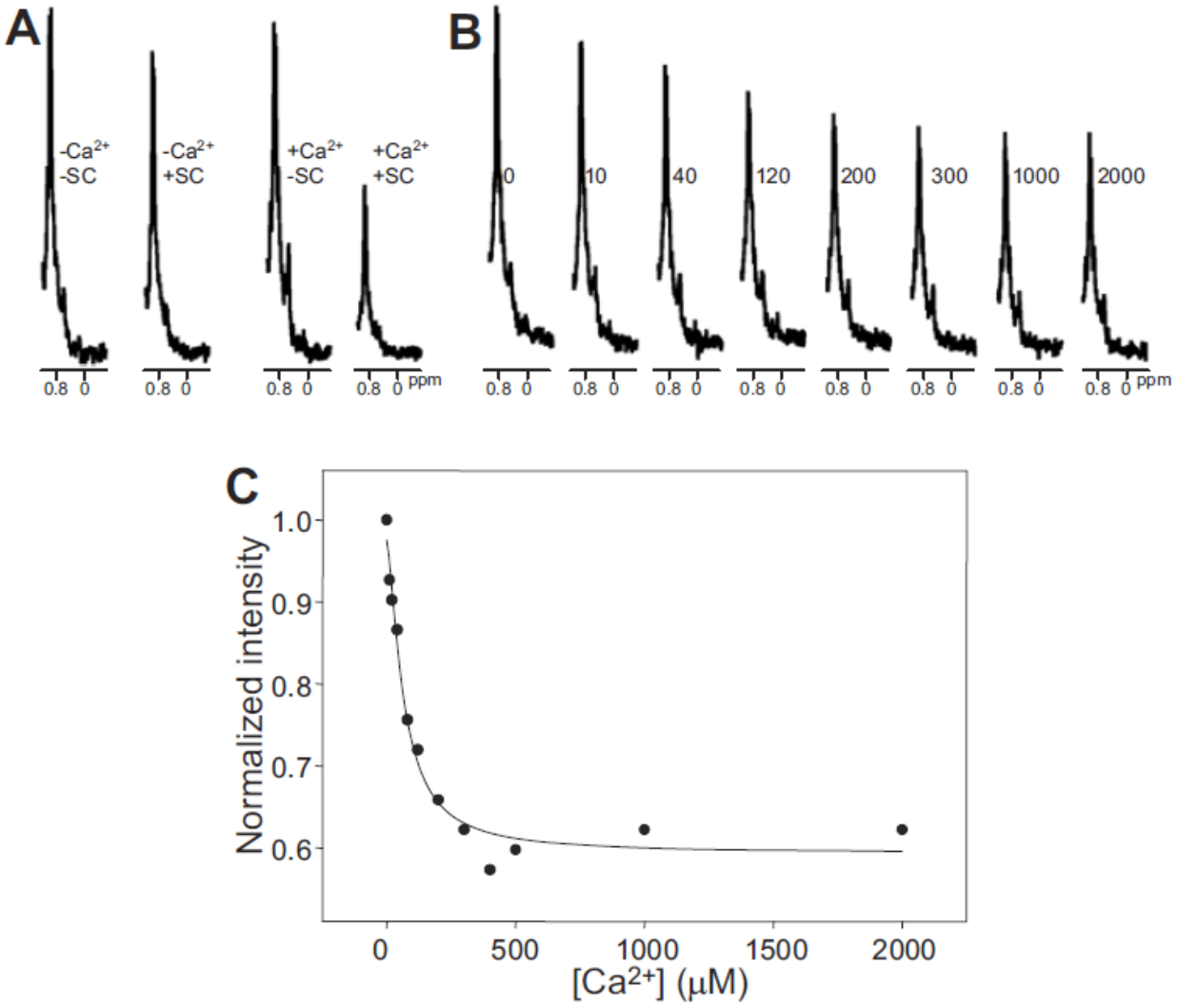

Figure 13. Calcium enhances the synaptotagmin-SNARE complex interaction. A. The SMR region of 1D ^{13}C-edited ^{1}H-NMR spectra of 3 µM ^{13}C-labeled C2AB fragment in the presence of 1 mM EDTA (-Ca^{2+}) or 1 mM Ca^{2+} (+Ca^{2+}), and without (-SC) or with (+SC) 3.5 µM SNARE complex. **B.** Analogous spectra of 3 µM labeled C2AB with 3.5 µM SNARE complex and the indicated concentrations of Ca^{2+} in µM. **C.** Plot of the normalized SMR intensities of a calcium titration. A subset of the raw data corresponding to this titration is shown in panel B. The curve shows the fit to a Hill equation.

The observed microscopic dissociation constant is primarily mediated by the C2B domain because the SNARE complex interaction is mostly due to C2B (see section 2.3.6). The apparent EC_{50} of 58 ± 8 μM is considerably lower than the intrinsic dissociation constants of the individual Ca^{2+} binding sites of the C2B domain which are 300-600 μM (Fernandez et al. 2001). This would imply some cooperativity between Ca^{2+} binding and SNARE binding to synaptotagmin. Such cooperativity may arise from long-range electrostatic interactions, as the SNARE complex is strongly negatively charged (Sutton et al. 1998) and Ca^{2+} increases the positive charge of the C2 domains (Shao et al. 1997; Fernandez et al. 2001).

The experiment was also repeated for different SNARE complex concentrations at a constant C2AB concentration of 3 μM. The difference between the 1 mM EDTA and 1 mM Ca^{2+} conditions indicate that the effect of calcium holds for all SNARE complex concentrations sampled (Figure 14).

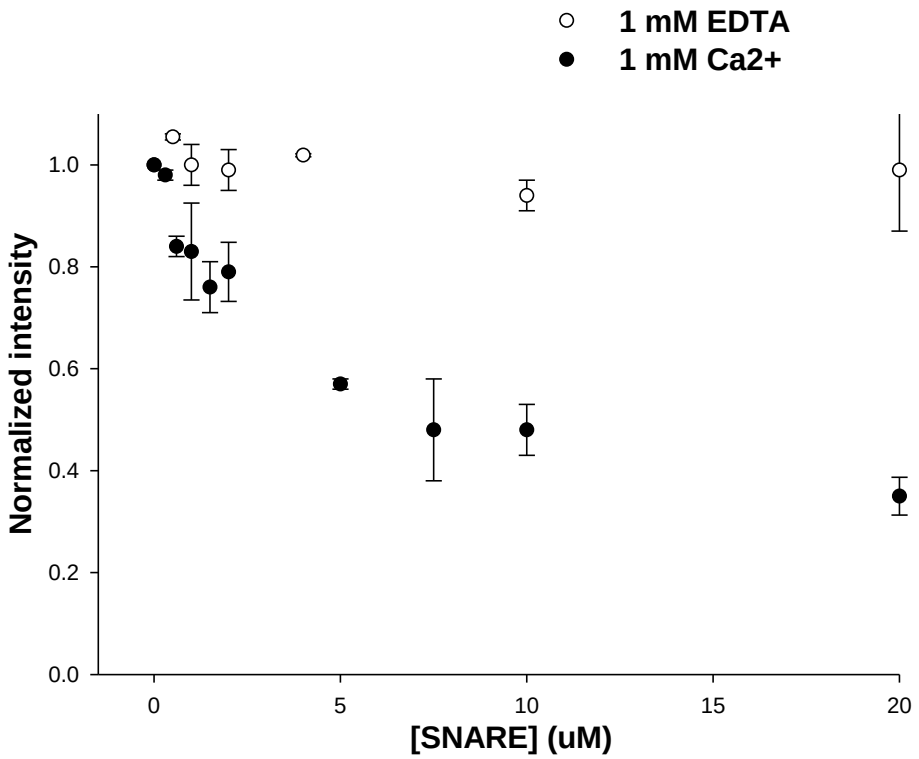

Figure 14. Calcium enhances synaptotagmin-SNARE complex binding at all SNARE complex concentrations. 1D NMR binding assay of 3 μM labeled synaptotagmin-1 C2AB fragment with increasing concentrations of the SNARE complex. The conditions were either 1 mM EDTA (open circles) or 1 mM Ca^{2+} (closed circles). Each data point represents the average of three trials, error bars represent the standard deviations.

2.3.5 Mutational analysis of the C2AB-SNARE complex interactions

To quantify the C2AB-SNARE complex affinity, I carried out titrations of ^{13}C-labeled C2AB with increasing concentrations of unlabeled SNARE complex. In the presence of 1 mM EDTA, the spectra showed only modest decreases in the SMR intensity far from saturation even at 20 μM SNARE complex. However, 1 mM Ca^{2+} instead of EDTA led to much stronger decreases in SMR intensity that appeared to be saturable (Figure 14 and Figure 16A). All the data were normalized to the intensity at zero SNARE complex concentration to allow for standardized comparison between samples on different days and different instruments. In order to do this, I first fitted each data set using the raw absolute intensities. The I_f from the fit was then used to normalize the data. Curve fitting of multiple titrations assuming a protein-ligand binding model of 1:1 stoichiometry yielded an apparent K_d of 2.32 ± 0.15 μM. See equation 1 and table 1.

Next, I sought to quantify the effects of mutations on the binding. The three mutations chosen (Figure 15) had previously been described to impair binding based on other analytical methods, but sometimes with contradictory results.

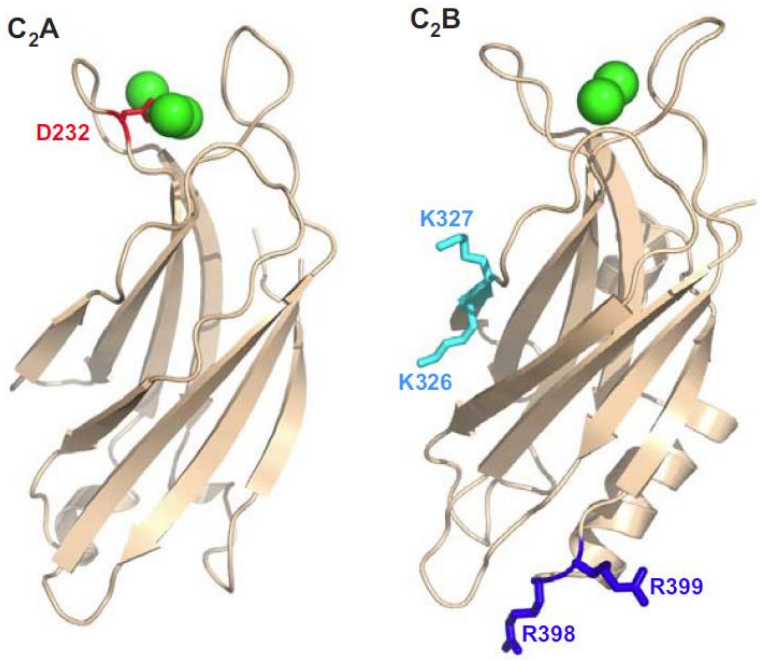

Figure 15. Ribbon diagrams of the synaptotagmin-1 C2A and C2B domains. Ca^{2+} ions are shown as green spheres. The side chains that were mutated are represented by stick models and labeled. D232 also referred to as DN, K326/K327 as KK, and R398Q/R399Q as RR.

The D232N, or DN mutation, abolishes Ca^{2+} binding at two of the three Ca^{2+} binding sites in the C2A domain (Ubach et al. 1998) and was described to paradoxically enhance neurotransmitter release as well as SNARE complex binding (Pang et al. 2006). R398Q/R399Q, or the RR mutation, is at the bottom of the C2B domain. It abolishes neurotransmitter release (Xue et al. 2008) and was reported to impair SNARE binding in one study (Gaffaney et al. 2008) but not in another (Xue, Ma et al. 2008). K326A/K327A, or the KK mutation, is in the polybasic region of C2B and impairs neurotransmitter release (Mackler and Reist 2001; Li et al. 2006). It was also found to decrease binding to the SNARE complex (Rickman et al. 2006; Dai et al. 2007) and to phosphatidylinositol phosphates (Bai et al. 2004; Li et al. 2006). Titrations of these labeled C2AB mutants with unlabeled SNARE complex (Figure 16) yielded the following apparent K_d values: 0.7 ± 0.3 μM for the DN mutant, 0.94 ± 0.01 μM for the RR mutant, and 3.7 ± 1.3 μM for the KK mutant (Table 1).

These results seem to suggest that the DN and RR mutations increase the affinity of C2AB for the SNARE complex, while the KK mutation decreases the affinity. However, comparison of the fitting curves between WT, DN and RR (Figure 16) shows that they are indistinguishable at SNARE complex concentrations below 5 μM, and diverged at higher concentrations. Hence, the differences in K_d is a result of differences in the fitted parameter I_b, which is the normalized signal intensity extrapolated at infinite SNARE complex concentration. The I_b values obtained were 0.29 ± 0.07 for the WT, 0.44 ± 0.01 for the DN mutant, and 0.48 ± 0.03 for the RR mutant (Table 1). Assuming 1:1 binding, which is the basis for equation 1, I_b is not expected to be altered by the mutations because it corresponds to the C2AB fragment fully bound to the SNARE complex.

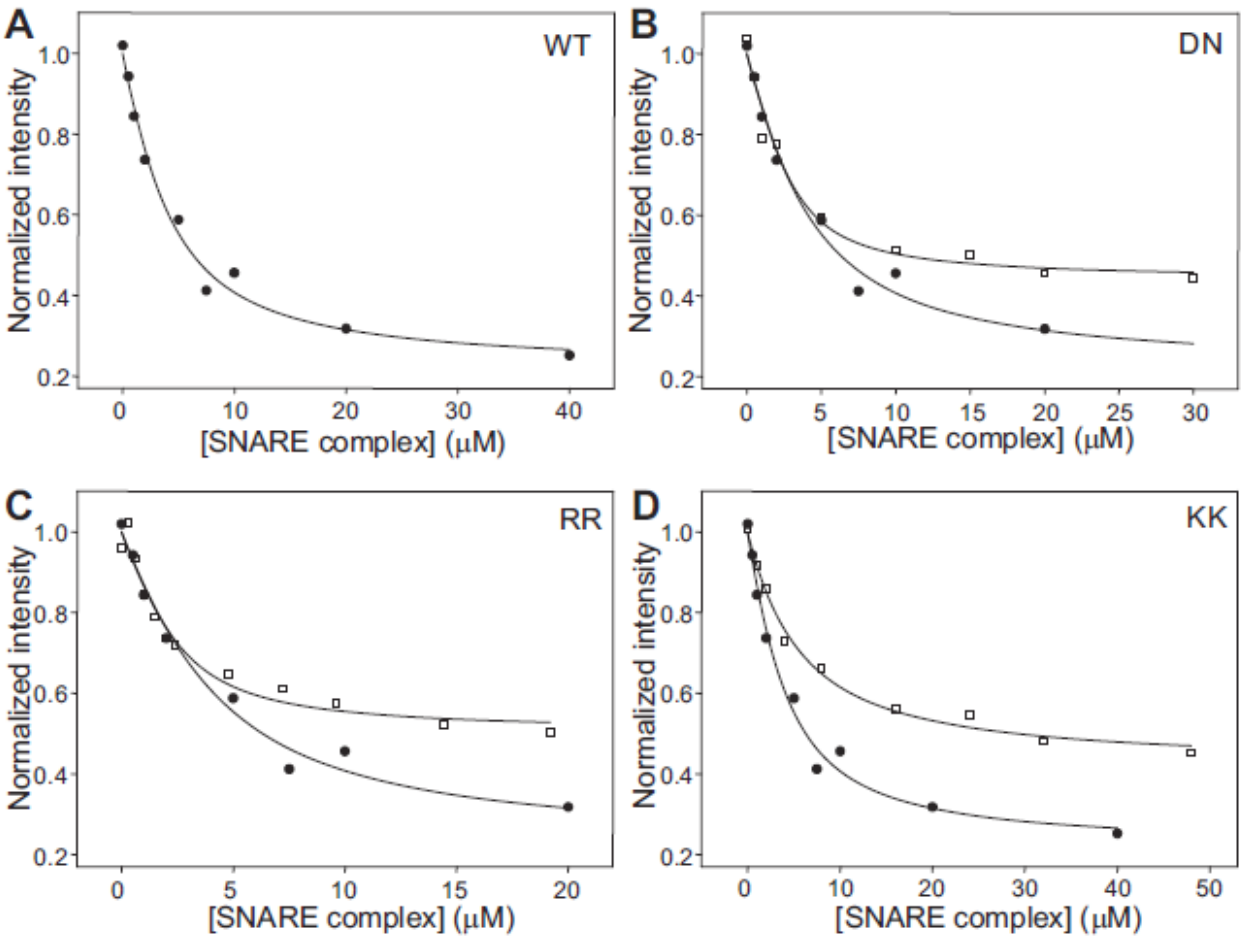

Figure 16. Sample titrations of 3 μM WT and mutant labeled C2AB with SNARE complex at 1 mM Ca^{2+}, monitored by 1D ^{13}C-edited proton NMR. **A.** Plot of the SMR intensities of WT as a function of unlabeled SNARE complex. This represents one of the three titrations summarized in Figure 14. **B-D.** Plots for analogous titrations performed with DN (**B**), RR (**C**) and KK (**D**) mutant C2AB fragments (open squares), superimposed with the WT plot (closed circles; same as (**A**). The curves show the fits of the data obtained with equation (1). The results of the fit reported in the text and table 1 are from 3-4 such titrations per mutant.

Table 1. Summary of the apparent K_d and I_b values from fitting the SNARE complex/synaptotagmin-1 fragment binding curves (Figure 16 and Figure 19).

	C2AB WT	C2AB DN	C2AB RR	C2AB KK
K_d (μM)	2.32 ± 0.15	0.7 ± 0.3	0.94 ± 0.01	3.7 ± 1.3
I_b	0.29 ± 0.07	0.44 ± 0.01	0.48 ± 0.03	0.34 ± 0.07
	C2B WT	C2B RR	C2B KK	
K_d (μM)	0.8 ± 0.2	0.4 ± 0.3	3.5 ± 0.7	
I_b	0.17 ± 0.05	0.51 ± 0.04	-0.03 ± 0.09	

These observations suggest that the intensities at low SNARE concentrations for the WT, DN and RR mutants reflect a primary, high affinity-binding mode that is not significantly affected by these two mutations. In addition, there appears to be one or more additional binding mode that is populated at higher SNARE complex concentrations and is impaired by the DN and RR mutations.

The 1D spectra in Figure 17 reveal further details: the SMR of most proteins is observed at ca. 0.8 ppm and includes resonances from highly mobile methyl groups, as well as structured methyl groups that have chemical shifts at 0.8 ppm. In the structured regions, most of the other methyl groups are observed at smaller chemical shifts, between 0.4 and 0.6 ppm. Because the molecular weights of the C2AB fragment and the SNARE complex are 35 and 32 kDa respectively, and because the SNARE complex is very elongated, formation of a 1:1 complex is expected to noticeably broaden the resonances from methyl groups in structured regions. Meanwhile, internal motions lead to sharp resonances for flexible regions regardless of the molecular size (Rizo et al. 2012). The resonances at 0.8 ppm from mobile methyl groups would therefore persist upon binding. In addition, based on the lab's experience in NMR analyses of the SNARE complex (Chen et al. 2002; Chen et al. 2005; Dai et al. 2007), resonances of methyl groups in structured regions, between 0.4 and 0.6 ppm, should still be detectable upon binding of labeled C2AB to the SNARE complex in 1:1 stoichiometry. This is indeed what was observed for the C2AB RR mutant at saturating SNARE complex concentration of 20 μM (Figure 17B), suggesting that the spectrum reflects 1:1 binding. Note that at 20 μM, the 1% natural abundance of ^{13}C in the unlabeled SNARE complex provides sufficient signal for detection. On the other hand, for the WT C2AB, there are no detectable resonances between 0.4 and 0.6 ppm under the

same condition of 20 µM SNARE complex. Only the sharp signal at the SMR position of 0.08 ppm is observed (Figure 17A).

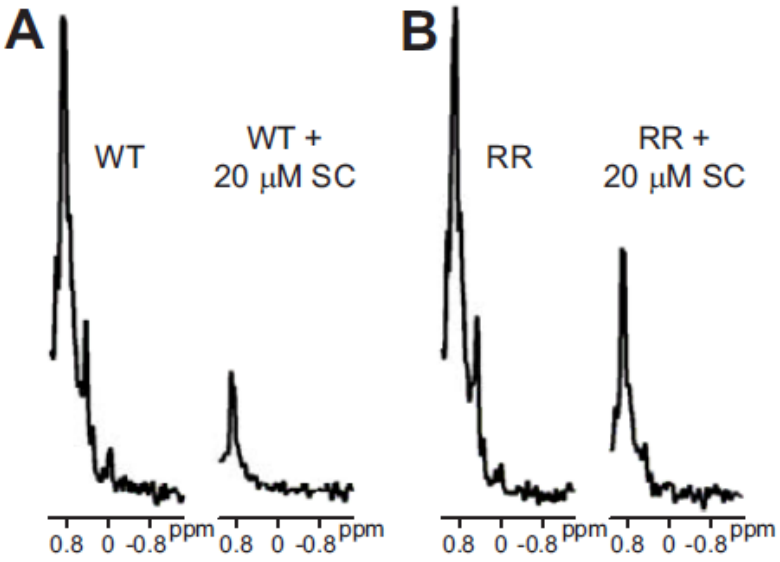

Figure 17. Expansions showing the methyl region of 1D ^{13}C-edited ^{1}H-NMR spectra of 3 µM WT and RR mutant C2AB, in the absence or presence of 20 µM SNARE complex (SC). **A.** WT does not display detectable resonances in the 0.4-0.6 ppm region in the presence of 20 µM SC. **B.** RR mutant with visible resonance signal in the 0.4-0.6 ppm region in the presence of 20 µM SC.

These observations imply that the additional binding mode(s) for WT C2AB at high SNARE complex concentrations involve the formation of larger complexes. The residual signal observed at 0.08 ppm under these conditions corresponds to the highly mobile methyl groups that are observable regardless of the molecular weight.

The interpretation is further supported by the tendency of the WT C2AB fragment to precipitate with the SNARE complex when both concentrations are in the 10 μM range (sections 2.3.2 and 2.3.7). Hence, the apparent K_d measured from the WT titration is not reliable, and the corresponding I_b does not correspond to 1:1 binding stoichiometry. Because the RR mutation disrupts, at least in part, the formation of larger complexes, the K_d measured for the RR mutant of 0.94 μM may be a better estimate of the dissociation constant for the primary C2AB/SNARE complex binding mode. 1:1 binding likely leads to an I_b value equal to or larger than the 0.48 measured for the RR mutant. Similar conclusions can be drawn for the DN mutant, although it appears to be less efficient at disrupting formation of large complexes than the RR mutation, as described in section 2.3.7.

The I_b value obtained from the KK mutant titrations was 0.34 ± 0.07. Although this is not statistically different from the WT I_b of 0.29 ± 0.07, it does not rule out the possibility that the mutation perturbed some secondary binding mode(s). More importantly, the higher K_d of the KK mutant (3.7 ± 1.3 μM) cannot arise from differences in I_b because, all else being equal, a higher I_b would yield a tighter affinity and therefore lower K_d. Moreover, the KK titration curves exhibited clear divergence from the WT even at low SNARE complex concentrations (Figure 16D). Hence, the KK mutation impairs the primary binding mode between the synaptotagmin-1 C2AB fragment and the SNARE complex. Admittedly, the presence of higher order binding

mode(s) pose complications to the data analysis: they hinder the measurement of reliable K_d and the quantification of mutational effects on the primary binding mode.

2.3.6 Contributions of the two synaptotagmin-1 C2 domains to SNARE complex binding

The previous section suggests the primary site for SNARE binding is located at or near the K326/K327 polybasic region of the synaptotagmin C2B domain. There are limitations to the data analysis possibly due to some higher-order, non-primary interactions between the proteins. To further dissect this, I wanted to see whether working with the WT and mutant versions of the C2B domain alone would yield clearer data.

In order to gauge whether SNARE complex binding to the C2B domain alone would be of functional significance, it was first of all important to quantify the relative contributions of the two C2 domains to binding. I performed SNARE titrations with isolated ^{15}N,^{13}C-labeled C2A and C2B domains (Figure 18). The SNARE-C2B domain gives an apparent affinity of K_d = 0.8 ± 0.4 μM (Table 1).

Titrations of the C2A domain with the SNARE complex revealed a gradual decrease in intensity. Because the overall SMR intensity change was small, it is unclear whether saturation was indeed reached. Fitting of the data suggested an apparent K_d ~ 2 μM, but this is not meaningful given the uncertainty in saturation. The small intensity decrease suggests there is a loose binding mode that results in only limited immobilization of the C2A domain. The region of contact on the C2A domain may be in a Ca^{2+} binding loop (Lynch et al. 2007). In contrast, the much stronger decrease observed for the C2B domain suggests the formation of a macromolecular assembly with a more extensive binding surface and considerable immobilization of the C2B domain. This conclusion agrees with extensive evidence that

synaptotagmin-1 binds to the SNARE complex primarily through the C2B domain (Rickman et al. 2004; Bowen et al. 2005; Dai et al. 2007; Choi et al. 2010).

The C2B domain signal decreases more than the C2AB fragment's because the former is of smaller molecular weight and hydrodynamic radius. SNARE complex binding to C2B would therefore induce a larger fractional drop in signal.

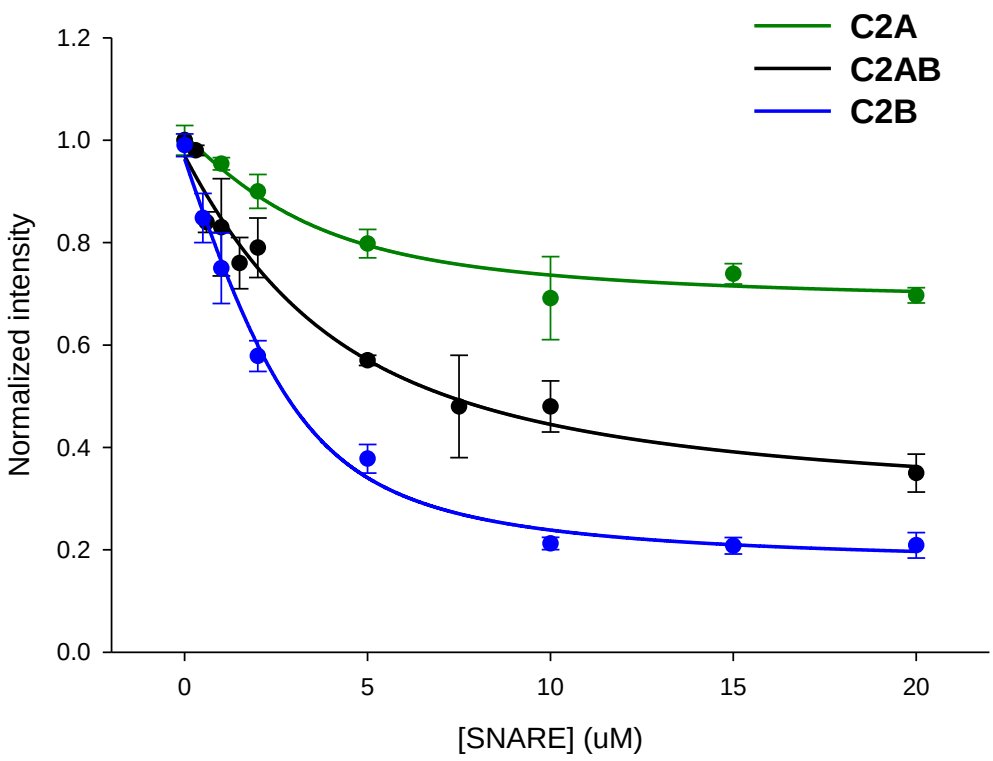

Figure 18. The C2AB-SNARE complex interaction is primarily mediated by the C2B domain. SMR intensities observed in the 1D spectra of 3 µM synaptotagmin-1 C2A domain (green), C2B domain (blue) and C2AB fragment (black) as a function of unlabeled SNARE complex concentration in the presence of 1 mM Ca^{2+}. The C2AB data is the same as presented in Figure 14. The C2B domain signal decreases more than the C2AB fragment's because the former is of smaller molecular weight and hydrodynamic radius. SNARE complex binding to C2B would therefore cause a larger fractional drop in signal. Data points represent the average from 3-4 titration series, and the error bars are the standard deviations. Curve fitting was done using equation 1.

2.3.7 The KK mutation impairs the primary binding mode and the RR mutation impairs aggregation of the synaptotagmin-SNARE complex assemblies

To investigate whether the polybasic lateral side and/or the double-arginine bottom region of C2B mediate binding to the SNARE complex, I performed SNARE titrations with the labeled C2B domain KK and RR mutants (Figure 19). The results were similar to the mutational effects in the C2AB fragment.

C2B RR yielded an apparent K_d of 0.4 ± 0.3 μM (Table 1) that was slightly lower than C2AB WT, but there is considerable uncertainty in the mutant K_d because of the intrinsic limitation of measuring K_d values below 1 μM given the protein concentrations used in this assay. Nevertheless, there are other similarities of the C2B RR to the C2AB RR results: it saturated at substantially higher I_b value (0.51 ± 0.04) than for C2B WT (0.17 ± 0.05). Moreover, comparison of the spectra acquired in the presence of 20 μM SNARE complex again showed the resonances from methyl groups in structured regions (e.g. between 0.4 and 0.6 ppm) remained observable for C2B RR but not for C2B WT (Figure 20). Therefore, it can be concluded that the higher SNARE complex concentrations lead to the formation of large complexes for the WT C2B domain, but such oligomerization is hindered by the RR mutation, leading to a 1:1 SNARE complex/C2B domain assembly.

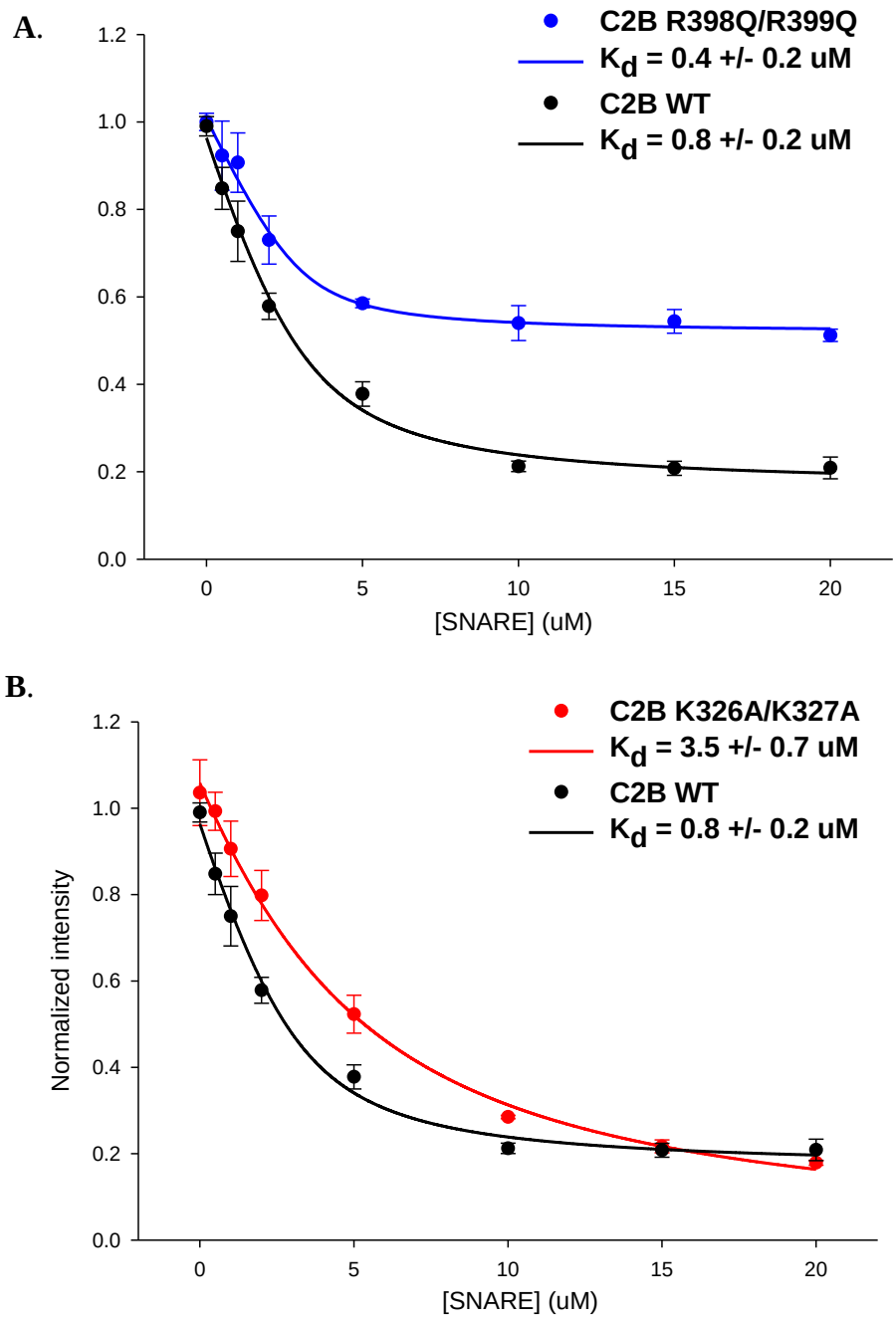

Figure 19. Titrations of WT and mutant ^{13}C-C2B domain with SNARE complex, monitored by 1D ^{13}C-edited ^{1}H-NMR spectra. Plot of the SMR intensities observed for 3 µM RR **(A)** and KK **(B)** mutant C2B domain as a function of unlabeled SNARE complex concentration in the presence of 1 mM Ca^{2+}, superimposed with WT C2B domain (black). Data points represent the average from 3-4 titration series, and the error bars are the standard deviations. The curves show the fits of the data obtained with equation (1).

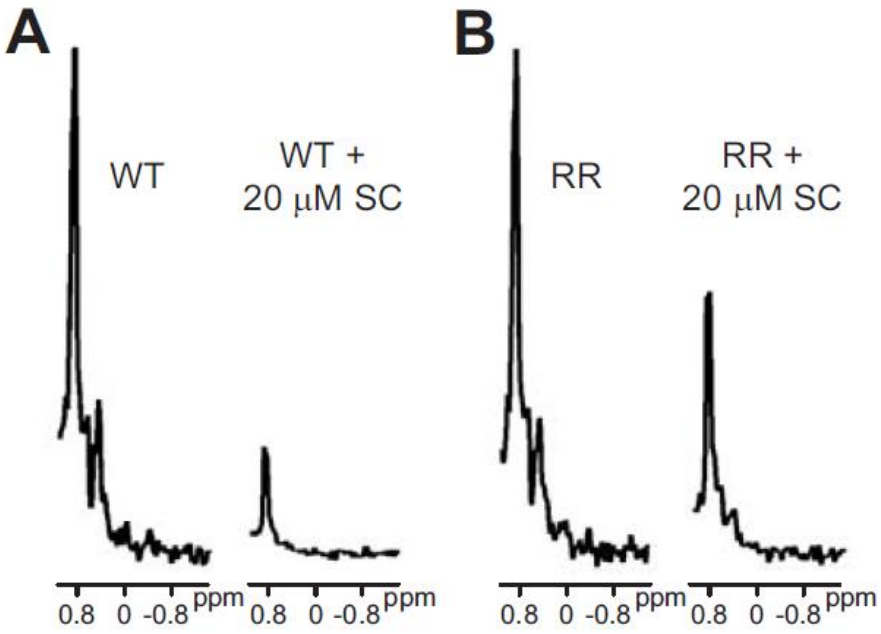

Figure 20. Expansions showing the methyl region of the 1D spectra of 3 μM WT and RR mutant C2B domain, in the absence or presence of 20 μM SNARE complex, or SC. **A.** WT does not display detectable resonances in the 0.4-0.6 ppm region in the presence of 20 μM SC. **B.** RR mutant with visible resonance signal in the 0.4-0.6 ppm region in the presence of 20 μM SC. These are analogous to the results for the C2AB fragment in Figure 17.

The results of the C2B KK mutant also resembled the C2AB KK mutant: C2B KK increased the apparent K_d from 0.8 ± 0.2 μM to 3.5 ± 0.7 μM. The calculated I_b for the C2B KK mutant was close to 0 (-0.03 ± 0.09; Table 1), which can be attributed to the uncertainty in this value when saturation is not reached at the high SNARE complex concentrations. Overall, these results show that the KK mutation in the polybasic region impairs the major SNARE complex binding mode while having much less effect, if any, on oligomerization.

To test the above conclusions by another method, I carried out precipitation assays with synaptotagmin-1 fragments and the SNARE complex (Figure 21). At both 10 and 20 μM SNARE complex, a substantial fraction of the WT C2AB fragment precipitated, but the RR mutation decreased the precipitation. The DN mutation induced slight decrease in precipitation at 10 μM SNARE complex, but to a much lesser extent than RR. The KK mutation did not impair precipitation. Similar results were obtained when the assay was repeated with the WT or mutant C2B domain. It is notable that in this case, the inhibition of precipitation by the RR mutation was even more dramatic. As mentioned in section 2.3.2, the C2AB fragment, C2B domain and SNARE complex alone are all highly soluble in the presence and absence of 1 mM Ca^{2+}. They yield excellent 2D NMR data at concentrations much higher than those used in these experiments (Fernandez et al. 2001; Ubach et al. 2001; Chen et al. 2002; Chen et al. 2005; Arac et al. 2006). Therefore, the precipitation is a direct consequence of aggregation of the synaptotagmin-1 fragments with the SNARE complex in the presence of calcium.

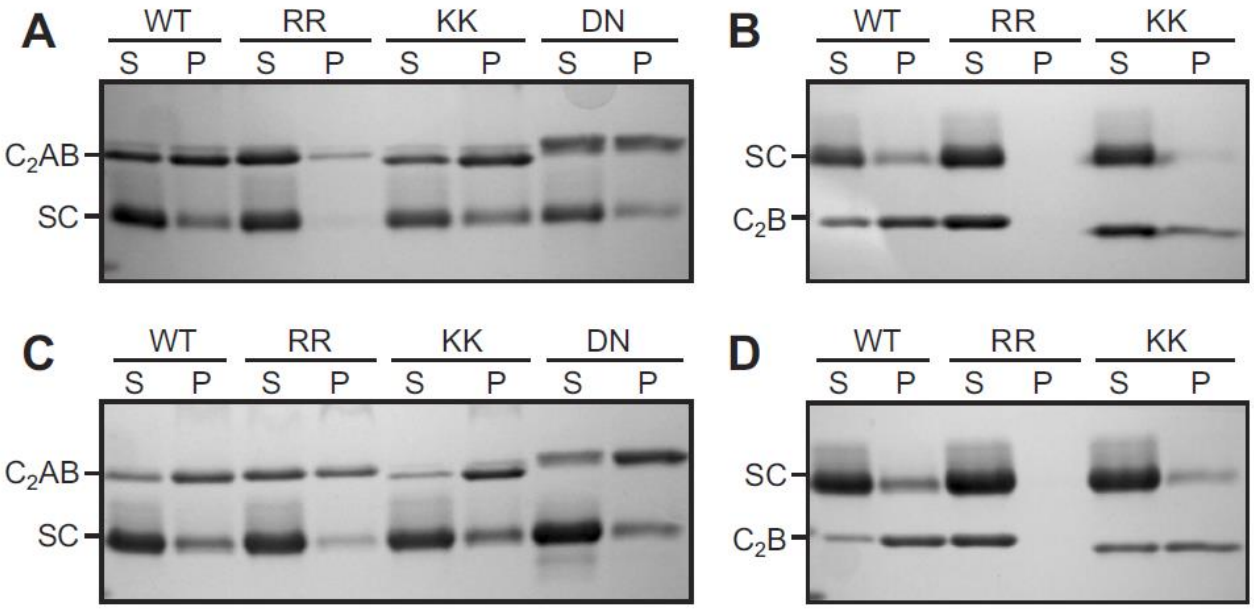

Figure 21. The RR mutation hinders precipitation of synaptotagmin-1 fragments with the SNARE complex. Samples containing 10 µM C2AB fragment (**A**,**C**) or 10 µM C2B domain (**B**,**D**) were incubated with 10 µM (**A**,**B**) or 20 µM (**C**,**D**) SNARE complex for 5 min in the presence of 1 mM Ca^{2+}. The soluble fractions (S) and the precipitates (P) were separated by centrifugation and analyzed by SDS PAGE followed by Coomassie blue staining.

In addition, I tried to quantify the amount of aggregation by dynamic light scattering, but any significant aggregation or precipitation that crossed path with the detector led to signal saturation. When I attempted to quantify the amount of precipitation using the fluorescence turbidity assay, whereby I monitored the amount of scattering at 350 nm, the precipitate formed a suspension that led to irreproducible data depending on how much of the suspension lay in the path of light of the detector. In the end, the precipitation assay above was the ideal method for probing the interactions, because it represents an average of the entire sample and does not require sample homogeneity in solution.

2.4 Discussion

Synaptotagmin-1 functions in the final, Ca^{2+} triggering step of neurotransmitter release, therefore its interactions with the SNARE complex are particularly important. Their interactions are widely believed to couple Ca^{2+} sensing to membrane fusion. Despite numerous studies describing such interactions, it has been difficult to characterize them with quantitative biophysical methods and to define the binding sites involved. I have used 1D ^{13}C-edited ^{1}H-NMR spectra to shed light on the nature of these interactions. My results firstly highlight the difficulties in the analysis of such interactions because of the tendency of synaptotagmin-1 fragments to aggregate with the SNAREs. Such aggregation can severely hinder the interpretation of the data. My data reveal the two arginine residues at the bottom of the synaptotagmin-1 C2B domain as contributing to such aggregation. Further, my data support the model that the polybasic region of the C2B domain constitutes the primary binding site for the SNARE complex.

The propensity of the synaptotagmin-1/SNARE complex assemblies to aggregate and precipitate in the presence of Ca^{2+} has hindered application of standard 2D heteronuclear NMR methods which can otherwise be used to map the binding sites involved in protein complexes (Rizo et al. 2012). Even in the absence of Ca^{2+}, TROSY-HSQC revealed multiple binding sites in the interaction that may reflect binding modes that are not primary or specific, but can lead to oligomers at the protein concentrations used for these experiments ($\geq$ 40 μM) (Dai et al. 2007). Compared to 2D, 1D NMR lacks of much of the residue-specific information and compromises the resolution of the data. However, it allows for a dramatic gain in sensitivity at regions where multiple resonances overlap. In particular, this applies to the most intense methyl region referred to as SMR (Arac et al. 2003). The gain in sensitivity, combined with the use of ^{13}C-editing to

select the proton signals of only the ^{13}C-labeled protein, allowed for the analysis of interactions at synaptotagmin-1 fragments concentration of 3 µM. Although such low concentrations prevented visible precipitation, titrations monitored by 1D NMR showed that higher SNARE complex concentrations still lead to the formation of large oligomer complexes with the WT C2AB fragment and C2B domain. Such aggregation phenomena can be assumed to be in line with the mechanism that leads to precipitation at higher synaptotagmin concentrations.

The RR and KK mutations at the bottom and in the polybasic region of the C2B domain, respectively, have different effects on the interactions according to my data. The RR mutation prevents the formation of larger complexes and precipitation, leading to titration curves that most likely correspond to 1:1 stoichiometric binding. Thus, although the titrations with the WT cannot be used to derive meaningful dissociation constants, those with the C2AB and C2B RR mutants provide more reliable data to estimate the affinity involved in the primary binding mode with the SNARE complex. Admittedly, because of the need to use unlabeled SNARE complex in the µM range to obtain sufficient dynamic range in the titration data, I still cannot calculate the K_d accurately if the interaction is relatively tight (<µM). The K_d values calculated from the titrations above (0.94 ± 0.01 µM and 0.4 ± 0.3 µM; Table 1) suggest the actual dissociation constant is 1 µM or lower.

As with the WT, the K_d measurements with the C2AB and C2B KK mutants cannot be considered reliable either because the KK mutation does not noticeably prevent aggregation. It is clear though, that the KK mutation impairs the primary binding mode between synaptotagmin-1 and the SNARE complex. This is based on the smaller decreases in SMR intensities at low SNARE complex concentrations for both the C2AB fragment (Figure 16) and C2B domain (Figure 19), relative to their WT counterparts. These results and those obtained with the RR

mutation strongly support the current working model that the primary binding mode involves the polybasic region of the C2B domain but not the bottom region of the C2B domain. This conclusion agrees with some of the previous studies (Rickman et al. 2006; Dai et al. 2007; Xue et al. 2008; Choi et al. 2010) but not others (Gaffaney et al. 2008; Choi et al. 2010). The existence of such a primary binding site, as concluded from my data, is not a novel concept but was not clear from the available literature. Such conclusion will pave the way for understanding how the functions of synaptotagmin-1 and SNAREs are coupled.

While much of the surface of the SNARE complex is highly negative (Fasshauer et al. 1998; Sutton et al. 1998), most of the synaptotagmin-1 C2B domain and part of the C2A domain are highly positive, especially upon Ca^{2+} binding (Ubach et al. 1998; Fernandez et al. 2001; Dai et al. 2007). These characteristics, along with the aggregation tendency of C2AB/SNARE and reports implicating different regions in binding (see section 2.1.1), raise the possibility that not all of the reported interactions are specific. Such features have greatly hindered the development of well-defined models for synaptotagmin-1/SNARE coupling as well as the validation of existing models. My data show that it is now possible to disentangle the primary binding mode from other interactions that favor oligomerization.

The contributions of the C2A domain to SNARE complex binding are still unclear. The titrations of the isolated C2A domain (Figure 18) indicate that, in contrast to C2B, it does not have an extensive, strong interaction with the SNARE complex. However, the small signal decrease suggests some dynamic interactions that may involve a small surface on C2A. Because the DN mutation had a similar effect on C2AB-SNARE complex binding as the RR mutation (Figure 16), the weak C2A-SNARE interaction observed may be disrupted by the DN mutation. However, the DN mutation did not impair precipitation as the RR mutation did (Figure 21).

Perhaps the interactions of the C2A Ca^{2+} binding loops (where D232N is located) with the SNARE complex simply add to those involving the key surfaces of the C2B domain.

The observation of oligomers and/or precipitate of protein complexes may simply reflect their insolubility and carry little physiological significance. It is therefore possible that the tendency of synaptotagmin-1 fragments to precipitate with the SNARE complex, as well as the impairment of such tendency by the RR mutation, do not have functional relevance. Furthermore, the impaired ability of the synaptotagmin-1 RR mutant to bring two membranes together already provided an explanation for its *in vivo* effect (Xue et al. 2008). Hence, the membranes are likely the real targets for the positively charged RR region *in vivo*. But in the absence of membranes, these regions are expected to be avid for negatively charged surfaces such as those present around much of the SNARE complex. This could explain the tendency of synaptotagmin-1 to aggregate with the SNARE complex. It is still possible, however, that the synaptotagmin-1/SNARE complex oligomers are functionally important, and their presence *in vivo* are modulated by the phospholipid membranes. Disruption of such oligomers could lead to the functional effects of the RR mutation.

There is still much to be discovered about the interactions and their role in neurotransmitter release. The results presented here show that disentangling the primary binding mode from additional interactions that favor aggregation is crucial to addressing these questions, and that 1D NMR is a powerful tool for this purpose.

Chapter 3. Alternative methods for probing synaptotagmin/SNARE complex interactions

3.1 Competition Assay

3.1.1 Introduction

Based on the results in chapter 2, I sought to develop a robust method to derive more definitive affinity of the synaptotagmin-1/SNARE complex primary binding mode, as well as the effects of mutations on this affinity. The new but related assay, hereon referred to as the competition assay, utilizes the same NMR pulse sequence to acquire 1D ^{13}C-edited ^{1}H-NMR spectra. The difference from before is that, in addition to a fixed 3 μM concentration of ^{15}N,^{13}C-labeled WT C2AB fragment, the concentration of unlabeled SNARE complex is fixed at well, at 3.5 μM. This SNARE concentration was chosen to give sufficient SMR intensity decrease and dynamic range, while avoiding the higher concentrations that could populate the secondary binding mode(s) and lead to precipitation. Increasing amount of unlabeled WT or mutant C2AB fragments were then introduced. They are expected to displace the labeled WT C2AB from the SNARE complex, which would lead to a recovery of the SMR signal intensity (Figure 22). It is assumed that the ^{13}C isotope does not change the chemical properties of C2AB, therefore binding is not affected. The amount of recovery is determined by how well the mutant binds to the SNARE complex compared to the WT. The key advantage of this method is that the concentration of SNARE complex can be kept relatively low throughout the experiment, thus sampling mostly the primary binding site with little interference of the other binding mode(s).

In theory, the competition assay is superior to the direct titration assay for examining the primary binding mode. Unfortunately, experimental artifacts have hindered the application of the assay to my system, as shown in Results and Discussion.

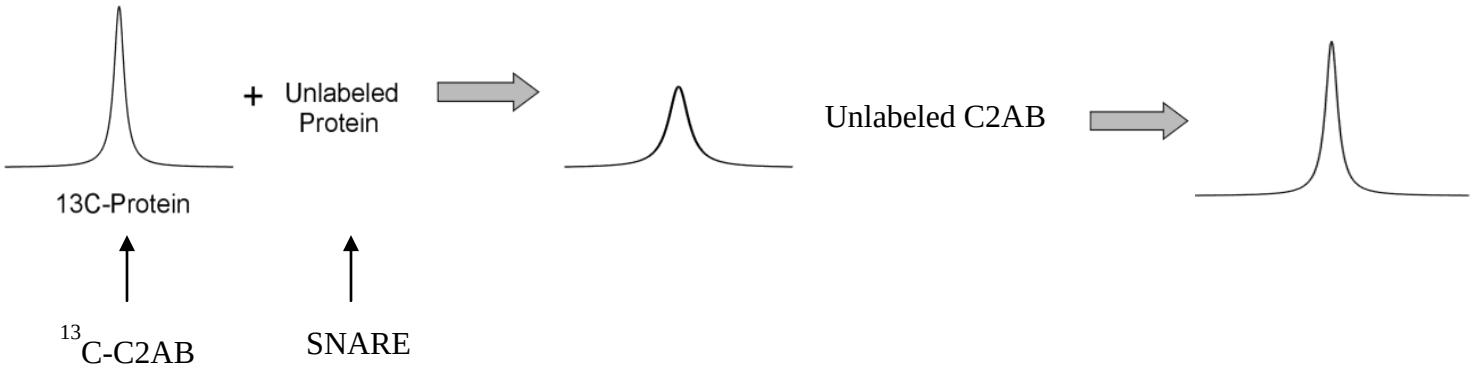

Figure 22. Competition between ^{13}C-labeled and unlabeled C2AB fragment for SNARE complex binding, as monitored through 1D ^{13}C-edited ^{1}H-NMR spectra. The diagram summarizes the principles of the approach. The SMR signal from the ^{13}C-labeled C_2AB fragment (left) is expected to decrease upon addition of SNARE complex (middle) and recover towards its initial intensity when it is displaced from the SNARE complex by increasing amount of unlabeled C2AB fragment.

Nevertheless, a thorough quantitative analysis of the assay is provided in the Method section because I believe it is a powerful method with general applicability to studying protein-protein interactions. Its limitation arises if there are significant interactions of the protein(s) with the reaction vessel.

3.1.2 Methods & Materials

Samples contained 3 μM of uniformly ^{15}N,^{13}C-labeled C_2AB fragment, 3.5 μM SNARE complex, and a variable amount of unlabeled WT or mutant C2AB fragment. A new sample was prepared for each unlabeled C_2AB concentration, and the 1% natural abundance of ^{13}C isotope in the unlabeled SNARE complex was accounted for as described in section 2.2.3. Assuming a 1:1 equilibrium-binding model, the SMR intensity (I) can be expressed as a function of the total unlabeled WT C2AB fragment added (U_T) by equation (2):

$$(2) \quad I = I_f\left(1+\frac{U_T}{100P_T}\right)+(I_b-I_f)\left(1+\frac{U_T}{100P_T}\right)\frac{P_T+U_T+L_T+K_d-\sqrt{(P_T+U_T+L_T+K_d)^2-4(P_T+U_T)L_T}}{2(P_T+U_T)}$$

This equation is analogous to equation (1), with P_T replaced by P_T+U_T, since both the labeled and unlabeled C2AB contribute equally to SNARE complex binding. The factor $[1+(U_T/100P_T)]$ accounts for the 1% natural abundance of ^{13}C in the unlabeled C2AB fragment. Unlike in chapter 2, I_f was determined from an average of multiple spectra acquired for 3 μM labeled C2AB fragment, rather than included as a parameter of data fitting. The I_f value was then used to normalize all the intensities, and fitting the experimental data to equation (2) yielded the K_d and normalized I_b.

For competitions with mutant C2AB, *r* was introduced as the ratio between the mutant and WT dissociation constants. *r* can be expressed by equation (3):

(3) $$r = \frac{\left[M_T - L_T + P_L + \left(\frac{K_d P_L}{P_T - P_L} \right) \right] P_L}{\left(P_T - P_L \right) \left[L_T - P_L - \left(\frac{K_d P_L}{P_T - P_L} \right) \right]}$$

where M_T is the total concentration of unlabeled mutant C_2AB fragment, P_L is the concentration of WT labeled C_2AB fragment bound to the SNARE complex, and K_d remains the dissociation constant for the wildtype protein. To express the observed SMR intensity (I) as a function of the variable M_T and the parameters I_f, I_b, P_T, L_T, K_d and r, it is necessary to isolate P_L in the equation. However, equation (3) has a cubic dependence on P_L, leading to a complex expression for I that is difficult to fit to the experimental data because of instability of the fitting algorithms. In principle, since P_T, L_T are known and I_f, I_b can be obtained from the competitions with WT C_2AB, this problem can be overcome by deriving the value of P_L from the SMR intensity I observed at a particular M_T value using equation (4):

(4) $$I = I_f \left(\frac{M_T}{100 P_T} + 1 \right) + \frac{I_b - I_f}{P_T} \left(\frac{L_T}{100} - \frac{L}{100} + 0.99 P_L \right)$$

where L is the concentration of free SNARE complex. Solving for P_L and removing the term $L/100$, which is negligible under the conditions of our experiments, we obtain equation (5):

(5) $$P_L = \frac{1}{0.99} \left[P_T \frac{I - I_f \left(\frac{M_T}{100 P_T} + 1 \right)}{I_f - I_b} - \frac{L_T}{100} \right]$$

The value of *r* obtained from equations (4) and (5) depends on the accuracy of the value of *I* measured for the particular M_T concentration. As an alternative approach, one can make the approximation that, at the higher M_T values, most of the SNARE complex is bound to either the labeled or unlabeled C_2AB, hence the concentration of free SNARE is negligible compared to the concentration of bound SNARE. Then, estimates of *r* can be obtained by fitting the observed *I* values to equation (6):

$$(6) \quad I = I_f\left(\frac{M_T}{100P_T}+1\right)+\left(I_b - I_f\right)\left(\frac{L_T}{100P_T}+0.99\frac{M_T - L_T + rP_T + rL_T - \sqrt{\left(M_T - L_T + rP_T + rL_T\right)^2 - 4r\left(r-1\right)P_T L_T}}{2P_T\left(r-1\right)}\right)$$

3.1.3 Results & Discussion

In order to measure the affinity of the different C2AB mutants for the SNARE complex, competition assays were carried out by adding unlabeled WT, DN, RR, and KK mutants. Each mutant set was repeated three times, and the WT four times. The data were reproducible, and only the KK mutant displayed significant difference from the WT (Figure 24A). This seemed to confirm the conclusion from chapter 2 that the KK mutation, but neither RR nor DN, disrupts the primary binding site to the SNARE complex.

However, the data were rendered inconclusive after the discovery of what appeared to be competition of the labeled and unlabeled C2AB for binding to the glass wall of the NMR tube. As shown in Figure 23, the addition of unlabeled C2AB to labeled C2AB significantly increased the peak intensity, even though no SNARE complex was present and hence no competition and signal recovery was expected.

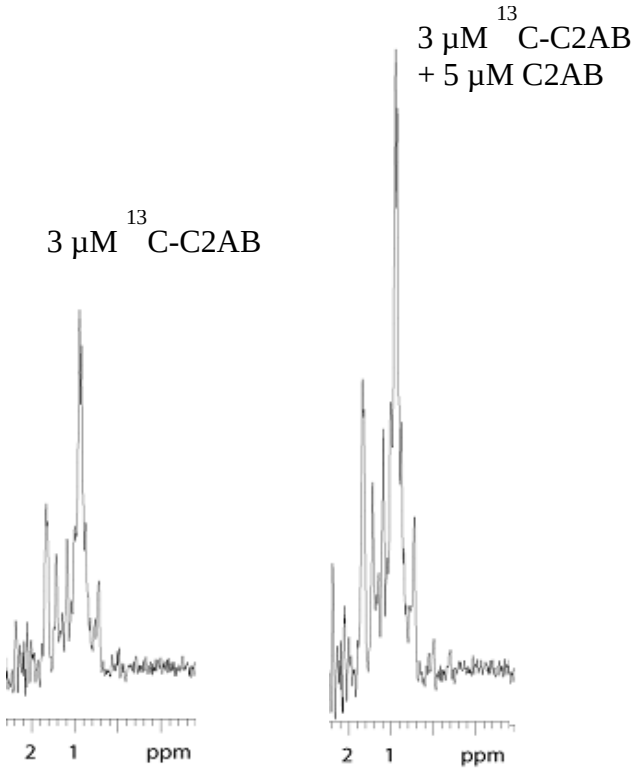

Figure 23. The addition of unlabeled C2AB results in an increase in the SMR signal intensity, despite the absence of SNARE complex. The two spectra are plotted on the same vertical scale. The addition of 5 µM unlabeled C2AB is not expected to alter the peak intensity of 3 µM labeled C2AB (left), except for the negligible 1% natural abundance in the unlabeled protein. But surprisingly, a large increase was observed (right), indicating that both species interact with the inner glass surface of the NMR tube: unlabeled C2AB binds to the glass, displacing and thereby mobilizing some of the labeled protein and causing the signal to increase.

Such a phenomenon could be explained by the binding of the overall positively charged C2AB fragments to the negatively charged inner glass surface of the NMR tube. Indeed, when SiO_2 particles were added to a sample of labeled C2AB, a substantial decrease in the signal was observed. This is despite the negligible volume introduced by the particles. Therefore, the signal change was not a result of dilution, but of the proteins binding to the significant surface area introduced by the particles, thereby becoming immobilized and therefore invisible in the spectrum.

I performed a series of competition experiments with glass, where 3 or 5 μM of unlabeled WT C2AB fragment was added to 3 μM labeled WT C2AB (Figure 24B). No SNARE complex was present in any of the samples. The results confirm the observation in Figure 23 that unlabeled C2AB competes with labeled C2AB for glass binding. The same holds for unlabeled C2AB mutants (data not shown). The competition assay results (Figure 24A) are therefore inconclusive, and the direct titration method presented in chapter 2 was applied to study the Syt1-SNARE system.

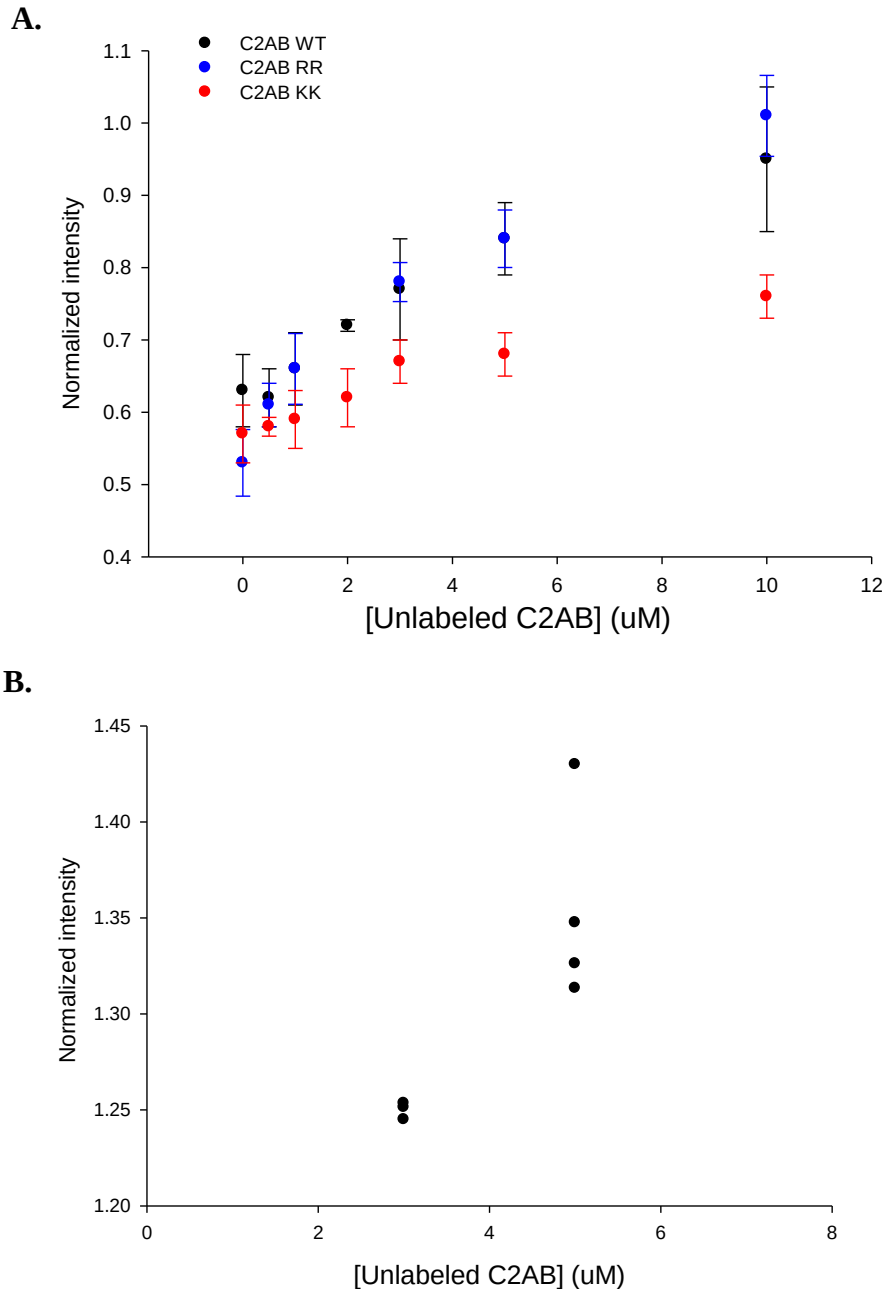

Figure 24. A. Competition assay of 3 μM ^{13}C-C2AB WT with various concentrations of WT and mutant unlabeled C2AB for SNARE complex binding. The KK mutant (red) seems to be different from the WT (black). Each point represents the average of 3-4 repeats. Error bars represent standard deviations. **B.** Competition of 3 μM ^{13}C-C2AB with 3 or 5 μM unlabeled WT C2AB for glass binding. Each point represents one repeat of the experiment. The intensities are much greater than unity, indicating that the addition of unlabeled protein mobilizes some of the labeled protein.

Because the above was an indirect way of addressing the problem and prone to different sources of error, I attempted to avoid the glass binding phenomenon altogether with a few approaches. First, I ascertained that there was no binding of the sample to the plastic Eppendorf tube in which the samples were prepared. Then, I used up to 50 μM of BSA to coat the glass surface in hopes of rendering it inert with respect to C2AB binding. However, subsequent addition of unlabeled C2AB to labeled C2AB still caused a non-trivial increase in the signal, though 10-20% less than before. It was suggested during my committee meeting that 50 μM is an insufficient concentration, so future applications of BSA for similar purposes should be attempted in the hundreds of μM range, or ~10-30 mg/ml.

Second, I tried to pacify the glass surface using AquaSil Siliconizing Fluid (Thermo Scientific). The functional groups react with the polar groups on the glass surface, resulting in a hydrophobic surface that resists nonspecific binding. The silanol bonds subsequently formed would be able to withstand even autoclaving conditions. However, the competition-with-glass phenomenon persisted. In retrospect, because the long pipettes used to transfer samples from the plastic Eppendorf tubes to the NMR tube are also made of glass, they introduced significant surface area for potential binding and should be silanized as well. This may help address the glass binding problem in the future.

3.2 LED diffusion experiment

3.2.1 Introduction

In order to circumvent the glass-binding problem described above, an NMR method that is independent of such binding would be ideal. One approach is to measure the self-diffusion coefficient D_s of the synaptotagmin C2AB fragment as a function of the amount of SNARE complex bound. As long as the concentration present in solution is constant, the amount of protein bound to the glass would not complicate the data analysis. D_s is inversely related to the hydrodynamic radius, and therefore the size of the molecule. It is often used to infer the oligomerization or aggregation states of the proteins. In this case, it is used to infer how much SNARE complex is bound to synaptotagmin: the greater the affinity between the two, the larger the average size of the molecules in solution, and the lower the D_s. The hypothesis is that the KK mutation would weaken the binding of synaptotagmin-1 C2AB fragment to the SNARE complex. Therefore the same amount of SNARE complex would lead to a smaller change in D_s for the mutant compared to the WT.

The experiment applied here is the LED: the longitudinal encode-decode or longitudinal eddy current delay experiment. It is based on pioneering work using pulsed field gradients (PFG) to measure the D_s of molecules in solution (Tanner 1970). The gradient pulse dephases the magnetization because the field strength increases along the length of the sample. The molecules then diffuse for a fixed amount of time before a re-focusing pulse is applied and the signal amplitude measured. As the strength of the PFG pulse increased in successive experiments, the signal amplitude became increasingly attenuated due to translational diffusion (see Figure 25). The faster the molecules diffused, the less of the original magnetization is recovered in the z-

direction, and the more the signal would become attenuated. The signal amplitude is therefore a function of D_s. The value of D_s can be extracted by fitting this relationship to the data obtained at different PFG strengths. This technique has since been optimized to eliminate residual eddy currents (Gibbs and Johnson 1991), which allowed for longer diffusion times and the study of larger molecules (in the 40+ kDa range) with slower motion. Water suppression has also been added to allow for greater dynamic range at any given PFG strength (Altieri et al. 1995).

As shown below, while this method generates reproducible data, it does not provide sufficient dynamic range in our system. Modifications could potentially be made in order to adopt LED self-diffusion as a viable assay.

3.2.2 Materials & Methods

Because the LED sequence monitors the protons directly bonded to the ^{13}C atoms, it allowed for the use of ^{13}C-labeled synaptotagmin-1 C2B domain, C2AB fragment, and the SNARE complex. See chapter 2 for purification protocols. All experiments were carried out at 25°C on Varian INOVA 600 MHz spectrometer equipped with a cold temperature probe. Samples were prepared in 25 mM HEPES, 125 mM NaCl and 1 mM Ca^{2+} at pH 7.4 with 5% D_2O. The gradient field strength was first calibrated using a 350 µM sample of ^{13}C-labeled synaptotagmin-1 C2B domain. Subsequently, the experiment was carried out with a 4 µM ^{13}C-C2AB sample and repeated at six different field strengths (Figure 25). Such a series of experiments lasted 2-4 hours and was repeated three times per sample. The other two samples contained 4 µM ^{13}C-C2AB and either 8 µM or 20 µM unlabeled SNARE complex.

The LED pulse sequence was courtesy of the Lewis Kay lab (U. Toronto). The curve fitting was performed in SigmaPlot by adapting the equation derived by the Kay lab. By plotting

the signal amplitude as a function of gzlvl5, the experimental parameter for field strength, one could extract the diffusion coefficient D_s from the curve fitting.

3.2.2 Results &Discussion

Figure 25 shows the raw traces from a series of six experiments on the same sample with increasing PFG strengths. As expected, the amplitude attenuates with increasing strength. When the peak amplitudes are plotted (Figure 26A), it is clear that the signal drops with increasing SNARE complex concentration. This is expected based on the findings in chapter 2, because SNARE complex binding increases the size of the detectable molecules. However, the diffusion coefficient does not depend on these raw values. Rather, it depends on how much the amplitude changes as a function of PFG strength relative to the zero-strength signal. In other words, the data fitting can be carried out with the normalized signal. For each sample, the normalization is done by taking the average of the three values at zero-strength and dividing it into all subsequent raw values (Figure 25B). It is clear from the normalized data that there are only slight differences at the different SNARE complex concentrations. Fitting the data gives:

$D \times 10^{11} = 4.22 \pm 0.10$ m^2/s for 4 μM C2AB,

$D \times 10^{11} = 4.12 \pm 0.12$ m^2/s for 4 μM C2AB + 8 uM SNARE, and

$D \times 10^{11} = 3.74 \pm 0.20$ m^2/s for 4 μM C2AB + 20 uM SNARE.

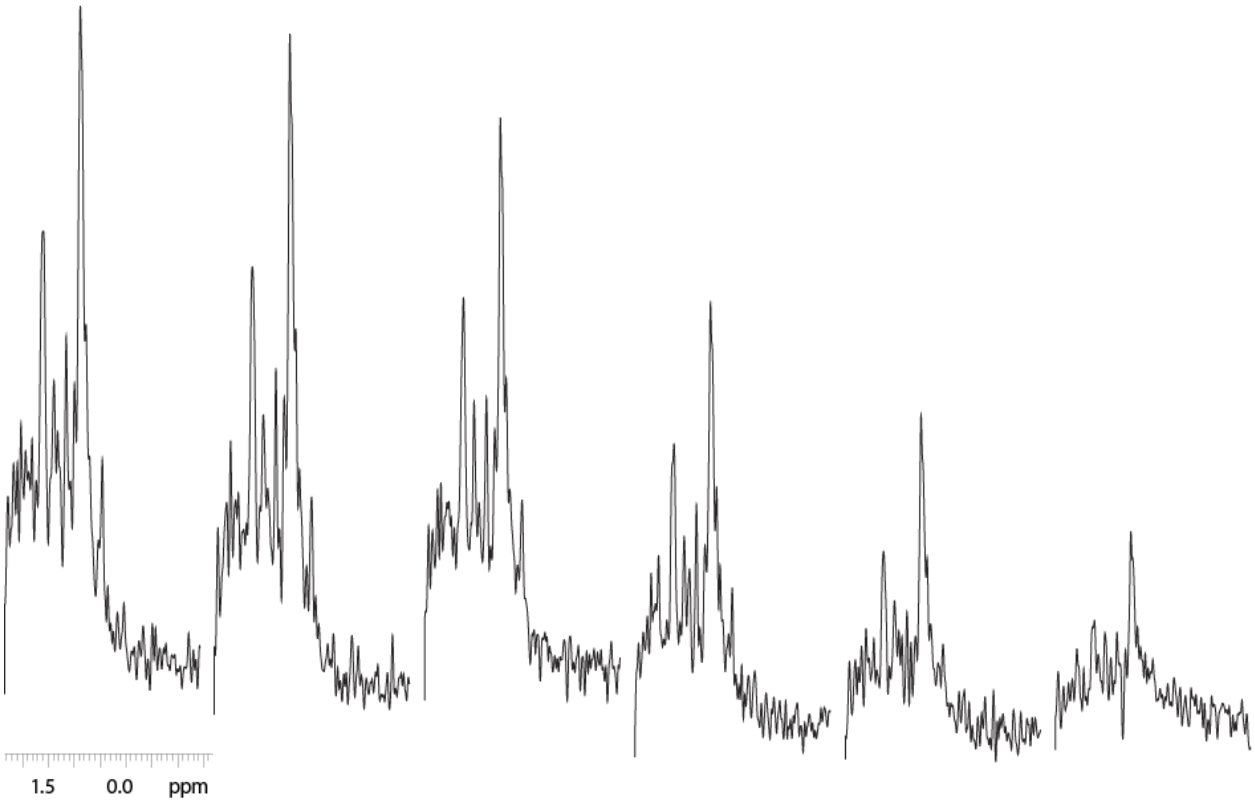

Figure 25. Raw traces from the LED diffusion experiment at increasing PFG strengths. The sample contained 4 μM ^{13}C-labeled Syt1 C2AB fragment and no SNARE complex. From left to right, the spectra represent the gradient field strength in units of Gauss/cm of 0.191, 4.019, 7.846, 11.673, 15.500, 19.327. The peak amplitudes are plotted in figure 26.

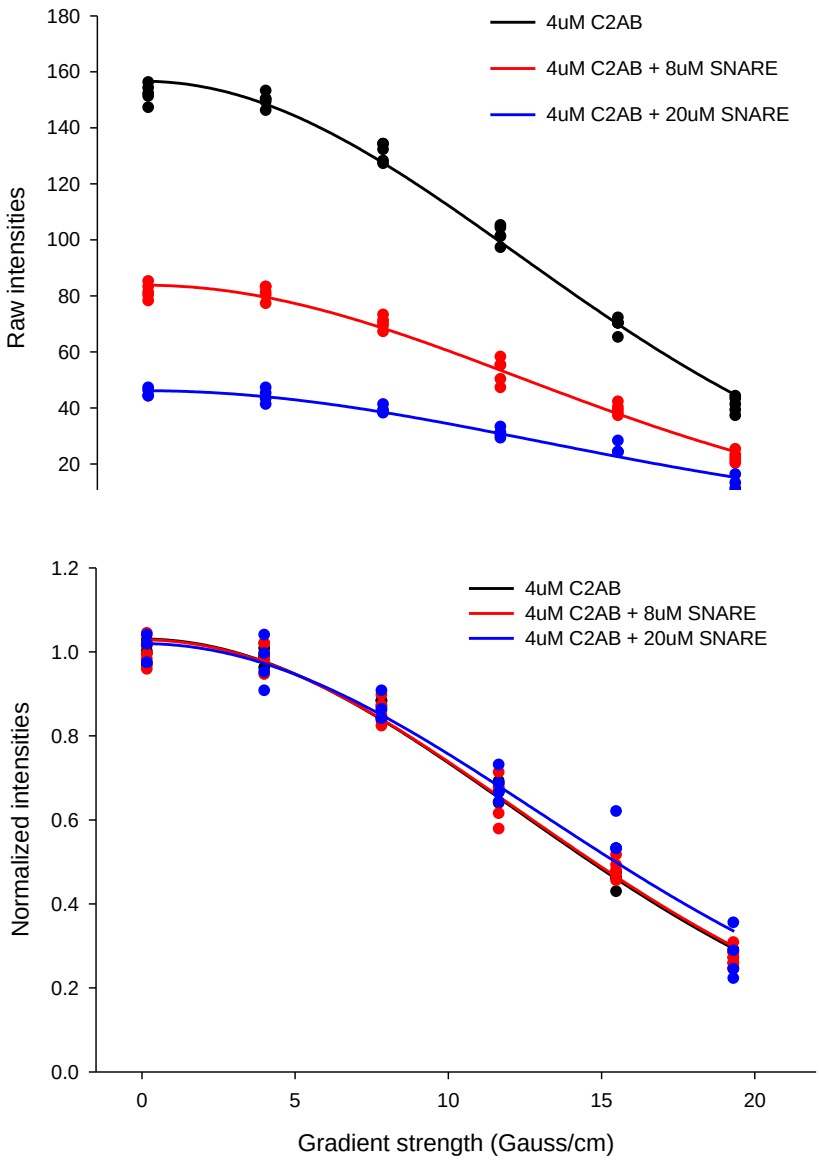

Figure 26. LED diffusion experiment of 4 µM ^{13}C-C2AB fragment at three different SNARE complex concentrations: 0 µM (black), 8 µM (red), and 20 µM (blue). **A.** The raw signal intensities as a function of the pulse strength. **B.** The signal intensities normalized to the average of the intensities at zero-strength. Each series was repeated three times, represented by three data points at each x-value.

Therefore, given a 4 μM WT C2AB sample, the decrease in the diffusion coefficient upon the addition of 20 μM SNARE complex is 11% ± 6%. The uncertainty is large compared to the dynamic range. Therefore, the experiment was not continued with the C2AB mutants.

From section 2.3.6 and Figure 18, it is clear that SNARE complex binding induces a larger fractional change in the molecular size of the C2B domain than for the C2AB fragment. Therefore, measuring LED diffusion for the C2B domain, rather than the C2AB fragment, may be a viable method for quantifying the differences between WT and mutants in binding to the SNARE complex.

Chapter 4. Characterization of an Extended Synaptotagmin-like Protein

4.1 Introduction

The extended synaptotagmin-like protein (E-Syt) was first reported as a 121 kDa protein in rat adipocytes with multiple C2 domains and an amino-terminal membrane-spanning domain (Morris et al. 1999). They are evolutionarily related to a family of yeast membrane proteins with three C2 domains, the tricalbins. As noted in chapter 1, while the SNARE proteins are known to be conserved through evolution as evidenced by their homologs in yeast and plants, synaptotagmins do not have clear homologs in yeast. The tricalbins may represent the only proteins resembling synaptotagmin that are conserved in yeast because of their tandem C2-domain feature. The tricalbins and their mammalian counterparts have not been examined in terms of their properties and expression profile. Although the tricalbins do not bind Ca^{2+} like the E-Syts do, the E-Syts are of interest because they can shed light on the evolution of synaptotagmins which are known to be important in Ca^{2+}-triggered neurotransmitter release (as summarized in chapters 1 and 2). In addition, ESyts have been implicated in cytoskeleton dynamics (Jean et al. 2012) and can reveal general governing principles of tandem C2-domain proteins.

There are three isoforms of E-Syt's (Figure 27). E-Syt1 is localized to intracellular membranes, while E-Syt2 and E-Syt3 are localized to the plasma membrane (PM). E-Syt2 and E-Syt3 were found to target to the PM by a mechanism that does not depend on their TMR, but on their third C2 domain, the C2C domain. E-Syts thus form a family of heterogeneous Ca^{2+}-binding membrane proteins (Min et al. 2007).

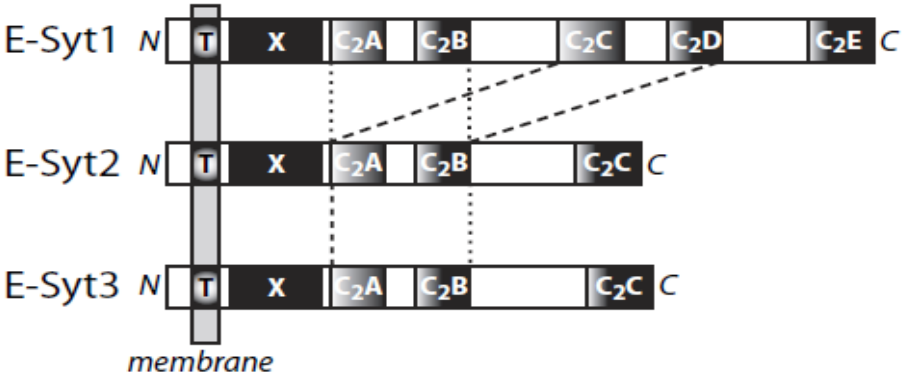

Figure 27. Domain diagrams of E-Syts. T denotes the TMR; X denotes a domain unique to E-Syts; C2A to C2E are the C2 domains. The C2C and C2D domains of E-Syt1 are highly homologous to the C2A and C2B domains of all E-Syts.

The Ca^{2+}-free structure of the E-Syt2 C2AB fragment was determined by Junjie Xu of the Rizo-Rey lab (Figure 28). The C2 domains display a similar eight-stranded β-sandwich structure as the synaptotagmin-1 counterparts (Figure 5). The linker region between the two C2 domains forms an α-helix. This is the first instance to date of a C2 linker region forming any secondary structure. The Ca^{2+}-free structure and calcium titration experiments of the WT protein led to the hypothesis that there are 1-2 high-affinity Ca^{2+} binding sites and one low-affinity site. The Ca^{2+}-bound structure was later determined as well (Junjie Xu) and allowed for the design of point mutations to disrupt the suspected binding sites. The D52N mutation disrupted high-affinity Ca^{2+} binding as expected, as shown by a lack of calcium-induced chemical shift changes compared to the WT.

Synaptotagmin-1 and its C2AB fragment are known to interact with phospholipids. Furthermore, most C2 domain-containing proteins are involved in membrane trafficking and signal transduction at the membrane interface. The tandem C2-domain feature of E-Syt therefore leads to the question of its lipid biding profile, if any. The co-floatation data showed that E-Syt C2AB does not interaction with phospholipids, at least not under the experimental conditions and lipid composition presented here. In addition, I found that the C2AB fragment does not interact with the SNARE complex.

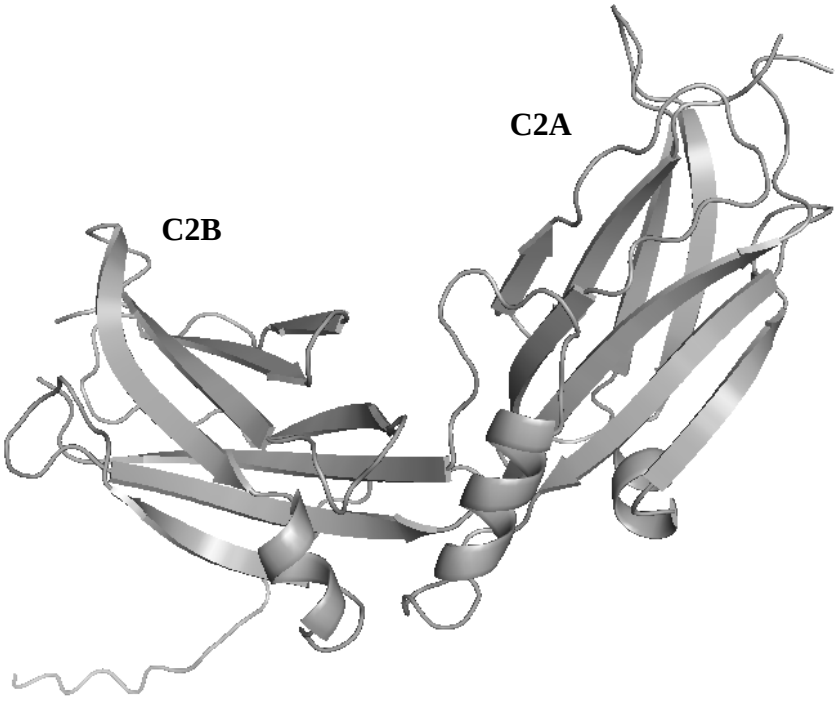

Figure 28. The Ca^{2+}-free structure of the E-Syt2 C2AB fragment (Junjie Xu, unpublished). Note that the linker region between the two C2 domains forms an α-helix. This is in contrast to the flexible linker of all other tandem C2 domain proteins studied so far.

4.2 Method & Materials

4.2.1 Protein expression and purification

Constructs for expression of human extended synaptotagmin-like protein isoform 2 (E-Syt 2) C2AB fragment and its point mutants were provided by Junjie Xu. Mutations were performed using the QuickChange site-directed mutagenesis kit (Stratagene). All proteins were expressed as GST-fusions in *Escherichia coli* BL21 DE3 cells. One colony of bacteria on the transformation plate was used to inoculate 50 ml of M9 minimal media broth with $^{15}NH_4Cl$ as the sole nitrogen source and $^{13}C_6$-glucose as the sole carbon source. 100 µg/ml Ampicillin and 100 µl of 0.5% thiamine were added immediately prior to incubation at 37 °C. This small culture was grown at 37 °C and 250 rpm overnight. The next day, it was transferred to 1 L of M9 media with 100 µg/ml ampicillin added. It was incubated at 37 °C and 250 rpm for 2.5-3 hours till the OD_{600} reached 0.9-1.0. The temperature was then lowered to 16°C and the media allowed to equilibrate at the new temperature for 30 minutes. Subsequently, 0.4 mM IPTG was added to induce protein expression. Induction was carried out at 16°C and 250 rpm for 20-22 hours to allow protein expression to proceed to completion.

The cells were centrifuged at 4000 rpm or around 10,000 g for 30 minutes in a swing bucket rotor (Sorvall RC-3C Plus). They were resuspended in STE buffer (150 mM NaCl, 10 mM Tris pH 8.0, 1mM EDTA, 2 mM DTT, 0.5 mM ABESF). The suspension was frozen in liquid nitrogen then stored at -80 °C until further purification took place. The cells were passed four times through an EmulsiFlex-C5 cell homogenizer (Avestin) at 13,000 psi and centrifuged at 19000 rpm or around 40,000 g for 30 minutes (Sorvall RC 6 Plus Centrifuge). The supernatant was passed through a 0.45 µm syringe filter before mixing with Glutathione Sepharose 4B beads (GE Healthcare) at a ratio of 1 ml of beads slurry per 1 L culture. The beads were prewashed

with the lysis buffer. Incubation was either two hours at RT or overnight at 4ºC. The resin was extensively washed with 50 ml each of the following buffers in sequence: STE buffer, PBS, PBS with 1% Triton, PBS with 1M NaCl, and PBS.

The resin was then equilibrated with Benzonase Buffer (50 mM Tris-HCl, pH 8.0, 2 mM $MgCl_2$, 2 mM DTT) before the addition of 20 ml Benzonase buffer and 5 µl Benzonase Nuclease (Novagen, 25 KUN) and rotation at RT for 2-3 hours. The Benzonase wash was discarded and the resin extensively washed with PBS followed by PBS with 1M NaCl. The resin was re-equilibrated then resuspended in 10 ml PBS with 0.4 ml TEV added (stock OD_{280} ~ 2). TEV cleavage was carried out at RT for 4 hours or 4ºC overnight. The cleavage fraction was collected and elution was repeated with PBS until UV Abs_{280} < 0.1 to recover the maximal amount of protein from the resin. 2 mM DTT was added to PBS throughout the procedure. The elution from the affinity column was further purified by gel filtration into 25 mM Tris pH 7.4, 125 mM NaCl, 0.5 mM TCEP which was analyzed for EDTA and Ca^{2+} content as described in section 4.2.3.

4.2.2 1D NMR titration for SNARE binding

In order to test for the ability of ESyt C2AB to bind the SNARE complex, the same procedure as described in chapter 2 was used for acquiring 1D ^{13}C-edited ^{1}H spectra, except 4 µM instead of 3 µM of ^{13}C-labeled protein was used.

4.2.3 Calcium titration using TROSY-HSQC

All spectra were acquired at 25°C on Varian INOVA 800 MHz spectrometer equipped with a cold temperature probe. 1D ^{1}H spectra of the buffer (25 mM Tris pH 7.4, 125 mM NaCl, 0.5 mM TCEP) were first acquired to ensure there is negligible amount of EDTA and calcium ions. The 1D spectrum of the buffer was recorded, followed by addition of 100 µM EDTA which

gave a sharp characteristic peak around 3.2 ppm. The subsequent addition of 50 µM Ca^{2+} led to a 50% drop in this peak. This confirms the absence of significant (µM scale) amount of EDTA and Ca^{2+} in the original buffer. For each WT and mutant sample, 160 µM of the ^{15}N-labeled protein free of calcium and EDTA was prepared in the aforementioned buffer for a total volume of 350 µl with 5% D_2O. A ^{1}H-^{15}N TROSY-HSQC spectrum was acquired for the calcium- and EDTA-free condition. Subsequent calcium ion additions were from respective stocks of 1 mM, 10 mM, 100 mM, and 1 M Ca^{2+} to minimize pipetting errors as well as extra volumes introduced to the sample. Each calcium concentration condition represented a distinct spectrum acquired for 2.5 hours.

4.2.4 Co-floatation assay

All lipids were purchased from Avanti Polar Lipids. Liposomes for samples 1 and 2 contained 55% POPC, 30% POPE, and 15% DOPS. Liposomes for samples 3 and 4 contained 54% POPC, 29% POPE, 15% DOPS, and 2% PIP. Liposomes for samples 5 and 6 contained 54% POPC, 29% POPE, 15% DOPS, and 2% PIP_2. Sample containing PIP_2 was suspended in two additional volumes of chloroform. The bottom of the glass tube was immersed in warm water. These procedures ensured the solubility of PIP_2. All lipid mixtures were dried in glass tubes with nitrogen gas, then under vacuum overnight. Lipid films were re-suspended in buffer A (25 mM HEPES, pH 7.4, 150 mM KCl) and vortexed for at least five minutes. The resuspended lipid films were frozen and thawed six times, then extruded through a 80 nm polycarbonate filter with an Avanti extruder for 23 times. The final 1 mM lipids were mixed with 5 µM ESyt2 C2AB fragment for a protein-lipid ratio of 1:200 and final sample volume of 165 µl. The liposomes and proteins were mixed by gentle pipetting followed by incubation at room temperature for 1 hour

with 1 mM fresh DTT added. The liposomes and bound protein were isolated by floatation on a Histodenz density gradient (40%:35%:30%) by centrifuging at 48,000 rpm for 4 hours (Beckmann Coulter Ultracentrifuge Optima L-90K). The centrifuged samples contained, from top to bottom, 50 µl buffer A, 150 µl 30%, 150 µl 35%, and 330 µl 40% which is a homogeneous mixture of 165 µl protein-liposome sample and 165 µl 80% Histodenz. 35 µl was taken from the top of the centrifuged sample for SDS-PAGE analysis and Coomassie blue staining.

4.3 Results & Discussion

4.3.1 E-Syt2 C2AB does not interact with the SNARE complex

As described in chapter 2, the 1D titration assay of a ^{13}C-labeled C2AB fragment with the SNARE complex can reveal binding between the two species. In particular, the 1D ^{13}C-edited ^{1}H spectra monitor the signal of the strongest methyl resonance (SMR). This value decreases with increasing size of the molecule. Therefore, binding of an unlabeled species to a labeled species would decrease the signal of the labeled species.

Figure 29 shows one sample titration of the ^{13}C-labeled E-Syt2 C2AB with increasing SNARE complex concentration. The C2AB concentration is held constant at 4 µM. The lack of signal decrease indicates that the two species do not bind. The experiment was repeated at 10 µM ^{13}C-C2AB with similar results (data not shown), leading to the conclusion that there is no interaction between E-Syt2 C2AB and the SNARE complex, at least not with tens of micromolar or tighter affinity. This suggests that the binding of synaptotagmin-1 C2AB to the neuronal SNARE complex (chapter 2) is specific, which highlights the selectivity of such physiologically relevant interactions *in vivo*.

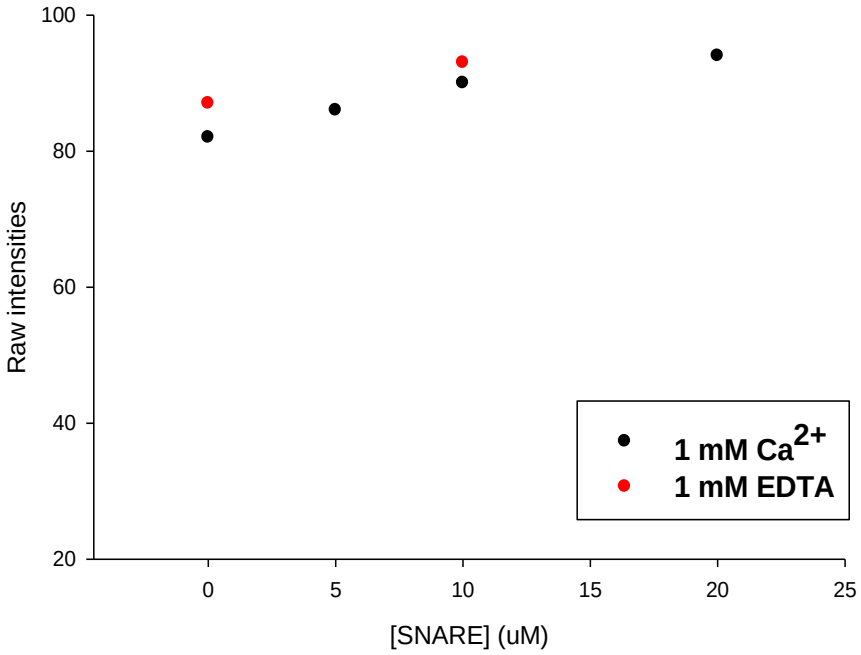

Figure 29. ESyt C2AB does not bind to the SNARE complex. 4 μM of ^{13}C-C2AB was titrated with increasing concentrations of the SNARE complex. Each data point represents a separate sample. A measurable interaction would lead to a decrease in the SMR intensity as described in chapter 2. The lack of binding is observed for both Ca^{2+}-free (1 mM EDTA, red) and 1 mM Ca^{2+} conditions (black).

4.3.2 E-Syt2 C2AB binds Ca^{2+} at more than one site with different affinities

TROSY-HSQC spectra were acquired for a 160 μM sample of ^{15}N-E-Syt2 C2AB WT protein at increasing Ca^{2+} concentrations. Figure 30 shows a few sample spectra overlay at low Ca^{2+} concentrations, showing that the protein is well-folded. Chemical shift changes are observed with increasing Ca^{2+} concentration, but only for some of the peaks (Figure 30), indicating that the interaction with Ca^{2+} is residue-specific. As an example, the inset expansion focuses on a single peak whose intensity decreases with increasing Ca^{2+}, as shown by the intensity plots from the contour cross section. Note that the surrounding peaks, as with many others in the spectrum, do not change in intensity. This change on the tens of μM scale is believed to represent one or two high-affinity calcium binding sites. This hypothesis will be tested with a point mutation.

At higher Ca^{2+} concentrations in the mM range, there are subtle changes as well but again, no overall changes that apply to all of the peaks. As an example, a new peak appeared when the concentration reached 2 mM Ca^{2+} (Figure 31). The inset expansion follows this peak at increasing Ca^{2+} concentrations and reveals a gradual shift. This observation is believed to be in line with the presence of a low-affinity Ca^{2+} binding site, and will be tested with a point mutation.

[Ca^{2+}]: 0 µM, 20 µM, 70 µM, 200 µM, 1000 µM

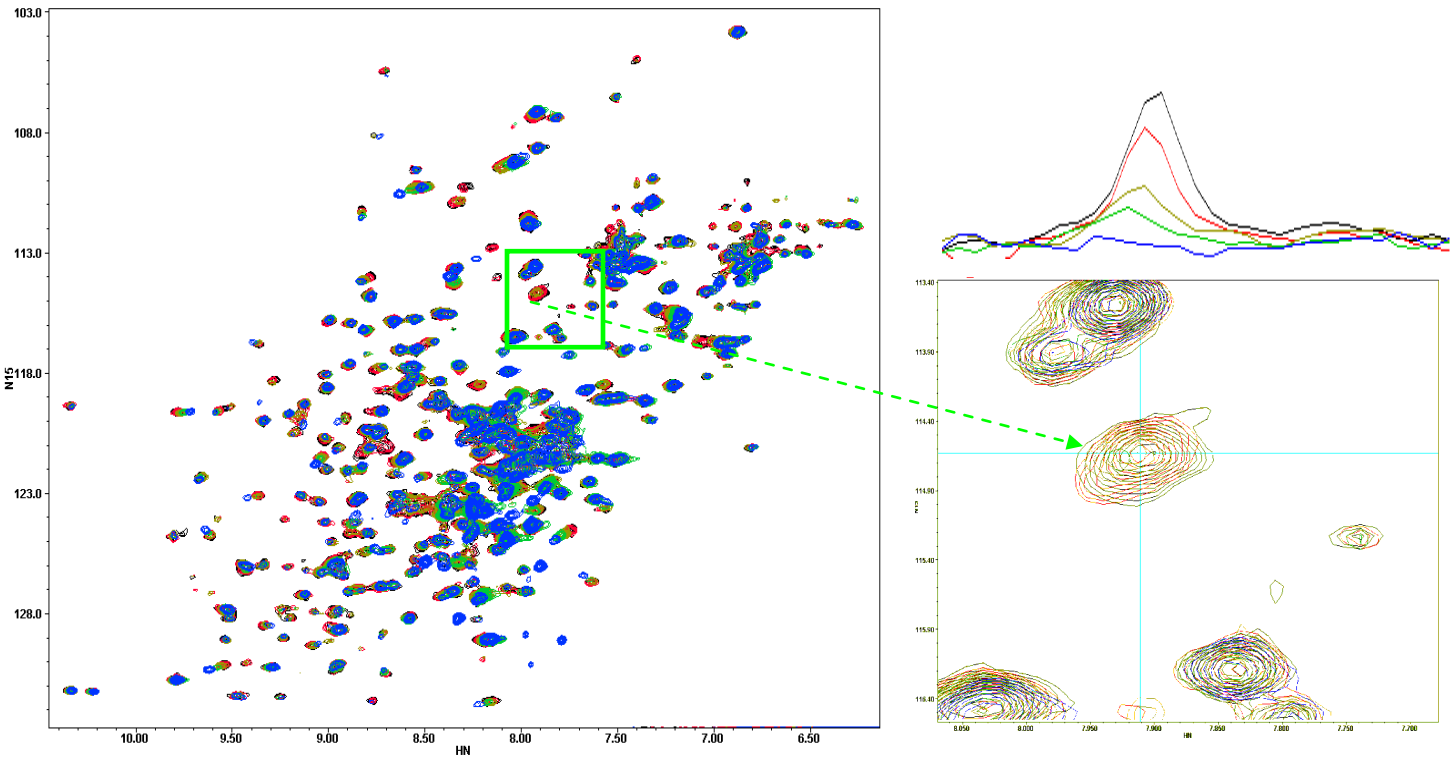

Figure 30. Calcium titration of E-Syt2 C2AB at low Ca^{2+} concentrations. The ^{1}H-^{15}N TROSY-HSQC spectrum (left panel) shows chemical shift changes for some but not all of the peaks. As an example illustration, the inset expansion focuses on a singular peak whose intensity decreased with increasing Ca^{2+} (right panel). The peak intensity is plotted above the inset. The representative Ca^{2+} concentrations shown are 0 µM (black), 20 µM (red), 70 µM (brown), 200 µM (green), 1000 µM (blue).

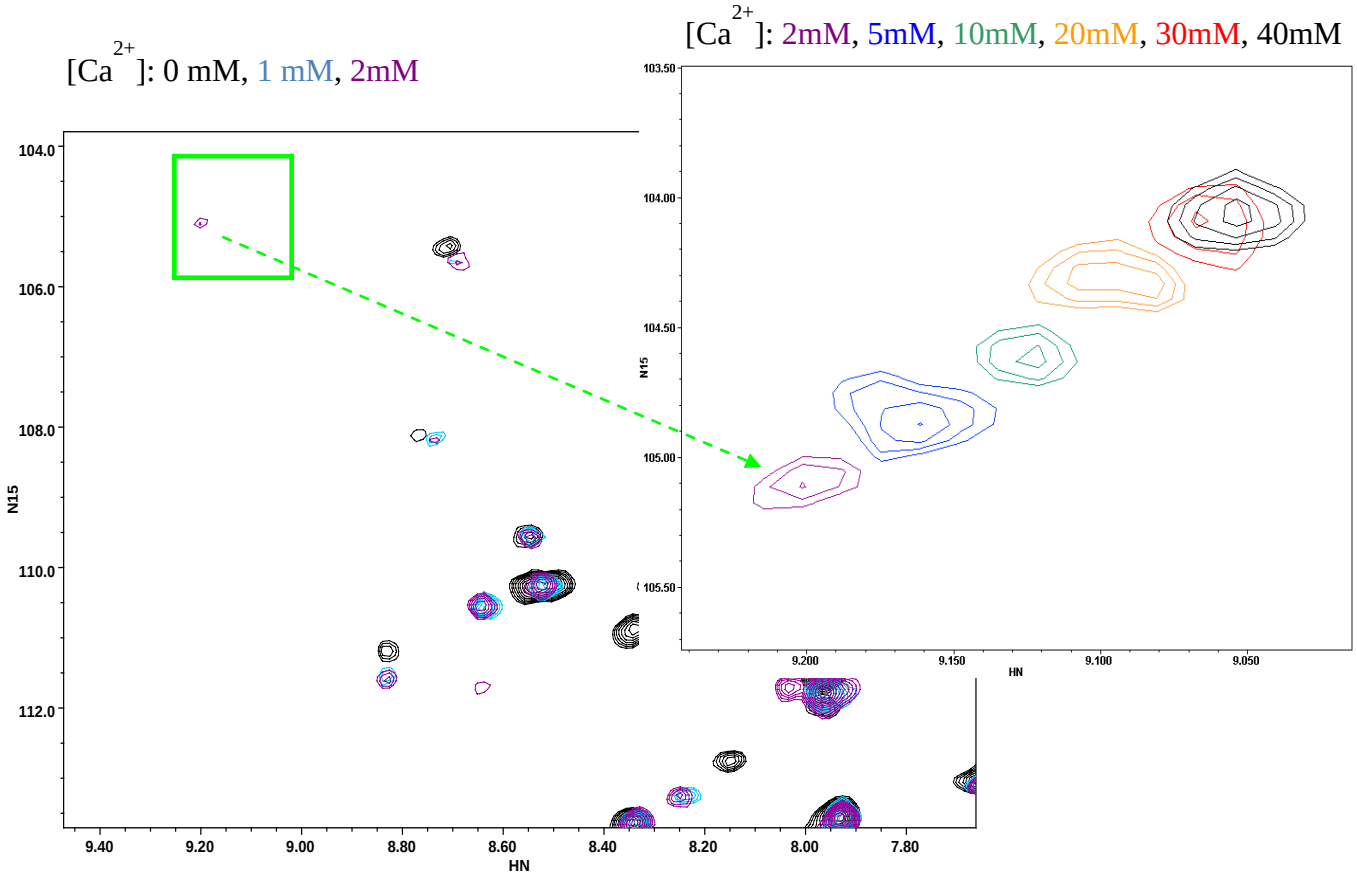

Figure 31. Calcium titration of E-Syt2 C2AB at high Ca^{2+} concentrations. The zoomed-in ^{1}H-^{15}N TROSY-HSQC spectrum (left panel) shows the appearance of a new peak at 2 mM Ca^{2+}. The inset expansion follows this peak at increasing Ca^{2+} concentrations. The concentrations shown are 0 mM (black), 1 mM (blue), and 2 mM (purple) in the left panel, and 2 mM (purple), 5 mM (blue), 10 mM (green), 20 mM (orange), 30 mM (red), and 40 mM (black) in the right panel.

4.3.3 Mutations in the Ca^{2+} binding loop disrupt Ca^{2+} binding

The crystal structure of the Ca^{2+}-bound form of E-Syt2 C2AB was determined by Junjie Xu after the above calcium titration experiments. The structure reveals that the Ca^{2+} binding region is in the C2A domain and confirms the presence of multiple (three) calcium binding sites (Figure 32). The binding sites involve residues that are conserved in tandem C2-domain proteins. In particular, the D52 residue is believed to be key for high-affinity binding because of its analogous structure and position to D178 of the synaptotagmin-1 C2A domain. Further examination reveals that the D52 residue is likely key in the coordination of high-affinity Ca^{2+} binding, while D105 may be responsible for low-affinity binding (Figure 32).

Calcium titration of the mutant E-Syt2 C2AB was carried out under the same conditions as the WT fragment. ^{1}H-^{15}N TROSY-HSQC spectra were acquired and the peaks were inspected for differences with increasing Ca^{2+} concentrations. The D52N mutation does not display any changes in chemical shifts at low Ca^{2+} concentrations: unlike the WT spectra, there were no movements in any of the peaks nor decreases in any peak intensities. One example of the difference between WT and D52N is shown in Figure 33.

The D105A mutant is expected to similarly disrupt low-affinity binding, so that for example, the new peak at 2 mM Ca^{2+} (Figure 31) would not appear. This is the next step in the characterization of the calcium-binding properties of E-Syt2.

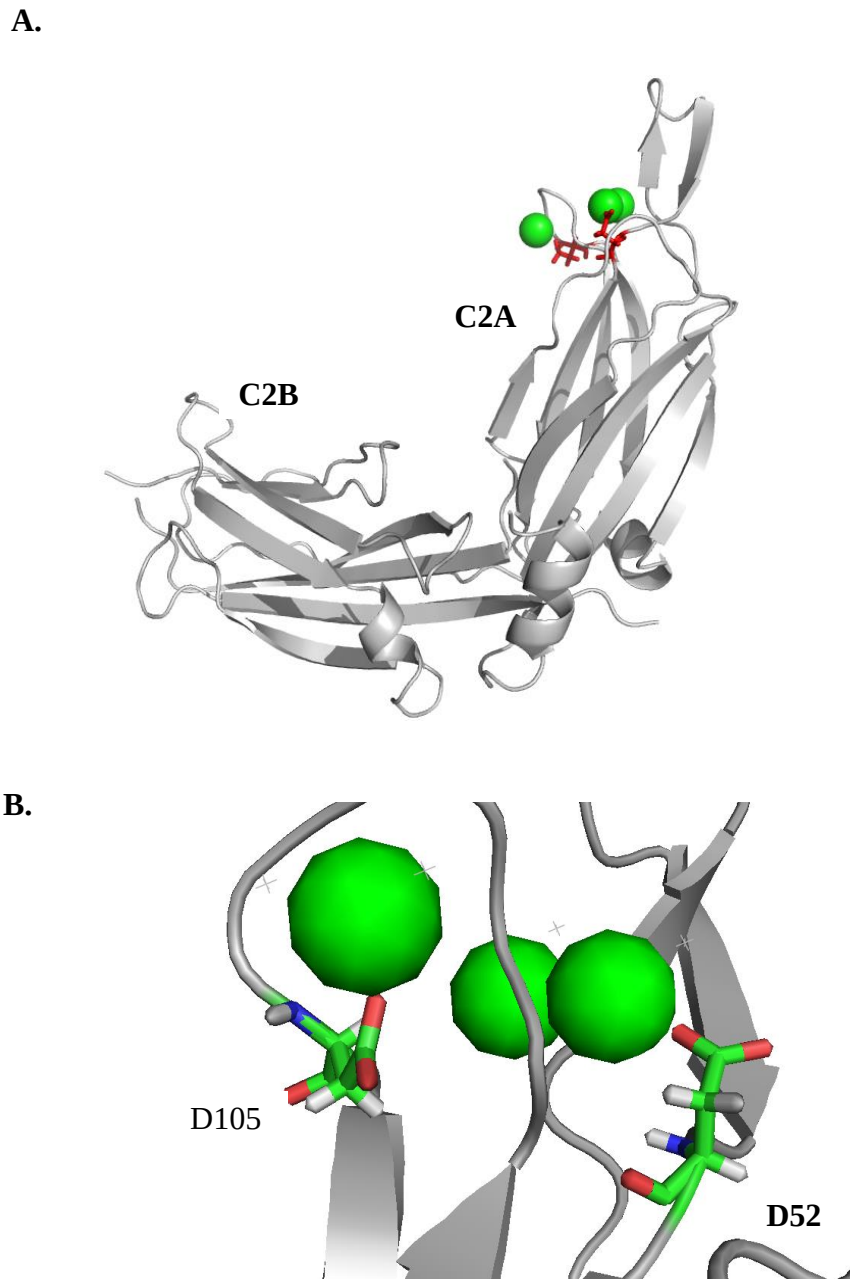

Figure 32. The Ca^{2+}-bound structure of the ESyt C2AB fragment (Junjie Xu, unpublished). **A.** Ribbon diagram of the C2AB fragment. Ca^{2+}-binding is exclusive to the C2A domain and involves three Ca^{2+} ions. **B.** Expansion of the Ca^{2+} binding region, with Ca^{2+} ions shown in green. Based on this structure, two mutations were designed to disrupt Ca^{2+} binding: D52N and D105A.

[Ca^{2+}]: 0 uM, 20 µM, 70 µM, 200 µM, 1000 µM

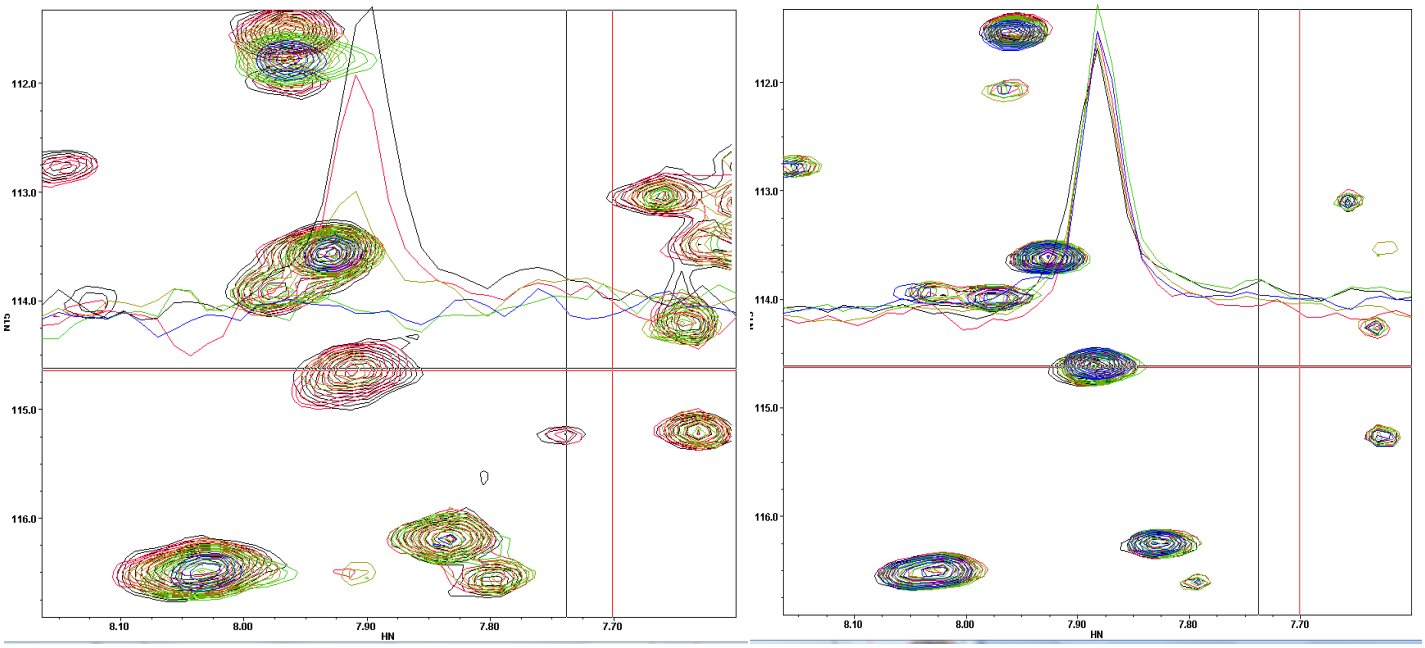

Figure 33. The high-affinity Ca^{2+} binding site is disrupted by the D52N mutation. As an example, the WT ^{1}H-^{15}N TROSY-HSQC spectrum (left) shows intensity decrease with increasing Ca^{2+} as in Figure 30. The D52N mutant spectrum (right) does not show peak intensity changes for the same calcium concentrations. The representative Ca^{2+} concentrations shown are 0 uM (black), 20 µM (red), 70 µM (brown), 200 µM (green), 1000 µM (blue).

4.3.4 E-Syt2 C2AB does not bind lipids

A co-floatation assay was carried out in both 1 mM EDTA or 1 mM Ca^{2+}, because phospholipid binding can often be Ca^{2+}-dependent, as is the case for synaptotagmin-1 (see chapter 1). The assay was performed with liposomes that did or did not contain 2% PIP or PIP_2. This is because the synaptotagmin-1 C2AB domain is known to interact with phosphatidylinositol phosphates (Bai et al. 2004). As shown in Figure 34, the lack of visible bands suggests no protein was bound to the liposomes under any of these conditions. This could be in line with the finding that it is the C2C domain of E-Syt that is responsible for membrane targeting (Min et al. 2007). However, while the lipid composition chosen here is representative of the plasma membrane and used in many lipid binding assays in the lab, one cannot rule out the possibility that a different composition could lead to different results.

Sample #	0 (input)	1	2	3	4	5	6
1 mM EDTA		x		x		x	
1 mM Ca^{2+}			x		x		x
2% PIP				x	x		
2% PIP_2						x	x

Figure 34. E-Syt2 C2AB fragment does not bind liposomes. Lane 0 represents the 5 µM E-Syt2 C2AB input of the assay. The odd-numbered samples contained 1 mM EDTA while the even-numbered samples contained 1 mM Ca^{2+}. Samples 3 & 4 contained liposomes with 2% PIP, while samples 5 & 6 contained liposomes with 2% PIP_2.

Chapter 5. Conclusion & Future Directions

Calcium-triggered neurotransmitter release depends critically on synaptotagmin, which senses the intracellular Ca^{2+} concentration, and on the SNARE complex which mediates fusion between the synaptic vesicle and plasma membrane. This dissertation is based on the current working model that synaptotagmin facilitates the role of the SNAREs in a Ca^{2+}-dependent manner. The precise mechanism by which this occurs is still unknown, despite the many attempts to study their interactions. This is because of the technical difficulties in probing the synaptotagmin-SNARE system. Current literature in the field presents conflicting evidence as to the Ca^{2+}-dependence of the interaction and protein domains involved in binding.

In chapter 2, I applied an analytical method that overcame these limitations, allowing for high sensitivity at low micromolar protein concentrations. My data suggest the interaction is Ca^{2+}-dependent and mediated primarily by the Syt1 C2B domain. Furthermore, the polybasic region of C2B constitutes the primary binding site for the SNARE complex and the two arginine residues at the bottom of the domain mediate additional, weaker interactions that lead to aggregation and precipitation of the macromolecular assembly. These results help clarify the complex mechanism of synaptotagmin-1/SNARE coupling, as well as to illustrate the usefulness of 1D NMR to study such protein-protein interactions.

These results can inform structural studies of the Syt1/SNARE complex – to minimize sample precipitation and to isolate the domain of functional interest, for example. This is being done in the Rizo-Rey lab to determine an NMR and possibly crystal structure of the macromolecular complex.

The structure will help elucidate many aspects of the interaction. For example, why is the Syt1-SNARE complex interaction Ca^{2+}-dependent in solution? They are known to function *in vivo* in a Ca^{2+}-dependent manner. But in the absence of membrane phospholipids, which residues or surfaces are conferring the Ca^{2+}-dependence? The answer is not immediately clear from the available data, since the major binding site has been shown to be in the polybasic region of the C2B domain away from the calcium binding loops: the rigid 4-helix SNARE bundle cannot contact the polybasic region and the calcium loops simultaneously. Our current working hypothesis is that Ca^{2+} binding confers additional positive charges to the C2 domains (three ions or six positive charges to C2A, and four positive charges to C2B). In particular, the C2B domain (pI = 9.2) is positively charged even in the absence of Ca^{2+} at physiological pH. The addition of Ca^{2+} therefore strengthens its electrostatic interaction with the SNARE complex which carries an overall negative charge. In the absence of a structure of the macromolecular complex, we can test this hypothesis by mutating negatively charged residues in the Ca^{2+} binding loops to positively charged residues, thereby disrupting Ca^{2+}-binding but mimicking the electrostatic effect of Ca^{2+}-binding. It is also important to study the interactions in the context of membranes.

Chapter 3 explores alternative methods to probe such protein-protein interactions. The advantage of the competition assay lies in the low concentration of SNARE complex used, thus sampling mostly the primary binding site with little interference of the other binding mode(s). In theory, this is superior to the direct titration assay for examining the primary binding mode. Unfortunately, experimental artifacts have hindered the application of the assay to my system. Nevertheless, it is a powerful method with general applicability to studying weak, low solubility protein-protein interactions. Its limitation arises if there are significant interactions of the protein(s) with the reaction vessel. The sample holder, as well as all other equipment that come

in contact with the sample, should be rigorously pacified and shown to be inert prior to substantial commitment to data acquisition. The technical difficulties encountered here highlight the complexity of the system and can inform the characterization of other protein-protein systems.

The diffusion-based method is also a possible route for studying such protein-protein interactions. The key lies in labeling a protein whose diffusion coefficient would change by a detectable amount (sufficient signal-to-noise) upon binding of an unlabeled protein. Application of the method to the ^{13}C-C2B domain, rather than the C2AB fragment, may be a viable method for quantifying the differences between WT and mutants in binding to the SNARE complex.

In chapter 4, the Ca^{2+}-, SNARE- and lipid-binding properties of an extended synaptotagmin-like protein, E-Syt2, were characterized. The D52N mutation disrupts high-affinity calcium binding and the D105A mutation has been shown to disrupt low-affinity binding (data courtesy of Junjie Xu, not shown). However, because the crystal structure reveals the presence of three calcium ions (Figure 32), there are three or possibly more ions bound. This in turn suggests that each of the two mutations may affect one or more binding pockets. Further analysis of the NMR Ca^{2+} titration data will help address these uncertainties. These studies can shed light on the evolution of synaptotagmins, as well as the general properties of calcium-binding tandem C2-domain proteins.

BIBLIOGRAPHY

Altieri, A., D. Hinton and R. Byrd (1995). "Association of Biomolecular Systems via Pulsed Field Gradient NMR Self-Diffusion Measurements." Journal of American Chemical Society **117**: 7566.

Arac, D., X. Chen, H. A. Khant, J. Ubach, S. J. Ludtke, M. Kikkawa, A. E. Johnson, W. Chiu, T. C. Sudhof and J. Rizo (2006). "Close membrane-membrane proximity induced by Ca(2+)-dependent multivalent binding of synaptotagmin-1 to phospholipids." Nat Struct Mol Biol **13**(3): 209-17.

Arac, D., T. Murphy and J. Rizo (2003). "Facile detection of protein-protein interactions by one-dimensional NMR spectroscopy." Biochemistry **42**(10): 2774-80.

Augustine, G. J., M. P. Charlton and S. J. Smith (1985). "Calcium entry and transmitter release at voltage-clamped nerve terminals of squid." J Physiol **367**: 163-81.

Bai, J., W. C. Tucker and E. R. Chapman (2004). "PIP2 increases the speed of response of synaptotagmin and steers its membrane-penetration activity toward the plasma membrane." Nat Struct Mol Biol **11**(1): 36-44.

Basu, J., N. Shen, I. Dulubova, J. Lu, R. Guan, O. Guryev, N. V. Grishin, C. Rosenmund and J. Rizo (2005). "A minimal domain responsible for Munc13 activity." Nat Struct Mol Biol **12**(11): 1017-8.

Bennett, M. K. (1995). "SNAREs and the specificity of transport vesicle targeting." Curr Opin Cell Biol **7**(4): 581-6.

Bennett, M. K., N. Calakos and R. H. Scheller (1992). "Syntaxin: a synaptic protein implicated in docking of synaptic vesicles at presynaptic active zones." Science **257**(5067): 255-9.

Blasi, J., E. R. Chapman, E. Link, T. Binz, S. Yamasaki, P. De Camilli, T. C. Sudhof, H. Niemann and R. Jahn (1993). "Botulinum neurotoxin A selectively cleaves the synaptic protein SNAP-25." Nature **365**(6442): 160-3.

Blasi, J., E. R. Chapman, S. Yamasaki, T. Binz, H. Niemann and R. Jahn (1993). "Botulinum neurotoxin C1 blocks neurotransmitter release by means of cleaving HPC-1/syntaxin." EMBO J **12**(12): 4821-8.

Block, M. R., B. S. Glick, C. A. Wilcox, F. T. Wieland and J. E. Rothman (1988). "Purification of an N-ethylmaleimide-sensitive protein catalyzing vesicular transport." Proc Natl Acad Sci U S A **85**(21): 7852-6.

Boeree, C. G. (2009). "The Neuron." Retrieved March 16, 2013, from http://webspace.ship.edu/cgboer/theneuron.html.

Bowen, M. E., K. Weninger, J. Ernst, S. Chu and A. T. Brunger (2005). "Single-molecule studies of synaptotagmin and complexin binding to the SNARE complex." Biophys J **89**(1): 690-702.

Brewer, K. D., W. Li, B. E. Horne and J. Rizo (2011). "Reluctance to membrane binding enables accessibility of the synaptobrevin SNARE motif for SNARE complex formation." Proc Natl Acad Sci U S A **108**(31): 12723-8.

Brose, N., A. G. Petrenko, T. C. Sudhof and R. Jahn (1992). "Synaptotagmin: a calcium sensor on the synaptic vesicle surface." Science **256**(5059): 1021-5.

Brunger, A. T. (2005). "Structure and function of SNARE and SNARE-interacting proteins." Q Rev Biophys **38**(1): 1-47.

Cajal, S. R. Y. (1906). "Nobel Lecture: The Structure and Connexions of Neurons." Retrieved Feb. 27, 2013, from http://www.nobelprize.org/nobel_prizes/medicine/laureates/1906/cajal-lecture.html.

Ceccarelli, B., W. P. Hurlbut and A. Mauro (1973). "Turnover of transmitter and synaptic vesicles at the frog neuromuscular junction." J Cell Biol **57**(2): 499-524.

Chapman, E. R. and A. F. Davis (1998). "Direct interaction of a Ca2+-binding loop of synaptotagmin with lipid bilayers." J Biol Chem **273**(22): 13995-4001.

Chapman, E. R., P. I. Hanson, S. An and R. Jahn (1995). "Ca2+ regulates the interaction between synaptotagmin and syntaxin 1." J Biol Chem **270**(40): 23667-71.

Chen, X., J. Tang, T. C. Sudhof and J. Rizo (2005). "Are neuronal SNARE proteins Ca2+ sensors?" J Mol Biol **347**(1): 145-58.

Chen, X., D. R. Tomchick, E. Kovrigin, D. Arac, M. Machius, T. C. Sudhof and J. Rizo (2002). "Three-dimensional structure of the complexin/SNARE complex." Neuron **33**(3): 397-409.

Choi, U. B., P. Strop, M. Vrljic, S. Chu, A. T. Brunger and K. R. Weninger (2010). "Single-molecule FRET-derived model of the synaptotagmin 1-SNARE fusion complex." Nat Struct Mol Biol **17**(3): 318-24.

Coussens, L., P. J. Parker, L. Rhee, T. L. Yang-Feng, E. Chen, M. D. Waterfield, U. Francke and A. Ullrich (1986). "Multiple, distinct forms of bovine and human protein kinase C suggest diversity in cellular signaling pathways." Science **233**(4766): 859-66.

Dai, H., N. Shen, D. Arac and J. Rizo (2007). "A quaternary SNARE-synaptotagmin-Ca2+-phospholipid complex in neurotransmitter release." J Mol Biol **367**(3): 848-63.

Davis, A. F., J. Bai, D. Fasshauer, M. J. Wolowick, J. L. Lewis and E. R. Chapman (1999). "Kinetics of synaptotagmin responses to Ca2+ and assembly with the core SNARE complex onto membranes." Neuron **24**(2): 363-76.

Davletov, B. A. and T. C. Sudhof (1993). "A single C2 domain from synaptotagmin I is sufficient for high affinity Ca2+/phospholipid binding." J Biol Chem **268**(35): 26386-90.

De Robertis, E. D. and H. S. Bennett (1955). "Some features of the submicroscopic morphology of synapses in frog and earthworm." J Biophys Biochem Cytol **1**(1): 47-58.

Del Castillo, J. and B. Katz (1954). "Changes in end-plate activity produced by presynaptic polarization." J Physiol **124**(3): 586-604.

Del Castillo, J. and B. Katz (1954). "Quantal components of the end-plate potential." J Physiol **124**(3): 560-73.

Del Castillo, J. and B. Katz (1956). "Localization of active spots within the neuromuscular junction of the frog." J Physiol **132**(3): 630-49.

Fasshauer, D., R. B. Sutton, A. T. Brunger and R. Jahn (1998). "Conserved structural features of the synaptic fusion complex: SNARE proteins reclassified as Q- and R-SNAREs." Proc Natl Acad Sci U S A **95**(26): 15781-6.

Fatt, P. and B. Katz (1952). "The electric activity of the motor end-plate." Proc R Soc Lond B Biol Sci **140**(899): 183-6.

Fernandez-Chacon, R., A. Konigstorfer, S. H. Gerber, J. Garcia, M. F. Matos, C. F. Stevens, N. Brose, J. Rizo, C. Rosenmund and T. C. Sudhof (2001). "Synaptotagmin I functions as a calcium regulator of release probability." Nature **410**(6824): 41-9.

Fernandez-Chacon, R., O. H. Shin, A. Konigstorfer, M. F. Matos, A. C. Meyer, J. Garcia, S. H. Gerber, J. Rizo, T. C. Sudhof and C. Rosenmund (2002). "Structure/function analysis of Ca2+ binding to the C2A domain of synaptotagmin 1." J Neurosci **22**(19): 8438-46.

Fernandez, I., D. Arac, J. Ubach, S. H. Gerber, O. Shin, Y. Gao, R. G. Anderson, T. C. Sudhof and J. Rizo (2001). "Three-dimensional structure of the synaptotagmin 1 C2B-domain: synaptotagmin 1 as a phospholipid binding machine." Neuron **32**(6): 1057-69.

Fernandez, I., J. Ubach, I. Dulubova, X. Zhang, T. C. Sudhof and J. Rizo (1998). "Three-dimensional structure of an evolutionarily conserved N-terminal domain of syntaxin 1A." Cell **94**(6): 841-9.

Fykse, E. M., K. Takei, C. Walch-Solimena, M. Geppert, R. Jahn, P. De Camilli and T. C. Sudhof (1993). "Relative properties and localizations of synaptic vesicle protein isoforms: the case of the synaptophysins." J Neurosci **13**(11): 4997-5007.

Gaffaney, J. D., F. M. Dunning, Z. Wang, E. Hui and E. R. Chapman (2008). "Synaptotagmin C2B domain regulates Ca2+-triggered fusion in vitro: critical residues revealed by scanning alanine mutagenesis." J Biol Chem **283**(46): 31763-75.

Geppert, M., B. T. Archer, 3rd and T. C. Sudhof (1991). "Synaptotagmin II. A novel differentially distributed form of synaptotagmin." J Biol Chem **266**(21): 13548-52.

Geppert, M., Y. Goda, R. E. Hammer, C. Li, T. W. Rosahl, C. F. Stevens and T. C. Sudhof (1994). "Synaptotagmin I: a major Ca2+ sensor for transmitter release at a central synapse." Cell **79**(4): 717-27.

Gerona, R. R., E. C. Larsen, J. A. Kowalchyk and T. F. Martin (2000). "The C terminus of SNAP25 is essential for Ca(2+)-dependent binding of synaptotagmin to SNARE complexes." J Biol Chem **275**(9): 6328-36.

Gibbs, S. and C. Johnson (1991). "A PFG NMR experiment for accurate diffusion and flow studies in the presence of Eddy currents." Journal of Magnetic Resonance **93**(2): 395.

Hata, Y., C. A. Slaughter and T. C. Sudhof (1993). "Synaptic vesicle fusion complex contains unc-18 homologue bound to syntaxin." Nature **366**(6453): 347-51.

Hayashi, T., H. Mcmahon, S. Yamasaki, T. Binz, Y. Hata, T. C. Sudhof and H. Niemann (1994). "Synaptic vesicle membrane fusion complex: action of clostridial neurotoxins on assembly." EMBO J **13**(21): 5051-61.

Heidelberger, R., C. Heinemann, E. Neher and G. Matthews (1994). "Calcium dependence of the rate of exocytosis in a synaptic terminal." Nature **371**(6497): 513-5.

Heuser, J. E. and T. S. Reese (1973). "Evidence for recycling of synaptic vesicle membrane during transmitter release at the frog neuromuscular junction." J Cell Biol **57**(2): 315-44.

Hodgkin, A. L. and A. F. Huxley (1952). "Propagation of electrical signals along giant nerve fibers." Proc R Soc Lond B Biol Sci **140**(899): 177-83.

Jahn, R., T. Lang and T. C. Sudhof (2003). "Membrane fusion." Cell **112**(4): 519-33.

Jahn, R. and R. H. Scheller (2006). "SNAREs--engines for membrane fusion." Nat Rev Mol Cell Biol **7**(9): 631-43.

Jean, S., M. G. Tremblay, C. Herdman, F. Guillou and T. Moss (2012). "The endocytic adapter E-Syt2 recruits the p21 GTPase activated kinase PAK1 to mediate actin dynamics and FGF signalling." Biol Open **1**(8): 731-8.

Kandel, E., J. Schwartz and Jessel Tm (2000). Principles of Neural Science, McGraw-Hill.

Katz, B. and R. Miledi (1967). "Ionic requirements of synaptic transmitter release." Nature **215**(5101): 651.

Kee, Y. and R. H. Scheller (1996). "Localization of synaptotagmin-binding domains on syntaxin." J Neurosci **16**(6): 1975-81.

Lai, A. L., H. Huang, D. Z. Herrick, N. Epp and D. S. Cafiso (2011). "Synaptotagmin 1 and SNAREs form a complex that is structurally heterogeneous." J Mol Biol **405**(3): 696-706.

Li, C., B. Ullrich, J. Z. Zhang, R. G. Anderson, N. Brose and T. C. Sudhof (1995). "Ca(2+)-dependent and -independent activities of neural and non-neural synaptotagmins." Nature **375**(6532): 594-9.

Li, L., O. H. Shin, J. S. Rhee, D. Arac, J. C. Rah, J. Rizo, T. Sudhof and C. Rosenmund (2006). "Phosphatidylinositol phosphates as co-activators of Ca2+ binding to C2 domains of synaptotagmin 1." J Biol Chem **281**(23): 15845-52.

Linial, M. (1997). "SNARE proteins--why so many, why so few?" J Neurochem **69**(5): 1781-92.

Link, E., L. Edelmann, J. H. Chou, T. Binz, S. Yamasaki, U. Eisel, M. Baumert, T. C. Sudhof, H. Niemann and R. Jahn (1992). "Tetanus toxin action: inhibition of neurotransmitter release linked to synaptobrevin proteolysis." Biochem Biophys Res Commun **189**(2): 1017-23.

Littleton, J. T., M. Stern, K. Schulze, M. Perin and H. J. Bellen (1993). "Mutational analysis of Drosophila synaptotagmin demonstrates its essential role in Ca(2+)-activated neurotransmitter release." Cell **74**(6): 1125-34.

Lopez-Munoz, F., J. Boya and C. Alamo (2006). "Neuron theory, the cornerstone of neuroscience, on the centenary of the Nobel Prize award to Santiago Ramon y Cajal." Brain Res Bull **70**(4-6): 391-405.

Lynch, K. L., R. R. Gerona, E. C. Larsen, R. F. Marcia, J. C. Mitchell and T. F. Martin (2007). "Synaptotagmin C2A loop 2 mediates Ca2+-dependent SNARE interactions essential for Ca2+-triggered vesicle exocytosis." Mol Biol Cell **18**(12): 4957-68.

Ma, C., L. Su, A. B. Seven, Y. Xu and J. Rizo (2013). "Reconstitution of the vital functions of Munc18 and Munc13 in neurotransmitter release." Science **339**(6118): 421-5.

Mackler, J. M., J. A. Drummond, C. A. Loewen, I. M. Robinson and N. E. Reist (2002). "The C(2)B Ca(2+)-binding motif of synaptotagmin is required for synaptic transmission in vivo." Nature **418**(6895): 340-4.

Mackler, J. M. and N. E. Reist (2001). "Mutations in the second C2 domain of synaptotagmin disrupt synaptic transmission at Drosophila neuromuscular junctions." J Comp Neurol **436**(1): 4-16.

Matos, M. F., J. Rizo and T. C. Sudhof (2000). "The relation of protein binding to function: what is the significance of munc18 and synaptotagmin binding to syntaxin 1, and where are the corresponding binding sites?" Eur J Cell Biol **79**(6): 377-82.

Matthew, W. D., L. Tsavaler and L. F. Reichardt (1981). "Identification of a synaptic vesicle-specific membrane protein with a wide distribution in neuronal and neurosecretory tissue." J Cell Biol **91**(1): 257-69.

Mcmahon, H. T., M. Missler, C. Li and T. C. Sudhof (1995). "Complexins: cytosolic proteins that regulate SNAP receptor function." Cell **83**(1): 111-9.

Meinrenken, C. J., J. G. Borst and B. Sakmann (2003). "Local routes revisited: the space and time dependence of the Ca2+ signal for phasic transmitter release at the rat calyx of Held." J Physiol **547**(Pt 3): 665-89.

Min, S. W., W. P. Chang and T. C. Sudhof (2007). "E-Syts, a family of membranous Ca2+-sensor proteins with multiple C2 domains." Proc Natl Acad Sci U S A **104**(10): 3823-8.

Morris, N. J., S. A. Ross, J. M. Neveu, W. S. Lane and G. E. Lienhard (1999). "Cloning and preliminary characterization of a 121 kDa protein with multiple predicted C2 domains." Biochim Biophys Acta **1431**(2): 525-30.

Nishiki, T. and G. J. Augustine (2004). "Dual roles of the C2B domain of synaptotagmin I in synchronizing Ca2+-dependent neurotransmitter release." J Neurosci **24**(39): 8542-50.

Nonet, M. L., K. Grundahl, B. J. Meyer and J. B. Rand (1993). "Synaptic function is impaired but not eliminated in C. elegans mutants lacking synaptotagmin." Cell **73**(7): 1291-305.

Palay, S. L. (1956). "Synapses in the central nervous system." J Biophys Biochem Cytol **2**(4 Suppl): 193-202.

Palay, S. L. (1960). "The fine structure of secretory neurons in the preoptic nucleus of the goldish (Carassius auratus)." Anat Rec **138**: 417-43.

Pang, Z. P., O. H. Shin, A. C. Meyer, C. Rosenmund and T. C. Sudhof (2006). "A gain-of-function mutation in synaptotagmin-1 reveals a critical role of Ca2+-dependent soluble N-ethylmaleimide-sensitive factor attachment protein receptor complex binding in synaptic exocytosis." J Neurosci **26**(48): 12556-65.

Pang, Z. P. and T. C. Sudhof (2010). "Cell biology of Ca2+-triggered exocytosis." Curr Opin Cell Biol **22**(4): 496-505.

Perin, M. S., V. A. Fried, G. A. Mignery, R. Jahn and T. C. Sudhof (1990). "Phospholipid binding by a synaptic vesicle protein homologous to the regulatory region of protein kinase C." Nature **345**(6272): 260-3.

Poirier, M. A., W. Xiao, J. C. Macosko, C. Chan, Y. K. Shin and M. K. Bennett (1998). "The synaptic SNARE complex is a parallel four-stranded helical bundle." Nat Struct Biol **5**(9): 765-9.

Purves, D., G. Augustine, D. Fitzpatrick and E. Al. (2001). Neuroscience. Sunderland (MA), Sinauer Associates.

Rhee, J. S., L. Y. Li, O. H. Shin, J. C. Rah, J. Rizo, T. C. Sudhof and C. Rosenmund (2005). "Augmenting neurotransmitter release by enhancing the apparent Ca2+ affinity of synaptotagmin 1." Proc Natl Acad Sci U S A **102**(51): 18664-9.

Rickman, C., D. A. Archer, F. A. Meunier, M. Craxton, M. Fukuda, R. D. Burgoyne and B. Davletov (2004). "Synaptotagmin interaction with the syntaxin/SNAP-25 dimer is mediated by an evolutionarily conserved motif and is sensitive to inositol hexakisphosphate." J Biol Chem **279**(13): 12574-9.

Rickman, C. and B. Davletov (2003). "Mechanism of calcium-independent synaptotagmin binding to target SNAREs." J Biol Chem **278**(8): 5501-4.

Rickman, C., J. L. Jimenez, M. E. Graham, D. A. Archer, M. Soloviev, R. D. Burgoyne and B. Davletov (2006). "Conserved prefusion protein assembly in regulated exocytosis." Mol Biol Cell **17**(1): 283-94.

Rizo, J., X. Chen and D. Arac (2006). "Unraveling the mechanisms of synaptotagmin and SNARE function in neurotransmitter release." Trends Cell Biol **16**(7): 339-50.

Rizo, J., M. K. Rosen and K. H. Gardner (2012). "Enlightening molecular mechanisms through study of protein interactions." J Mol Cell Biol **4**(5): 270-83.

Rizo, J. and C. Rosenmund (2008). "Synaptic vesicle fusion." Nat Struct Mol Biol **15**(7): 665-74.

Rizo, J. and T. C. Sudhof (1998). "C2-domains, structure and function of a universal Ca2+-binding domain." J Biol Chem **273**(26): 15879-82.

Robinson, I. M., R. Ranjan and T. L. Schwarz (2002). "Synaptotagmins I and IV promote transmitter release independently of Ca(2+) binding in the C(2)A domain." Nature **418**(6895): 336-40.

Rothman, J. E. (1994). "Mechanisms of intracellular protein transport." Nature **372**(6501): 55-63.

Sabatini, B. L. and W. G. Regehr (1996). "Timing of neurotransmission at fast synapses in the mammalian brain." Nature **384**(6605): 170-2.

Schiavo, G., F. Benfenati, B. Poulain, O. Rossetto, P. Polverino De Laureto, B. R. Dasgupta and C. Montecucco (1992). "Tetanus and botulinum-B neurotoxins block neurotransmitter release by proteolytic cleavage of synaptobrevin." Nature **359**(6398): 832-5.

Schiavo, G., M. Matteoli and C. Montecucco (2000). "Neurotoxins affecting neuroexocytosis." Physiol Rev **80**(2): 717-66.

Shao, X., B. A. Davletov, R. B. Sutton, T. C. Sudhof and J. Rizo (1996). "Bipartite Ca2+-binding motif in C2 domains of synaptotagmin and protein kinase C." Science **273**(5272): 248-51.

Shao, X., C. Li, I. Fernandez, X. Zhang, T. C. Sudhof and J. Rizo (1997). "Synaptotagmin-syntaxin interaction: the C2 domain as a Ca2+-dependent electrostatic switch." Neuron **18**(1): 133-42.

Shatz, C. J. (2001). The Scientific American Book of the Brain, Lyons Press.

Shin, O. H., J. Xu, J. Rizo and T. C. Sudhof (2009). "Differential but convergent functions of Ca2+ binding to synaptotagmin-1 C2 domains mediate neurotransmitter release." Proc Natl Acad Sci U S A **106**(38): 16469-74.

Simpson, L. L. (2004). "Identification of the major steps in botulinum toxin action." Annu Rev Pharmacol Toxicol **44**: 167-93.

Sollner, T., M. K. Bennett, S. W. Whiteheart, R. H. Scheller and J. E. Rothman (1993). "A protein assembly-disassembly pathway in vitro that may correspond to sequential steps of synaptic vesicle docking, activation, and fusion." Cell **75**(3): 409-18.

Sollner, T., S. W. Whiteheart, M. Brunner, H. Erdjument-Bromage, S. Geromanos, P. Tempst and J. E. Rothman (1993). "SNAP receptors implicated in vesicle targeting and fusion." Nature **362**(6418): 318-24.

Sollner, T. H. (2003). "Regulated exocytosis and SNARE function (Review)." Mol Membr Biol **20**(3): 209-20.

Sudhof, T. and J. Rizo (2012). Synaptic Vesicle Exocytosis. The Synapse. Cold Spring Harbor, Cold Spring Harbor Laboratory Press**:** 49-62.

Sudhof, T. C. (2008). "Neuroligins and neurexins link synaptic function to cognitive disease." Nature **455**(7215): 903-11.

Sudhof, T. C. (2012). "Calcium control of neurotransmitter release." Cold Spring Harb Perspect Biol **4**(1): a011353.

Sudhof, T. C., P. De Camilli, H. Niemann and R. Jahn (1993). "Membrane fusion machinery: insights from synaptic proteins." Cell **75**(1): 1-4.

Sudhof, T. C. and J. E. Rothman (2009). "Membrane fusion: grappling with SNARE and SM proteins." Science **323**(5913): 474-7.

Sutton, R. B., B. A. Davletov, A. M. Berghuis, T. C. Sudhof and S. R. Sprang (1995). "Structure of the first C2 domain of synaptotagmin I: a novel Ca2+/phospholipid-binding fold." Cell **80**(6): 929-38.

Sutton, R. B., D. Fasshauer, R. Jahn and A. T. Brunger (1998). "Crystal structure of a SNARE complex involved in synaptic exocytosis at 2.4 A resolution." Nature **395**(6700): 347-53.

Tang, J., A. Maximov, O. H. Shin, H. Dai, J. Rizo and T. C. Sudhof (2006). "A complexin/synaptotagmin 1 switch controls fast synaptic vesicle exocytosis." Cell **126**(6): 1175-87.

Tanner, J. (1970). "Use of the Stimulated Echo in NMR Diffusion Studies " Journal of Chemical Physics **52**(5): 2523.

Ubach, J., Y. Lao, I. Fernandez, D. Arac, T. C. Sudhof and J. Rizo (2001). "The C2B domain of synaptotagmin I is a Ca2+-binding module." Biochemistry **40**(20): 5854-60.

Ubach, J., X. Zhang, X. Shao, T. C. Sudhof and J. Rizo (1998). "Ca2+ binding to synaptotagmin: how many Ca2+ ions bind to the tip of a C2-domain?" EMBO J **17**(14): 3921-30.

Ullrich, B., C. Li, J. Z. Zhang, H. Mcmahon, R. G. Anderson, M. Geppert and T. C. Sudhof (1994). "Functional properties of multiple synaptotagmins in brain." Neuron **13**(6): 1281-91.

Van Den Bogaart, G., M. G. Holt, G. Bunt, D. Riedel, F. S. Wouters and R. Jahn (2010). "One SNARE complex is sufficient for membrane fusion." Nat Struct Mol Biol **17**(3): 358-64.

Walch-Solimena, C., K. Takei, K. L. Marek, K. Midyett, T. C. Sudhof, P. De Camilli and R. Jahn (1993). "Synaptotagmin: a membrane constituent of neuropeptide-containing large dense-core vesicles." J Neurosci **13**(9): 3895-903.

Weber, T., B. V. Zemelman, J. A. Mcnew, B. Westermann, M. Gmachl, F. Parlati, T. H. Sollner and J. E. Rothman (1998). "SNAREpins: minimal machinery for membrane fusion." Cell **92**(6): 759-72.

Xue, M., C. Ma, T. K. Craig, C. Rosenmund and J. Rizo (2008). "The Janus-faced nature of the C(2)B domain is fundamental for synaptotagmin-1 function." Nat Struct Mol Biol **15**(11): 1160-8.

Zhang, P., Y. Sun, H. Hsu, L. Zhang, Y. Zhang and M. Y. Lee (1998). "The interdomain connector loop of human PCNA is involved in a direct interaction with human polymerase delta." J Biol Chem **273**(2): 713-9.

Zhang, X., M. J. Kim-Miller, M. Fukuda, J. A. Kowalchyk and T. F. Martin (2002). "Ca2+-dependent synaptotagmin binding to SNAP-25 is essential for Ca2+-triggered exocytosis." Neuron **34**(4): 599-611.

Zhang, X., J. Rizo and T. C. Sudhof (1998). "Mechanism of phospholipid binding by the C2A-domain of synaptotagmin I." Biochemistry **37**(36): 12395-403.